Stochastic Approaches to Solute Transport in Heterogeneous Porous Media

Dissertation

der Mathematisch-Naturwissenschaftlichen Fakultät
der Eberhard Karls Universität Tübingen
zur Erlangung des Grades eines
Doktors der Naturwissenschaften
(Dr. rer. nat.)

vorgelegt von
M.Sc. Marie-Madeleine Stettler
aus Muttenz/Schweiz

Tübingen
2025

Gedruckt mit Genehmigung der Mathematisch-Naturwissenschaftlichen Fakultät der Eberhard Karls Universität Tübingen.

Tag der mündlichen Qualifikation:	24.02.2026
Dekan:	Prof. Dr. Thilo Stehle
1. Berichterstatter/-in:	Prof. Dr.-Ing. Olaf A. Cirpka
2. Berichterstatter/-in:	Prof. Dr. Insa Neuweiler

Abstract

While substantial amounts of global drinking and irrigation water consumption are supplied from groundwater, its storage is increasingly threatened by depletion and pollution. Thus, in order to remediate and protect it, understanding how solutes are distributed in the subsurface by and within groundwater is very important. However, this poses a challenge because solute transport in natural porous media is highly affected by the spatial variability of hydraulic properties, which is never fully known in real-world applications. Thus, there is a need for approaches which deal with uncertainty in a stochastic manner. While tremendous progress has been made in the past decades to characterize solute transport in heterogeneous media, there is still confusion between advective spreading and diffusive mixing, and closed-form expressions relating geostatistical properties of the formation to transport characteristics are often restricted to cases of mild heterogeneity.

In this thesis, these research gaps are addressed by applying two different stochastic methods: a stochastic advective-diffusive Spatial Markov Model (Study A) and an analytical solution applying linear stochastic theory (Study B). Numerical Monte-Carlo simulations serve as a synthetic reality to confirm the new approaches which are advantageous concerning the computational effort. In both studies, the main methodical angle lies in determining first and second temporal or spatial moments (mean and variance) of a moving plume from which dispersion coefficients can be computed. Ensemble dispersion measures the increase of second central temporal or spatial moments with distance and time, respectively, after taking the average of concentration either over a large cross-sectional area or over many realizations. By construction it includes the variance of first moments. In effective dispersion, by contrast, second central moments are computed for individual plumes first and are then averaged over the cross-sectional area or ensemble. Thus, ensemble dispersion incorporates uncertainty about the field and effective dispersion is more representative for a single plume.

The main goal of Study A is to advance Spatial Markov Models (SMM), which are generally applicable to fields of unlimited heterogeneity, such that advection and diffusion are derived analytically and mechanistically, rather than based on empirical transition matrices. SMM parameterize advective transport as transitions between consecutive observation planes assuming random velocity transitions that are conditioned on the directly preceding increments. The SMM introduced in Study A draws advective velocities from a conditional distribution which is analytically derived from geostatistical properties of the hydraulic conductivity field. Diffusion is conceptualized as lateral jumps between advective trajectories. At every transition, the current advective travel time and the diffusion time necessary for a particle to leave its trajectory by going beyond a certain radius in transverse direction are compared. Whichever process acts faster produces the next transition. After a diffusive exchange, the advective correlation chain is reset. With this model, I evaluate temporal ensemble moments and breakthrough curves under different degrees of heterogeneity and Péclet regimes.

Study B applies an existing linear stochastic theory solution for the evolution of

concentration fields and their moments to transport with flow reversal. The key idea behind subjecting a plume to flow reversal is the following: While spreading is determined by velocity variability caused by the geometry and structure of the subsurface, mixing is purely random. In a thought experiment where the two processes can be switched on and off and can thus act isolated from each other, spreading alone would be completely reversible upon flow reversal, while mixing alone is completely irreversible independent of the direction of flow. In reality, the processes are interconnected and act simultaneously, rendering dispersion partially reversible. Thus, by looking at plume deformation over a flow reversal cycle, information about the relative strengths and the interplay of spreading and mixing can be inferred. With this approach, I evaluate spatial ensemble and effective moments and dispersion coefficients.

Combining the results from both studies, applied to a point-injection, the following effects of increasing diffusion strength are supported: (i) Ensemble dispersion decreases because the velocity correlation is interrupted by diffusion. (ii) Effective dispersion increases because point plumes are enabled to sample a range of velocities by diffusive plume expansion. (iii) The reversibility of dispersion decreases because diffusion destroys path memory.

Further, from Study B I deduce that effective moments are not a metric for pure mixing because they are affected by flow reversal, albeit not as strongly as ensemble moments. Nevertheless, effective moments are much more appropriate for mixing quantification. Also, it becomes evident how strongly spreading and mixing are interconnected, since flow reversal alone does not allow to completely identify the separate impacts of the two processes on dispersion. However, qualitatively the influence strengths can be determined: The lower the degree of reversibility of dispersion the stronger diffusion dominates over advection.

Building on the present work, the advective-diffusive SMM could be refined by enabling it to capture effective dispersion for which considering the longitudinal velocity correlation normal to the direction of flow is most likely necessary. Additionally, it would be of high interest to perform laboratory flow reversal experiments which allow for the assessment of specific mixing metrics like the dilution index besides ensemble and effective dispersion.

Zusammenfassung

Weltweit wird ein erheblicher Teil des Bedarfs an Trink- und Bewässerungswasser aus dem Grundwasser gespiesen. Gleichzeitig ist dessen Speicher zunehmend durch Verbrauch und Verschmutzung bedroht. Um die Grundwasservorkommen zu sanieren und zu schützen, ist es daher sehr wichtig, zu verstehen, wie sich gelöste Stoffe im Untergrund durch und innerhalb des Grundwassers verteilen. Eine grosse Herausforderung dabei ist, dass der Transport gelöster Stoffe in natürlichen porösen Medien stark von der räumlichen Variabilität der hydraulischen Eigenschaften beeinflusst wird, die in realen Anwendungen nie vollständig bekannt ist. Owohl in den letzten Jahrzehnten enorme Fortschritte bei der Charakterisierung von Stofftransport in heterogenen Medien erzielt wurden, besteht weiterhin Bedarf an Ansätzen, die diesen Unsicherheiten stochastisch begegnen. Dies ist insbesondere deswegen der Fall, weil nach wie vor Unschärfe in der Abgrenzung zwischen advektiver Spreitung und diffusiver Vermischung besteht und weil geschlossene Ausdrücke, die geostatistische Formationseigenschaften mit Transporteigenschaften in Beziehung setzen, oft auf Fälle mit geringer Heterogenität beschränkt sind.

In dieser Arbeit werden diese Forschungslücken durch die Anwendung zweier verschiedener stochastischer Methoden angegangen: einem stochastischen advektiv-diffusiven Spatial Markov Modell (Studie A) und einer analytischen Lösung unter Anwendung von linearer stochastischer Theorie (Studie B). Numerische Monte-Carlo-Simulationen liefern dazu eine künstliche Realität, um die neuen, hinsichtlich des Rechenaufwand vorteilhaften Ansätze zu bestätigen. Der methodische Schwerpunkt beider Studien liegt auf der Bestimmung der ersten und zweiten zeitlichen oder räumlichen Momente (Mittelwert und Varianz) einer sich bewegenden Stoffwolke, aus denen Dispersionskoeffizienten berechnet werden können. Ensemble-Dispersion misst den Anstieg des zweiten zentralen zeitlichen oder räumlichen Moments mit der Entfernung bzw. der Zeit, nachdem die Durchschnittskonzentration entweder über einen grossen Querschnitt oder über viele Realisierungen ermittelt wurde. Sie umfasst konstruktionsbedingt die Varianz der ersten Momente. Bei der effektiven Dispersion hingegen werden zunächst die zweiten zentralen Momente für einzelne Stoffwolken berechnet und dann über den Querschnitt oder das Ensemble gemittelt. Somit beinhaltet Ensemble-Dispersion Unsicherheit über das Feld, während effektive Dispersion repräsentativer für eine einzelne Stoffwolke ist.

Das Hauptziel von Studie A ist die methodische Weiterentwicklung von Spatial Markov Modellen (SMM), welche im Allgemeinen auf Felder beliebiger Heterogenität anwendbar sind, so dass Advektion analytisch und neu auch Diffusion mechanistisch hergeleitet werden, statt auf empirische Übergangsmatrizen gestützt. SMM parameterisieren advektiven Transport als zufällige Geschwindigkeitsübergänge zwischen aufeinanderfolgenden Beobachtungsebenen konstanten Abstands, wobei die nächste Geschwindigkeit ausschliesslich von der direkt vorgängigen abhängig ist. Im hier in Studie A vorgestellten SMM, werden die advektiven Geschwindigkeiten aus einer konditionellen Verteilung gezogen, die aus den geostatistischen Eigenschaften des Durchlässigkeitsfeldes analytisch hergeleitet

ist. Die Diffusion wird als laterale Sprünge zwischen advektiven Trajektorien konzipiert. Bei jedem Schritt wird die aktuelle advektive Transportzeit mit der Diffusionszeit verglichen, die ein Partikel benötigt, um seine Trajektorie über einen bestimmten Radius in Querrichtung zu verlassen. Derjenige Prozess, der schneller abläuft, bewirkt den nächsten Übergang. Nach einem diffusiven Austausch wird die advektive Korrelationskette zurückgesetzt. Mit diesem Modell bewerte ich zeitliche Ensemble-Momente und Durchbruchskurven unter verschiedenen Heterogenitätsgraden und Péclet-Regimen.

Studie B erweitert eine bestehende Lösung für die Entwicklung von Konzentrationsfeldern und deren Momenten mit linearer stochastischer Theorie auf Transport mit Strömungsumkehr. Die Grundidee dahinter, eine Stoffwolke Strömungsumkehr auszusetzen, basiert darauf, dass Vermischung rein zufällig geschieht, wohingegen Spreitung durch Geschwindigkeitsvariabilität verursacht wird, die wiederum durch die Geometrie des Untergrunds bestimmt ist. In einem Gedankenexperiment, in dem die beiden Prozesse ein- und ausgeschaltet werden und somit isoliert voneinander wirken können, wäre Vermischung allein unabhängig von der Strömungsrichtung vollständig irreversibel, während Spreitung allein vollständig reversibel wäre. In der Realität sind die Prozesse miteinander verbunden und wirken gleichzeitig, wodurch Dispersion teilweise reversibel wird. Durch die Analyse der Stoffwolkenverformung über einen Transportzyklus mit Strömungsumkehr lassen sich somit Informationen über die relative Stärke und das Zusammenspiel von Spreitung und Vermischung ableiten. Mit diesem Ansatz untersuche ich räumliche Ensemble- und effektive Momente sowie Dispersionskoeffizienten. Auf eine Punktinjektion angewandt, bestätigt die Kombination der Ergebnisse von Studie A und Studie B, dass die Erhöhung der Diffusionsstärke folgende Auswirkungen hat: (i) Die Ensemble-Dispersion wird verringert, da die Geschwindigkeitskorrelation durch Diffusion unterbrochen wird. (ii) Die effektive Dispersion wird erhöht, da Punktstoffwolken durch diffusive Ausdehnung ein Geschwindigkeitsspektrum erfahrbar wird. (iii) Die Reversibilität der Dispersion wird verringer, da Diffusion das Weggedächtnis zerstört.

Aus Studie B leite ich ausserdem ab, dass effektive Momente kein Mass für reine Vermischung sind, weil sie von der Strömungsumkehr beeinflusst werden. Dennoch sind effektive Momente für die Quantifizierung von Vermischung viel besser geeignet als Ensemble-Momente. Zudem wird deutlich, wie stark Spreitung und Vermischung miteinander verbunden sind, da die Strömungsumkehr nicht ausreicht, um die getrennten Auswirkungen der beiden Prozesse auf die Dispersion vollständig zu identifizieren. Qualitativ lassen sich die Einflussstärken hingegen bestimmen: Je geringer die Reversibilität der Dispersion ist, desto stärker dominiert die Diffusion gegenüber der Advektion.

Basierend auf der vorliegenden Arbeit könnte das advektiv-diffusive SMM auf Anwendungen für effektive Dispersion erweitert werden, indem die Korrelation der longitudinalen Geschwindigkeiten senkrecht zur Strömungsrichtung berücksichtigt wird. Darüber hinaus wäre es von grossem Interesse, Laborversuche zur Strömungsumkehr durchzuführen, die neben der Ensemble- und effektiven Dispersion auch die Ermittlung spezifischer Vermischungskennzahlen wie z.B. des Verdünnungsindex ermöglich.

Acknowledgements

To my dear grandmothers whose formal education and careers were restricted.
We have come a long way. Let us keep going.

Collaboration lays the groundwork for my scientific endeavours. Many fine people have supported me throughout my doctoral studies to whom I am deeply indebted.

- To my first supervisor, Olaf Cirpka: Thank you for entrusting me with this topic, for providing both freedom and guidance and for creating a work environment that fosters both academic and personal growth.
- To my second supervisor, Marco Dentz: Thank you for bringing your enthusiastic and contagious passion about science and your optimism about always finding a solution into our collaborations.
- To Yves Méheust: Thank you for joining and enriching my PhD committee with your precision and focus and for openly and kindly sharing your expertise and opinion.
- To Insa Neuweiler, Peter Grathwohl, Christiane Zarfl: Thank you for agreeing to evaluate this thesis and my oral defense of it. Also I'm grateful for your ready and helpful advice at selected moments during my PhD time.
- To Carsten Leven: Thank you for sharing your incessant cascade of nifty ideas and valuable experience as well as your good sense of humour.
- To Cora Strobel and Philippa Hennessey: Thank you for being such close companions, advice-givers and role models during my PhD time. Our regular exchange in the office and online about our projects and all imaginable other topics were invaluable to me.
- To the hydrogeology workgroup members, Michael, Simon, Anna, Jonas, Adrian, Tao, Janek, Frederick, Konstantin, Mauricio, Anne, Sina: Thank you for bringing all your different perspectives into our group and for shaping an encouraging, friendly and humorous atmosphere.
- To the Barcelona work group: Thank you for welcoming me so warmly during my research stay. It was very inspiring to visit and learn from you. Special thanks to Animesh and Jordi for being fabulous office mates and Barcelona guides.
- To the administration staff at GUZ, especially Gabriele Stimmler, Patricia König, Iris Dreher, Uli Nasarek: Thank you for dealing with all the paperwork so cordially and efficiently and for offering such great support in any conceivable situation.

Science may follow winding roads. Although it did not make it into this thesis, I did perform some laboratory work which many people helped me perform.

- To the technical staff who substantially supported my experimental work, Annegret Walz, Alexander Schnapper, Thomas Siller, Barbara Maier: Thank you for generously investing your time, hand and brain power into my project.

- To the laboratory staff at GUZ, especially Bernice Nisch, Stephanie Nowak, Björn Spranglewski, Sara Wild: Thank you for teaching me many things about lab work and for creating a supportive and easy work climate.

- To the master's students who supported my work as Hiwis, Maria Sánchez, Josefine Schulte, Anees Kizhakkekara-Asharaf, Rebekka Knauer, Aleena Baby: Thank you for your assistance. I really enjoyed our interactions and I hope learning from the collaboration was mutual.

Balance is key. All the support I experience from outside of it helps me thrive in science.

- To my AEG classmates, especially, Akash, Amir, Kleio, Sary: Thank you for your precious company during our master's journey (which led me to this doctoral position) and well beyond.

- To my fantastic flatmates at Rappenberghalde 11, Flo, Justina, Manuel: Thank your for making me truly feel at home in Tübingen.

- To my closest friends from home, especially Annegret, Ladina, Nivitha, Sabren, Sebastian: Thank you for sharing both the silly and serious with me. It's such a privilege to grow alongside you even though we ended up scattered around the globe.

- To my family and my beloved partner: My deepest gratitude goes to you. My boat was built with your unwavering support and your unconditional love is the wind in my sails.

Contents

List of Figures

List of Abbreviations

ADE	Advection-Dispersion/Diffusion Equation
BTC	Breakthrough Curve
CTRW	Continuous Time Random Walk
MRMT	Multirate Mass Transfer
PTRW	Particle-Tracking Random-Walk
SMM	Spatial Markov Model

List of Symbols

A	coefficient related to local dispersion in spectral domain
B	coefficient related to mean advection in spectral domain
C	covariance function of K field
c	concentration
D	diffusion/dispersion coefficient
$\mathbf{d}$	distance vector
e	vertical-to-horizontal anisotropy ratio
$\mathbf{e_1}$	unit vector
h	hydraulic head
I_v	Eulerian velocity integral scale
I_Y	integral scale of $\ln K$, equals λ_h
$\mathbf{J}$	hydraulic gradient vector
K	hydraulic conductivity
K_g	geometric mean of hydraulic conductivity
L	dimension of periodic unit cell
m_0	zeroth spatial moment
$\mathbf{m_x}$	vector of first spatial moments
$\mathbf{M_{x\otimes x}}$	matrix of second spatial moments
Pe	Péclet number
$\mathbf{q}$	specific discharge vector
R	stream-tube radius
$\mathbf{S}_{\mathbf{v}'_0\otimes\mathbf{v}'_0}$	power spectrum of velocity fluctuations
$S_{Y'Y'}$	power spectrum of log-conductivity fluctuation
S_0	specific storage coefficient
$\mathbf{s}$	vector of spatial frequencies
s	Laplace variable
T	reversal time
t	time
t_s	setting time
t_{sh}	shrinking time

u	particle velocity
$\mathbf{v}$	Eulerian velocity vector
W_0	source/sink term
w	normal score transforms of u
$\mathbf{x}$	vector of spatial coordinates
Y	normal logarithm of K, equals $\ln K$
Δd	numerical grid spacing
$\mathcal{E}$	inverse Péclet number
θ	effective porosity
λ_h	horizontal correlation length, equals I_Y
λ_v	vertical correlation length
μ_τ	first temporal moment
σ_v^2	Eulerian velocity variance
σ_Y^2	variance of $\ln K$
σ_τ^2	second temporal moment
τ_a	advection time
τ_D	diffusion time
τ_m	mean escape time
χ	tortuosity
ψ	escape-time distribution
ω^2	Cramér-von Mises criterion

Statement of Contributions

This thesis is based on two co-authored manuscripts. For both manuscripts I am the first author and have performed the major part of the work as indicated in the tables below.

Co-author contributions in % for Study A: Spatial Markov Model of Advective-Diffusive Transport in Heterogeneous Domains.

#	Author	Scientific ideas	Data generation	Analysis & interpretation	Paper writing
1	Marie-Madeleine Stettler	60	90	70	70
2	Marco Dentz	20	10	15	15
3	Olaf A. Cirpka	20	0	15	15

Status in publication process: Published (Stettler et al., 2026)

Co-author contributions in % for Study B: Linear Stochastic Analysis of the Partial Reversibility of Ensemble and Effective Dispersion in Heterogeneous Porous Media.

#	Author	Scientific ideas	Data generation	Analysis & interpretation	Paper writing
1	Marie-Madeleine Stettler	60	100	70	70
2	Marco Dentz	20	0	15	10
3	Olaf A. Cirpka	20	0	15	20

Status in publication process: Published (Stettler et al., 2023)

To ensure uniformity and to avoid repetitions, the manuscripts have been altered in the following way compared to the published versions:

The introductions of Study A and Study B have been shortened and some elements have been moved to the general introduction (Chapter 1). Section 2.1 and Section 2.2 have been extracted from Study B in large parts. The introduction of the covariance function in Section 2.1 has been extracted from Study A. The corresponding parts in the main manuscript chapters (Chapters 3 & 4) have been shortened accordingly. The design of the figures in Chapter 4 has been slightly adjusted to fit the format of this thesis. Few variable symbols have been changed to ensure consistency between the chapters.

Chapter 1

General Introduction

1.1 Importance of Solute Transport and Mixing in Groundwater

Groundwater is a resource of paramount importance for human life and is becoming more and more threatened by depletion and pollution (Kuang et al., 2024). It accounts for about 40% of global irrigation demands (Siebert et al., 2010) and the fraction of drinking water extracted from the subsurface is as high as 50% globally (Smith et al., 2016) and higher than 70% in Germany (Bannick et al., 2008). Groundwater storage quantity suffers from increased water demands for irrigation caused by climate change (Aeschbach-Hertig and Gleeson, 2012), while groundwater quality is threatened by pollution from a multitude of uses, including agriculture, industrial facilities and gasoline infrastructure (Foster and Bjerre, 2023; Santucci et al., 2018; Hilpert et al., 2015). Because groundwater is of such vital importance and faced with such substantial threats, it is of utmost importance to protect and remediate it, for which it is necessary to understand solute transport, which may be separated into the movement with mean flow, denoted advection, and variation about the mean movement, called dispersion. Investigating dispersion is the broad scope of this thesis.

In heterogeneous porous media like aquifers, there are two contributions to dispersion: advective spreading, which is the distortion of the plume due to the nonuniform flow field, and diffusive mixing, which is the dilution of the plume by Brownian motion (e.g., Dentz et al., 2011). Advectively, solutes are transported with the moving water parcels and diffusively, within and between water parcels. Spreading is deterministically caused by the geometry of the porous medium and the distribution of hydraulic conductivity. It leads to an increase of the plume surface while the plume volume remains constant. By contrast, mixing increases the volume over which the plume is distributed, implying a reduction of concentration in the plume center (Kapoor and Kitanidis, 1996; Dentz et al., 2023). The two processes are closely related. The efficiency of mixing is dramatically enhanced by advective spreading which (i) increases the surface area over which diffusive exchange can occur (Weeks and Sposito, 1998) and (ii) decreases diffusion distances due to compaction of fluid elements perpendicular to their stretching direction (Le Borgne et al., 2013). Conversely, transverse mixing leads to a more efficient sampling of different velocities and thus limits spreading (Andričević, 1998). Complex interactions between several parameters, including plume age, aquifer heterogeneity, and diffusion strength, influence the plume behavior under transport and, as a general rule, mixing becomes increasingly important with increasing travel time (Fiori et al., 2002; Tonina and Bellin, 2008). In sum, while advective spreading changes the spatial distribution of

solutes in the subsurface and usually is the much more efficient transport mechanism over large distances, diffusive mixing changes the quality of the solute-bearing groundwater - negatively when it leads to contamination of previously clean water (Ding et al., 2022), but also positively when it facilitates groundwater remediation via mixing-limited reactions (Piscopo et al., 2013). Since spreading and mixing are so strongly interconnected and mixing is both an amplifier of and a possible solution to pollution, it is very relevant to understand and quantify the processes' impact on solute transport in groundwater as well as their interplay, which are the overarching objectives of this thesis.

1.2 Relevant Concepts for Transport in Groundwater

Uncertainty in the Subsurface A ubiquitous issue for transport prediction and modeling in natural systems is the limited accessibility to the subsurface. It is impossible to know the aquifer structure and thus the heterogeneous flow field in full detail. Since field methods allow either for exact information about the subsurface at only specific places like boreholes, trenches or outcrops (Lowe and Zaccheo, 1991; Kruse et al., 2018) or for spatially expanded information via indirect measurements like geophysical investigation and hydraulic well tests (Maliva, 2016), one always has to rely on assumptions when describing the three-dimensional subsurface. One way to address the issue is by performing physical experiments in controlled settings, where the artificial sediment structure is fully known or by conducting numerical experiments in synthetic aquifers (Close et al., 2008; Larocque et al., 2009). A more versatile and widely applicable approach is to treat the uncertainty as a stochastic problem, which shifts the goal from knowing the exact distribution of heterogeneity to making statements about its statistical properties. A multitude of methods follows this approach. Two classical approaches are numerical Monte-Carlo simulations and stochastic small-perturbation theory.

In the Monte-Carlo approach, an ensemble of possible random field realizations given the statistical parameters is generated. The flow and transport problem is solved numerically for each individual realization, then the initial uncertainty is accounted for by averaging over the ensemble of realizations (e.g., Lu and Zhang, 2003; Pasetto et al., 2014). The advantage of Monte-Carlo simulations is that they are not restricted to small variances of log-conductivity and simple geometries. The disadvantage is that the computational effort is high, and a prediction of transport characteristics from geostatistical parameters without performing simulations is not possible. As Monte-Carlo simulations converge to the exact statistical distribution of the uncertain variables of interest in the limit of an infinite number of realizations, they often serve as ground truth for parameterizations that do not resolve the heterogeneity explicitly.

Stochastic small-perturbation theory treats the transport properties of an aquifer as random, typically second-order stationary space variables of given statistical properties (e.g., Dagan, 1989; Gelhar, 1993; Zhang, 2002; Rubin, 2003). Each variable is expressed by the sum of its deterministic mean and the random auto-correlated perturbations about it. The groundwater-flow and transport equations are then simplified by linearization, implying that only perturbations of first order with respect to the standard deviation of log-conductivity are considered (Yeh, 1992; Dagan, 2002). The objective of small-perturbation theory is to predict the statistical properties of dependent quantities from statistical properties of the formation and mean forcings. Its advantage is that it provides closed-form predictions of

solute behavior for given geostatistical properties of the log-conductivity field and given forcing. The disadvantage is that the approach is restricted to cases of mild heterogeneity and comparably simple overall settings, such as a uniform mean hydraulic gradient.

Spatial and Temporal Moments The uncertainty about the subsurface and the deduced flow field is transferred onto the shape and position of plumes in groundwater. Therefore, it is convenient to characterize plumes by their statistical moments, rather than aiming to describe their exact shape. Spatial and temporal moments give information about the spatial distribution of a plume at given times and about the distribution of arrival times at given locations, respectively (Dagan, 1987; Harvey and Gorelick, 1995). The zeroth, first, and second central spatial moments give information about the total mass of the plume, the position of its center of mass, and the spread around it, respectively. Spatial moments characterize the full plume and are robust to heterogeneity. However, a high measurement effort is required to capture data about the full extent of a plume. The zeroth, first, and second central temporal moments give information about the mass recovered at the observation point and the mean and the variance of arrival times, so they describe the shape of breakthrough curves (BTC) rather than the shape of a plume. Temporal moments represent a point measurement and are therefore in danger of not being representative for the full plume. However, they are very useful for long-term observations and require less measurement infrastructure than spatial moments (Rubin and Ezzedine, 1997).

Dispersion coefficients, the Advection-Dispersion Equation and Macrodispersion Additionally to moments, dispersion coefficients are a common metric to quantify dispersion. The assumption behind dispersion coefficients is that when flow is averaged over a large enough reference volume or after long enough travel times, dispersion processes can mathematically be treated as a Gaussian process just like diffusion. This means dispersive mass transfer is assumed to follow Fick's first law and thus to be proportional to the mean concentration gradient with the dispersion tensor $\mathbf{D}$ $[L^2T^{-1}]$ as the proportionality constant (Ferrara et al., 1999). This concept is a powerful tool for upscaling flow and transport as it spares describing flow through single pores at the Darcy scale and knowing the exact distribution of heterogeneity at the field scale. In the latter case, $\mathbf{D}$ is typically called macrodispersion tensor and it is related to second central moments as half their rate of change (Kitanidis, 1988). In this framework, solute transport is mathematically described with the advection-dispersion equation (ADE) (Bear, 1972):

$$\frac{\partial c}{\partial t} + \mathbf{v} \cdot \nabla c - \mathbf{D}\nabla^2 c = 0, \tag{1.1}$$

in which c and t denote concentration and time, respectively, and $\mathbf{v}$ is the velocity vector.

Applying classical macrodispersion, a solute plume undergoing advection with the mean velocity and dispersion by the macrodispersion tensor matches the moments of the ensemble-averaged concentration in the heterogeneous domain. Closed-form expressions for the second central spatial moments of the ensemble-averaged concentration were derived using Eulerian (e.g., Gelhar and Axness, 1983), Lagrangian (e.g., Dagan, 1984; Dagan, 1988; Dagan and Fiori, 1997), and Eulerian-Lagrangian approaches (e.g., Neuman et al., 1987). Shapiro and Cvetkovic

(1988) and Dagan et al. (1992) derived expressions for temporal-moment based equivalents.

Ensemble and Effective Dispersion I consider so-called ensemble and effective moments and dispersion coefficients as they give different information about the dispersive behavior of a plume. The two types of dispersion differ in the order of operations, namely taking moments and ensemble averaging. Ensemble moments are calculated as the variance of a concentration field averaged over many ensemble members, differing in their specifics but sharing statistical properties. By contrast, effective moments are calculated as the ensemble average of the second central moments in space or time of individual plumes (Attinger et al., 1999). Hence, ensemble moments contain information about an average plume and display the combined effect of average spreading and mixing, with mixing typically contributing only a small part of the total variance. Ensemble dispersion quantifies the net effect of dispersion, which is of interest in risk assessment of groundwater contamination (Li, 2007). Effective moments are more representative for the behavior of a single plume because they do not contain information about the uncertainty of the position of the center of mass, and are considered a more suitable metric of mixing than ensemble moments (Cirpka and Kitanidis, 2000; Benson et al., 2019).

The differences between ensemble and effective dispersion are the biggest for point injections and vanish in the limit of an infinite original plume size. Dentz et al. (2000) and Fiori and Dagan (2000) derived closed-form expressions for effective dispersion of a plume originating from a point injection in uniform-in-the-average velocity fields by linear Eulerian and Lagrangian analyses, respectively. Without local dispersion, the point-related effective dispersion is zero, and the ensemble dispersion can exclusively be related to the uncertainty of tagging the plume that remains a Dirac pulse at all times. When adding local dispersion, a point plume in a single realization experiences only pore-scale dispersion at early times, which slowly expands the plume so that it starts to be affected by velocity variations within the plume, leading to an acceleration of effective dispersion. At very late times, effective dispersion coefficients asymptotically reach the same values as ensemble dispersion coefficients.

Flow reversal and partial reversibility of dispersion Subjecting a plume to flow reversal and examining how its dispersion reacts to it is an important concept to investigate the respective influence of spreading and mixing on dispersion. The underlying idea is to exploit the differences in the behavior of spreading and mixing under reversed flow (cf. Gouze et al., 2008). For illustration, consider a thought experiment, where the processes act completely independently. A plume is transported forward until a certain time T, at which the velocity field is instantaneously inverted, and the plume is then transported backward over the same time span. Then, pure advective spreading is fully reversible. That is, upon reversal of the flow field, the plume exactly regains its initial spatial distribution, because the velocity variability is deterministic, albeit in most cases not known in full resolution. Conversely, pure mixing, prevalent for example in a set-up where the velocity is perfectly uniform, is completely irreversible as diffusion is a random process independent of the direction of flow. Upon flow reversal, the plume continues expanding by diffusion. Because in natural porous media spatially variable advection and diffusive mixing interact, dispersion is a partially reversible process. The spreading of the plume is partially reversed but the concentration distribution is more spread out than in the

initial state after equally long forward and backward motion than in the initial state (cf. Figure 4.1). Investigating transport under flow reversal is relevant for applications such as push-pull tests (Istok, 2013), subsurface storage (Zivar et al., 2021), and understanding tidally influenced aquifers (Pool et al., 2014).

1.3 A Brief Overview of Transport and Mixing Research

The classical description of solute transport with the advection-dispersion equation 1.1 as introduced above relies on assumptions whose validity is challenged. Studies from the field, Darcy and pore scale show that the use of a volume-averaged dispersion coefficient fitted from conservative transport experiments with the ADE overestimates mixing (Molz and Widdowson, 1988; Gramling et al., 2002; de Anna et al., 2014). In other cases, the ADE fails to represent conservative transport correctly altogether, because the transport is non-Fickian (e.g., Feehley et al., 2000; Moroni et al., 2007). This reveals two issues: First, real mixing processes are not represented properly by the scale-dependent dispersion coefficient, which grows much stronger with travel distance and time than the impact of diffusion processes (Cherry, 2023). Second, the ADE approach relies on averaging and homogenization in order to approximate Gaussian transport which is not reflected in many transport systems (Bolster et al., 2019). By averaging over the pore space, pore-scale effects which can influence the large-scale behavior are neglected (Berkowitz et al., 2006). At the other end of the scale, in field-scale transport it is almost impossible to find large enough volumes and long enough travel times to reach the so called asymptotic transport regime where dispersion through heterogeneous domains can truly be described with macrodispersion coefficients (Molz, 2015). Contrarily, heterogeneity is so relevant at all scales that the assumption that dispersion can be described diffusion-like as a Gaussian process with a constant coefficient rarely holds and the ADE is not applicable for the many cases of non-Fickian transport (Neuman and Tartakovsky, 2009).

Nevertheless, the ADE has many positive properties like its easy applicability and its flexible use in numerical implementations as well as analytical solutions. By using a time-dependent (macro)dispersion coefficient, the criticism of its scale-dependency is alleviated. Additionally, Jose and Cirpka (2004) argue that for most field applications initially incomplete pore-scale mixing is of little consequence because over the considered distances and travel times diffusion becomes strong enough to homogenize the solute distribution in the pore space.

However, it is beneficial to complement ADE-based approaches with other lines of research with a more explicit focus on mixing and the ability to represent non-Fickian transport. In the following, a selection of alternative approaches is presented.

Dilution Index The dilution index is based on the idea that by diffusion, the volume of a conservative solute plume can only ever increase. A decrease is impossible altogether, and in the limit of complete absence of diffusion the volume remains constant. Kitanidis (1994) introduced the dilution index as a metric of solute mixing based on the concept of information entropy. Increased dilution of a plume increases the entropy of the concentration distribution (interpreted as a spatial probability density function of particle locations), which is reflected in an increase in the dilution index, calculated as the exponential of the Shannon entropy. The reactor ratio is the dilution index normalized with an adequate theoretical maximum. In

the case of a batch reactor, the maximum dilution is achieved by a uniform solute distribution. In the case of a plume at the field scale in an infinite domain, maximum dilution corresponds to a Gaussian plume having the same zeroth to second central moments as the actual plume. The original dilution index was developed for evaluation of a constant mass. Rolle et al. (2009) developed the flux-related dilution index which is applicable for cases with a continuous injection and describes how a solute is distributed across a section normal to the flux, rather than how the solute is distributed across a given volume. In reactive transport, in contrast to conservative compounds, the volume occupied by a solute can indeed shrink, when it is transformed or consumed by a reaction. Thus, Chiogna et al. (2012) used the evolution of the dilution index in reactive transport to distinguish between regimes where diffusive dilution (dilution index increases) or reactive consumption are the dominant processes (dilution index decreases).

Multirate mass transfer models Coined by Haggerty and Gorelick (1995), Multirate Mass Transfer (MRMT) models are an upscaling approach for solute transport, in which not an exact or stochastic spatial representation of the aquifer geometry and heterogeneity is the goal, but the correct quantification of slow and fast exchange rates between a mobile zone and one or multiple immobile zones. All types of aquifer heterogeneity are represented by introducing the necessary number of mass-transfer rate coefficients which are coupled to the ADE for transport. The difficulty with MRMT models is to define or estimate the right number and values of exchange coefficients (Molz, 2015; Andrés et al., 2025). There exist advanced MRMT applications to modeling of two-phase flow in highly heterogeneous fracture networks (Tecklenburg et al., 2016) and to flow under transient conditions with rate coefficients as function of the flow velocity (Guo et al., 2020), for example.

Stream-Tube Approach In the advective-dispersive stream-tube approach of Cirpka and Kitanidis (2000), the longitudinal effective dispersion coefficient related to a point injection is used to parameterize mixing in effective models of mixing-controlled reactive transport in heterogeneous systems. The approach is based on calculating temporal moments of local breakthrough curves to assess mixing, as opposed to using averaged breakthrough curves for ensemble dispersion. The idea is, that the effects on the concentration that dilution and the variability in arrival time at different positions have, are blended in a volume-averaged BTC, whereas in a point measurement only the effect of dilution is observed. Along these lines, Vanderborght and Vereecken (2002) developed perturbation-theory expressions for effective and ensemble dispersivities and Jose et al. (2004) performed large-scale sandbox tracer experiments with point measurements, allowing for calculation of ensemble and effective dispersion coefficients. In a similar fashion, by following the evolution of point sources in space rather than observing solute arrival at one point, Cirpka (2002), Perez et al. (2019) and Perez et al. (2020) quantify reactive mixing by means of effective dispersion coefficients in flow at the Darcy scale, in a single channel and at the pore-scale, respectively.

Continuous Time Random Walk Rather than averaging over heterogeneities of some scales, continuous time random walk models (CTRW) aim to include the impact of heterogeneity at all scales in the transport description. CTRW are a probabilistic approach which conceptualize solute transport as random particle transitions in space and time, which are drawn from a probability distribution (Berkowitz

et al., 2006). By choosing the right shape of the probability distribution, CTRW can be applied at all scales (Rhodes et al., 2008; Raveh-Rubin et al., 2015; Gouze et al., 2023) as well as under transient (Engdahl and Aquino, 2022; Elhanati et al., 2023) and non-equilibrium conditions (Li and Ren, 2009). To obtain a predictive quality for solute transport, it is important to relate the distribution of transition times to the geostatistical properties of the medium (Akomolafe et al., 2024). This gives way to correlated CTRW which include memory of travel times reflecting velocity correlations inherent to heterogeneous porous media (Montero and Masoliver, 2007; Le Borgne et al., 2011). One type of correlated CTRW are Spatial Markov Models (SMM) (Le Borgne et al., 2008b; Le Borgne et al., 2008a). The key idea is that the spatial transitions of CTRW are deterministic, from one observation plane to the next, whereas the transition times are stochastic. They are derived from velocity statistics that are correlated from one transition to the next. As only correlation to the last transition is considered, the scheme is a first-order Markov process. (Sherman et al., 2021). Time-domain random walk (e.g., Cvetkovic et al., 2014) also considers sequences of travel times over fixed spatial transitions, albeit in most applications neglecting correlations between consecutive random jumps.

Lamellar Mixing Model Lamellar mixing models describe solute transport and mixing by looking at the stretching and folding of individual tracer filaments in 2-D or tracer sheets in 3-D. They have been developed for transport on both the Darcy and the pore scale and they are able to capture the full development from pre-asymptotic to asymptotic regimes for any heterogeneity and diffusion strength (Le Borgne et al., 2013; Le Borgne et al., 2015; Lester et al., 2016). Initially, individual lamellae are stretched in the mean direction of flow. As dictated by mass conservation, stretching demands compression in the direction normal to the mean flow. This steepens concentration gradients and thus enhances diffusive mixing. At later stages, when diffusion becomes more powerful than compression, individual lamellae coalesce and build aggregates. The lamellar mixing model has been successfully applied to reactive transport applications (e.g., Bandopadhyay et al., 2017; Yoon et al., 2021).

1.4 Research Objectives

As is obvious from the abundance of concepts and approaches presented above (which nota bene represent only a selection), quantifying dispersion and mixing is a diverse and engaging area of research. The ultimate aspiration would be to find a unified theory for both large-scale transport and spreading and local-scale mixing. In the mean time, it is worthwhile to pursue many different paths and advance the knowledge in increments. In general, there is an increasing complexity in quantifying and understanding ensemble dispersion over effective dispersion to actual mixing. I will follow this order of complexity in how I approach the topic with my research avenues about transport in heterogeneous porous media.

Figure 1.1 depicts the most important processes and concepts covered in this thesis. It shows how a solute plume in the subsurface undergoing transport is reshaped by advective spreading while it is simultaneously diluted by diffusive mixing acting over its enlarged surface area. The distinction between ensemble and effective dispersion is illustrated by the different plume widths they represent. Ensemble dispersion covers the maximum extent of the plume, from its rearmost to its foremost

point, including the spread resulting primarily from velocity contrasts. Effective dispersion covers the local extent of the plume, measuring its width locally along the direction of flow. In the figure, effective dispersion is indicated only at one position. In fact, it would have to be given by the average local width over the full height of the plume.

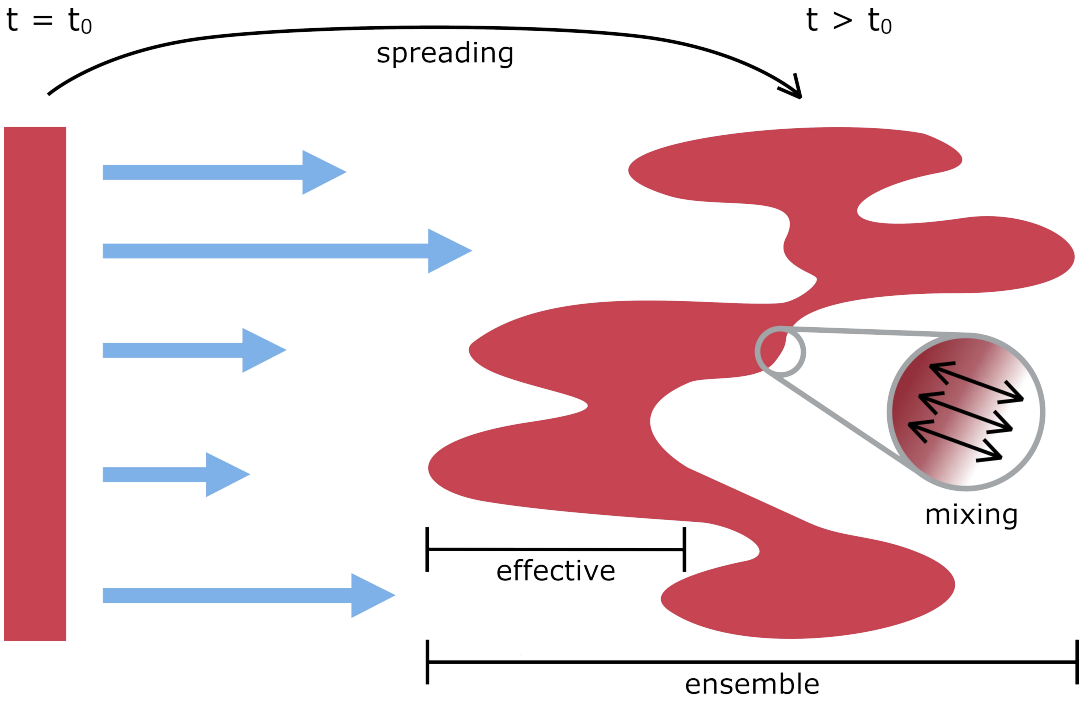

FIGURE 1.1: Concept figure illustrating advective spreading and diffusive mixing, as well as ensemble and effective dispersion. Blue arrows signify groundwater flowing at different velocities, the initial plume and the solute plume deformed by dispersion are depicted in red.

The overarching research questions of this thesis are the following:

- How does diffusion strength influence breakthrough curves, ensemble and effective moments and the degree of reversibility of dispersion?
- Are effective moments under flow reversal an adequate measure of mixing?
- How can flow reversal contribute to understanding the interplay between mixing and spreading?

To investigate these questions, I apply and advance two different methods. Study A examines the effect of diffusion strength and field heterogeneity on breakthrough curves in unidirectional flow by means of temporal moments of ensemble concentrations. To do so, a Spatial Markov Model with a velocity transition probability distribution inferred from properties of the porous medium is developed which allows for loss of correlation by diffusive exchange. Study B investigates the influence of flow reversal on the reversibility of dispersion under different conditions and evaluates how much information about mixing can be extracted from spatial ensemble and effective moments. Linear small-perturbation theory is applied to look into these topics. For both studies, I adapt numerical schemes to my requirements in order to use them as a synthetic reality and compare the results of the theoretical approaches to them.

1.5 Outline

Following the general introduction to the topic, its motivation and the research objectives presented in this chapter, the general theory and methods are provided in Chapter 2, which includes the governing equations for flow and transport and the numerical methods used to create the synthetic fields and simulate transport. Chapters 3 and 4 treat Study A and Study B, applying methods of Spatial Markov Models and linear stochastic theory, respectively. Finally, Chapter 5 summarizes and compounds the major findings of each study and opens possible further research directions adding on to the work of this thesis.

Chapter 2

Theory & Methods

In the following, the general theory and methods applicable to both Study A and Study B are introduced.

2.1 Governing Equations for Flow and Transport

3-D transient groundwater flow is described by the groundwater flow equation (Bear, 1972):

$$S_0 \frac{\partial h}{\partial t} - \nabla \cdot (K \nabla h) = W_0, \tag{2.1}$$

subject to initial and boundary conditions. Here $h(\mathbf{x}, t)$ $[L]$ is the hydraulic-head field depending on the spatial coordinates $\mathbf{x}$ $[L]$ and time t $[T]$, $K(\mathbf{x})$ $[LT^{-1}]$denotes the hydraulic conductivity, S_0 $[L^{-1}]$ is the specific storage, and W_0 $[T^{-1}]$ is an internal volumetric source/sink term. In the following, we assume incompressibility and neglect internal volumetric sources and the storage properties of an aquifer, resulting in steady-state flow:

$$\nabla \cdot (K \nabla h) = 0. \tag{2.2}$$

Under these conditions, groundwater flow through the medium can be described by Darcy's law:

$$\mathbf{q}(\mathbf{x}) = -K(\mathbf{x}) \nabla h(\mathbf{x}), \tag{2.3}$$

in which $\mathbf{q}(\mathbf{x})$ is the specific discharge vector $[LT^{-1}]$ which is related to the velocity vector $\mathbf{v}$ via the effective porosity θ, assumed spatially uniform, by:

$$\mathbf{v}(\mathbf{x}) = \frac{\mathbf{q}(\mathbf{x})}{\theta}. \tag{2.4}$$

Solute transport can be expressed with the advection-diffusion/dispersion equation (Bear, 1972):

$$\frac{\partial c}{\partial t} + \mathbf{v} \cdot \nabla c - \mathbf{D} \nabla^2 c = 0, \tag{2.5}$$

in which c denotes concentration $[ML^{-3}]$, and D denotes the diffusion-dispersion tensor $[L^2T^{-1}]$. In the present applications, $\mathbf{D}$ is simplified to be spatially uniform and isotropic, rendering it a scalar coefficient D.

We consider three-dimensional heterogeneous log-normally distributed hydraulic-conductivity fields, which are characterized by the geometric mean K_g, the variance σ_Y^2 of the log-hydraulic conductivity $\ln K(\mathbf{x})$ and an exponential

correlation structure with integral scale I_Y. The corresponding stationary covariance function $C(\mathbf{d})$ reads as:

$$C(\mathbf{d}) = \sigma_Y^2 \exp\left(\frac{\|\mathbf{d}\|_2}{I_Y}\right), \tag{2.6}$$

with the distance vector of coordinates $\mathbf{d}$ $[L]$ and its length $\|\mathbf{d}\|_2$ $[L]$. For exponential covariance functions, the integral scale I_Y and the correlation length λ are identical and can be used interchangeably.

The relative strength of advective and diffusive-dispersive transport processes are measured by the dimensionless Péclet number Pe, which gives the ratio between characteristic diffusion-dispersion and advection times, τ_D and τ_a respectively, over a characteristic length scale l (Fetter et al., 2017):

$$Pe = \frac{\tau_D}{\tau_a} = \frac{lv}{D}. \tag{2.7}$$

The characteristic length scale l has to be chosen appropriately for the considered system and the problem at hand (Huysmans and Dassargues, 2005). For the present applications, it is convenient to define Pe over a correlation length of the heterogeneous medium.

2.2 Numerical Simulations of Flow and Transport

The general procedure for the numerical simulations follows the approach of Hansen et al. (2018) and consists of creating Monte-Carlo simulations of random log-conductivity fields, calculating the corresponding head and velocity fields, and performing particle-tracking random-walk on the velocity fields. From the resulting distributions of particle displacements and arrival times, spatial and temporal moments are calculated.

To minimize boundary effects, the numerical simulations are performed for infinite periodic domains with periodic log-conductivity fields and flow subject to periodic boundary conditions with a trend in the hydraulic head as described by Hansen et al. (2018):

$$K(\mathbf{x} + nL_i\mathbf{e}_i) = K(\mathbf{x}) \; \forall n \in \mathbb{Z}, i \in \{1,2,3\}, \tag{2.8}$$

$$h(\mathbf{x} + L_i\mathbf{e}_i) = h(\mathbf{x}) - J_i L_i, i \in \{1,2,3\}, \tag{2.9}$$

in which L_1, L_2, and L_3 $[L]$ are the dimensions of the unit cell. The hydraulic gradient $\mathbf{J} = [J_1, J_2, J_3]^T$ $[-]$ is chosen such that the mean velocity is strictly oriented into direction x_1. Because the hydraulic-head and conductivity fields are periodic, the velocity fields are also periodic:

$$\mathbf{v}(\mathbf{x} + nL_i\mathbf{e}_i) = \mathbf{v}(\mathbf{x}) \; \forall n \in \mathbb{Z}, i \in \{1,2,3\}. \tag{2.10}$$

For the covariance function $C(\mathbf{d})$ of log-hydraulic conductivity, we choose the exponential model, adapted for periodicity:

$$C(\mathbf{d}) = \sigma_Y^2 \exp\left(-\sqrt{\left(\frac{\min(d_1, L_1\text{-}d_1)}{\lambda_h}\right)^2 + \left(\frac{\min(d_2, L_2\text{-}d_2)}{\lambda_h}\right)^2 + \left(\frac{\min(d_3, L_3\text{-}d_3)}{\lambda_v}\right)^2}\right), \tag{2.11}$$

in which λ_h and λ_v are the correlation lengths in horizontal and vertical direction, respectively. Because we analyze all properties in dimensionless terms, λ_h is chosen as unity and all velocities are normalized by the mean velocity before simulating solute transport, which means that arbitrary values can be assigned to the geometric mean of the hydraulic conductivity K_g and to the effective porosity θ.

For the particle-tracking random-walk simulations, the semi-analytical method of Pollock (1988), which effectuates particle transport along streamlines, is parallelized on the graphics processing units (GPU) (see Hansen et al., 2018).

In its standard configuration, the periodic unit cell has an isotropic covariance function and is discretized into $400 \times 200 \times 200$ cells of a uniform spatial resolution of $\Delta d = 0.1\lambda_h$, yielding dimensions of $L_1 = 40\lambda_h$, and $L_2 = L_3 = 20\lambda_h$.

Chapter 3

Spatial Markov Model of Advective-Diffusive Transport in Heterogeneous Domains

3.1 Introduction

A typical question in applied hydrogeology is: When does a compound introduced into the subsurface reach a receiver of interest? Also, groundwater age has been associated to the chemical status and is thus used as proxy for water quality (Sprenger et al., 2019). Therefore, investigating breakthrough curves in observation planes and their temporal moments is an approach relevant to application.

As stated before, solute transport is strongly influenced by the heterogeneity of the subsurface. A direct way to assess the effects of heterogeneity in a stochastic manner is given by numerical Monte-Carlo simulations. As examples for BTC applications, Gotovac et al. (2009) evaluated purely advective travel-time statistics in a Lagrangian framework performing two-dimensional Monte-Carlo simulations of transport in highly heterogeneous synthetic fields of isotropic multi-Gaussian correlation structure, Srzic et al. (2013) performed numerical transport simulations in highly heterogeneous fields with distinct connectivity structures to calculate concentration moments and uncertainty at different distances under both diffusion- and advection-dominated transport conditions, and Hansen et al. (2018) derived an empirical relationship between temporal moments and the geostatistical properties of heterogeneous porous media by performing a regression on results of Monte-Carlo transport simulations in isotropic multi-Gaussian fields.

An alternative stochastic approach is to apply small-perturbation theory. Shapiro and Cvetkovic (1988) applied small-perturbation theory to derive first and second central moments of travel times registered at observation planes for purely advective transport. Vanderborght and Vereecken (2002) expanded the theory to advective-diffusive transport by modeling local and flux-averaged dispersion from BTC measured in a natural-gradient tracer test in a fluvial aquifer. As a final example, Fernàndez-Garcia et al. (2005) found that temporal moments of breakthrough curves in a three-dimensional heterogeneous, anisotropic sandbox experiment were in good agreement with predictions by linear stochastic theory.

Continuous Time Random Walk models are an efficient and versatile alternative to the approaches mentioned above because (i) other than small-perturbation based approaches they are not limited to small variances of log-velocity, (ii) they require little knowledge about the medium geometry and are thus computationally efficient, and (iii) they do not assume that the effective transport equation resembles advective-diffusive transport, which enables them to capture anomalous transport

(Berkowitz et al., 2006; Sherman et al., 2021). CTRW approaches allow modeling non-Fickian transport in a variety of environments, including fractured rock (Mettier et al., 2006; Kang et al., 2011; Hyman and Dentz, 2021), karst aquifers (Goeppert et al., 2020), and porous media at the continuum (Le Borgne et al., 2008b; Fiori et al., 2015; Comolli et al., 2019), and pore scale (Morales et al., 2017; Dentz et al., 2018b; Puyguiraud et al., 2019). In the following, we focus on Spatial Markov Models, which can be seen as a CTRW with spatially correlated particle velocities or particle transit times.

When Le Borgne et al. (2008b) and Le Borgne et al. (2008a) introduced the concept of SMM, they used numerical transition matrices of particle velocities created from two-dimensional particle-tracking random-walk (PTRW) calculations and demonstrated that the simple first-order Markov model can predict mean transport properties. Some of the many SMM applications include pore-scale modeling of transport in a sandstone (Kang et al., 2014) and modeling the BTC of laboratory column tests (Sherman et al., 2018) and pumping tests in fractured aquifers (Kang et al., 2015), demonstrating the method's versatility.

Dentz et al. (2016) and Morales et al. (2017) provided analytical frameworks to model transitions of particle velocities. Based on the fact that the Lagrangian velocity distribution is identical to the flux-weighted Eulerian velocity distribution, Dentz et al. (2016) parameterized transport in the SMM framework making use of properties of the Eulerian velocity field only. Morales et al. (2017) reproduced experimental data showing intermittent and non-Fickian behavior based on bivariate log-normal distributions of consecutive particle velocities. These two analytical SMM have been applied for upscaling of purely advective anomalous transport in highly heterogeneous porous media (Comolli et al., 2019; Puyguiraud et al., 2019) and in fracture networks (Hyman and Dentz, 2021). Cirpka et al. (2022) developed a purely advective SMM based on velocity and slowness statistics derived from statistics of the hydraulic conductivity field, assuming that the distributions of all named properties are log-normal. These authors derived analytical expressions for ensemble dispersion based on travel-time statistics.

The approaches listed above neglect diffusion and local dispersion. In a review of SMM, Sherman et al. (2021) also identified a lack of mixing applications. Existing SMM for transport with finite finite Péclet number are based on transition matrices determined by numerical transport simulations (e.g., Le Borgne et al., 2011; Bolster et al., 2014; Sund et al., 2017b; Sherman et al., 2018) and most existing work with an explicit focus on mixing is based on velocity distributions from small-scale simulations with no process-based implementation of diffusion (Sund et al., 2017a; Wright et al., 2019; Wright et al., 2021). An exception is the study by Aquino and Le Borgne (2021) who developed an analytical mechanistic model incorporating advection as velocity transitions in longitudinal direction and diffusion in transverse direction based on a velocity-dependent shear rate. However, the latter authors did not apply their model to realistic heterogeneous velocity fields.

In summary, analytically derived SMM have so far been limited to purely advective transport, and SMM for finite Péclet numbers have taken the transition matrices for travel-time increments from numerical simulations of multi-dimensional flow-and-transport simulations. The objective of this study is thus to develop a process-based diffusion implementation in SMM and limit the use of empirical data for finite Péclet transport within the framework. However, this study is restricted to the BTC and their moments of the ensemble concentration, which may be interpreted as the BTC averaged over a very wide observation plane for injection also over a very wide

plane. These breakthrough curves are affected by diffusion (studied here), but do not address solute mixing relevant for chemical reactions.

In the following sections, we establish the governing equations for flow and transport and describe our PTRW simulations which we perform to validate our proposed SMM. We then introduce a purely advective SMM which we base on the work of Comolli et al. (2019) and Cirpka et al. (2022). Next, to account for diffusion, we introduce the option for particles to leave their current advective trajectory by transverse diffusion. The proposed diffusion algorithm is based on comparing the advection time over a spatial increment to the diffusion time over a characteristic radius for each particle and velocity transition. If the advection time is shorter than the diffusion time, the particle remains on its current advective trajectory and the next velocity is drawn from the distribution conditioned on the preceding velocity. If the advection time is longer than the diffusion time, the particle diffuses onto a different trajectory and the next velocity is drawn from the marginal distribution. Finally, we show that our results are in good agreement with numerical simulations of ensemble dispersion in second-order heterogeneous log-conductivity fields with stationary, isotropic exponential correlation structure.

3.2 Flow and Transport in Three-Dimensional Heterogeneous Porous Media

3.2.1 Governing Equations

Flow and transport through three-dimensional heterogeneous log-normally distributed hydraulic-conductivity fields $K(\mathbf{x})$ of an exponential correlation structure are described as given in Section 2.1.

In the SMM framework, it is convenient to use the Langevin equation as a particle-oriented equivalent to the ADE (equation 2.5) (Risken, 1996):

$$\frac{d\mathbf{x}(t)}{dt} = \mathbf{v}(\mathbf{x}(t)) + \sqrt{2D}\xi(t), \tag{3.1}$$

where $\xi(t)$ is Gaussian white noise with zero mean and a covariance of $\langle \xi(t)\,\xi(t')\rangle = \delta(t-t')$. The angular brackets denote the average over all noise realizations.

Here, we define the Péclet number (equation 2.7) as:

$$Pe = \frac{I_Y \overline{v}_1}{D}, \tag{3.2}$$

where the overline denotes averaging.

3.2.2 Ground-Truth Numerical Simulations in 3-D

We perform PTRW simulations in a periodic three-dimensional heterogeneous porous medium to test the validity of the advective-diffusive SMM introduced in Section 3.3. The periodic unit cell as described in Section 2.2 is calculated based on an isotropic exponential covariance function. 4×10^6 particles are injected across evenly spaced injection planes across the domain in 50 realizations of the conductivity fields for each value of σ_Y^2 considered in combination with each value of Pe.

After each advection step, random walk is implemented by displacing the particle in the x_2- and x_3-directions of the coordinate system by a random increment

drawn from a normal distribution with zero mean and variance of $2D\Delta t$ with Δt the advective travel time. To minimize the number of particles crossing the same observation plane several times and to ensure particle arrival at the exact position of the observation planes, diffusion in the x_1-direction of mean flow is disabled. Since the effect of said diffusion on longitudinal macrodispersion has been shown to be negligible (Fiori, 1996), we choose this approximation over techniques relying on interpolation. We limit Δt to a maximum value of $\frac{\Delta d^2}{4D}$ in order to prevent diffusive displacements that are larger than the spatial discretization Δd for the solution of the flow equation.

We record the distribution of breakthrough times at control planes perpendicular to the mean flow direction. Breakthrough times are defined as the times of first arrivals of particles at the control planes. Since the particles are injected at different injection planes, we consider the difference between the injection and the observation plane rather than actual longitudinal coordinates for the statistical evaluation. The PTRW simulations are performed with a uniform injection (i.e. volume-weighted). A flux-weighted injection condition is simulated by weighting the particle breakthrough times at control planes by the initial particle velocities.

All simulations are performed for variances of log-hydraulic conductivity ranging between 0.1 and 5, and for Péclet number Pe of 10, 30, 100, 1000, and in the limit $Pe \to \infty$. Transport is quantified by the mean μ_τ and variance σ_τ^2 of arrival times as well as the BTC at observation planes at different travel distances.

3.2.3 Temporal Moments

Temporal moments characterize a distribution of arrival times τ at given observation points. The nth raw temporal moment of concentration μ_n $[ML^{-3}T^n]$ at a given location is defined as (e.g., Harvey and Gorelick, 1995):

$$\mu_n\left(c\left(\mathbf{x},\tau\right)\right) = \int_0^\infty \tau^n c\left(\mathbf{x},\tau\right) d\tau. \tag{3.3}$$

The zeroth temporal moment $\mu_0\left(c\left(\mathbf{x},\tau\right)\right)$ indicates the mass recovered at the observation point.

The nth central temporal moment of concentration μ_n^c $[ML^{-3}T^n]$ is defined as:

$$\mu_n^c\left(c\left(\mathbf{x},\tau\right)\right) = \int_0^\infty \left(\tau - \overline{\tau}\left(\mathbf{x}\right)\right)^n c\left(\mathbf{x},\tau\right) d\tau, \tag{3.4}$$

in which $\overline{\tau} = \mu_1\left(c\left(\mathbf{x},\tau\right)\right)/\mu_0\left(c\left(\mathbf{x},\tau\right)\right) = \mu_\tau$ is the mean breakthrough time and the second central temporal moment $\mu_2^c = \sigma_\tau^2$ denotes the variance of arrival times, which corresponds to ensemble dispersion.

Numerically, including flux-weighting by the initial particle velocity, the temporal first and second central ensemble moments are expressed as follows:

$$\mu_\tau\left(\left\langle c\left(\mathbf{x},\tau\right)\right\rangle\right) = \tfrac{1}{n_p}\Sigma_{i=1}^{n_p} w_i\left(\tau_i\left(x_1\right) - \tau_i\left(0\right)\right), \tag{3.5}$$

$$\sigma_\tau^2\left(\left\langle c\left(\mathbf{x},\tau\right)\right\rangle\right) = \tfrac{1}{n_p-1}\Sigma_{i=1}^{n_p} w_i\left(\tau_i\left(x_1\right) - \tau_i\left(0\right) - \mu_\tau\left(x_1\right)\right)^2, \tag{3.6}$$

where n_p is the number of injected particles and $w_i = v_{1,i}(t=0)/\Sigma_{i=1}^{n_p} v_1, i(t=0)$ is the weight given to each particle.

3.3 Spatial Markov Model

3.3.1 Advective Transport

In a Spatial Markov Model, the movement of a particle is conceptualized along advective trajectories, which are discretized into spatial increments between observation planes of a fixed spacing Δx in the mean direction of flow. A random velocity u, and thus a transition time $\Delta x/u$, is assigned to each spatial increment, leading to the following equations for updating the particle position and travel time (Le Borgne et al., 2008b):

$$x_{i+1} = x_i + \Delta x, \tag{3.7}$$

$$\tau_{i+1} = \tau_i + \frac{\Delta x}{u_{x_i}}. \tag{3.8}$$

The series of particle velocities $\{u_x\}$ is modeled as a stationary first-order Markov process, that is, the velocity u_x can be attained by the knowledge of only a single previous velocity $u(x')$ at $x' < x$. The distribution of the velocity $u(x)$ conditional to the velocity $u(x') = u'$ is given by $p\left(u, x|u', x'\right) \equiv p(u, x - x'|u')$. Note that the conditional distribution depends only on the increment $x - x'$ due to the stationarity assumption. For the conditional distribution $p(u, x|u')$ the Chapman-Kolmogorov equation holds (Pavliotis, 2014):

$$p\left(u, x - x'|u'\right) = \int_0^\infty p\left(u, x - x''|x''\right) p\left(u'', x'' - x'|u'\right) \mathrm{d}u'', \tag{3.9}$$

with $x' \leq x'' \leq x$. The evolution of the one-point velocity distribution $p(u, x)$ from the initial velocity distribution $p(u, x = 0) \equiv p_0(u)$ is given by:

$$p(u, x) = \int_0^\infty p\left(u, x|u'\right) p_0\left(u'\right) \mathrm{d}u'. \tag{3.10}$$

We denote the stationary velocity distribution by $p_s(u)$. For $p_0(x) = p_s(u)$, the velocity distribution $p(u, x) = p_s(u)$ remains unchanged. This initial condition holds for an injection into the flux (Demmy et al., 1999; Dentz et al., 2016). In contrast, for a volume-weighted injection, the initial velocity distribution deviates from the stationary distribution and over time the velocity distribution evolves toward it as described by equation 3.10. With these relationships, the sampling of consecutive particle velocities along an advective trajectory in the spatial Markov process is fully defined. The first velocity is drawn from the initial distribution $p_0(u)$ and from the conditional distribution $p(u, x|u')$ in all subsequent steps.

Velocity Distributions

In the following, we derive the stationary velocity distribution $p_s\left(u\right)$ based on the Eulerian velocity distribution $p_e\left(u\right)$. They could also be called flux-weighted and volume-weighted velocity distributions, respectively. We consider a flux-weighted injection of particles into a three-dimensional heterogeneous porous medium with a log-normally distributed K field defined by its uniform geometric mean K_G, uniform variance σ_Y^2, integral scale I_Y, and functional form of the stationary correlation structure of log-conductivity. Rather than following true particle paths, we use the

path projection onto the x_1-coordinate which is identical to the direction of mean flow. In this framework, the calculated trajectories are shorter than the true paths by a factor of the advective tortuosity χ (Koponen et al., 1996; Puyguiraud et al., 2019), which we treat as a scalar. Thus, we transform the full velocity vector into the tortuosity-corrected velocity in x_1-direction which we denote u:

$$u(x) = \frac{\|\mathbf{v}(\mathbf{x})\|}{\chi}. \tag{3.11}$$

By that, negative velocities are avoided and the line perspective of the SMM is accounted for. Scaling with the mean tortuosity-corrected Eulerian velocity μ_u and the integral scale of the hydraulic conductivity field leads to the dimensionless velocity, spatial coordinate and time, u_*, x_* and t_*, respectively:

$$u_* = \frac{u}{\mu_u}, \quad x_* = \frac{x}{I_Y}, \quad t_* = t\frac{\mu_u}{I_Y}. \tag{3.12}$$

In the following, all asterisks are dropped for brevity.

For moderately heterogeneous media with $\sigma_Y^2 \lesssim 1$, the Eulerian velocity distribution can be approximated by a log-normal distribution (Fiori et al., 2006; Comolli et al., 2019):

$$p_e(u) = \frac{1}{u\sqrt{2\pi\sigma^2_{\ln u}}} \exp\left[-\frac{(\ln u - \mu_{\ln u})^2}{2\sigma^2_{\ln u}}\right], \tag{3.13}$$

where $\mu_{\ln u}$ and $\sigma^2_{\ln u}$ are the mean and variance of the log-velocity $\ln u$.

According to linear stochastic theory, the variance $\sigma^2_{\ln u}$ and integral scale $I_{\ln u}$ of the Eulerian log-velocity can be related to σ_Y^2 and I_Y as (Dagan, 1989; Gelhar, 1993):

$$\sigma^2_{\ln u} = \frac{8}{15}\sigma_Y^2, \qquad I_{\ln u} = \frac{15}{8} I_Y. \tag{3.14}$$

Using the general relationship between statistical properties of a pair of corresponding normal and log-normal distributions (e.g., Zerovnik et al., 2013), the mean log-velocity $\mu_{\ln u}$ is given in terms of the average flow velocity as:

$$\mu_{\ln u} = \ln(\mu_u) - \frac{\sigma^2_{\ln u}}{2} = -\frac{\sigma^2_{\ln u}}{2}, \tag{3.15}$$

where $\mu_u = 1$ has been used, which results from the normalization applied in equation 3.12.

The stationary velocity distribution $p_s(u)$ is given in terms of the distribution $p_e(u)$ of Eulerian flow velocities as (Dentz et al., 2016):

$$p_s(u) = \frac{u p_e(u)}{\mu_u}. \tag{3.16}$$

Combining equations 3.13 and 3.16 leads to the stationary velocity distribution $p_s(u)$ which is also log-normally distributed and given by:

$$p_s(u) = \frac{1}{u\sqrt{2\pi\sigma^2_{\ln u}}} \exp\left[-\frac{\left(\ln u - \mu_{\ln u} - \sigma^2_{\ln u}\right)^2}{2\sigma^2_{\ln u}}\right], \tag{3.17}$$

in which $u = \exp(\ln u)$ and $\mu_u = \exp\left(\mu_{\ln u} + \frac{\sigma^2_{\ln u}}{2}\right)$ have been used.

By inserting equation 3.15 into equation 3.17 it can be simplified to:

$$p_s(u) = \frac{1}{u\sqrt{2\pi\sigma^2_{\ln u}}} \exp\left[-\frac{(\ln u + \mu_{\ln u})^2}{2\sigma^2_{\ln u}}\right]. \tag{3.18}$$

Thus, for moderately heterogeneous media the velocity distribution $p_s(u)$ can be fully parameterized in terms of the statistics of the hydraulic conductivity field and the Eulerian mean flow velocity. For stronger heterogeneity with $\sigma^2_Y > 1$, however, $p_e(u)$ deviates from a log-normal distribution. Drawing from the Eulerian and the stationary velocity distributions corresponds to drawing from a volume- and a flux-weighted velocity distribution, respectively.

Velocity Transitions

We base particle velocity transitions on an Ornstein-Uhlenbeck process, closely related to the *outdrw* model described in Comolli et al. (2019). The initial velocity for each particle is drawn from the marginal flux-weighted velocity distribution (equation 3.18). Since Ornstein-Uhlenbeck processes are Gaussian (e.g., Pavliotis, 2014), the velocities need to be transformed into their normal scores w:

$$w(x) = \Phi^{-1}\{P_s[u(x)]\}, \tag{3.19}$$

where $\Phi(w)$ is the cdf of the normal distribution and $P_s(u)$ is the velocity cdf. For advective transport with injection into the flux, $P_s(u)$ corresponds to the integral of $p_s(u)$ (equation 3.17) from 0 to u. Then, the correlated evolution of the velocity normal score transforms $w(x)$ is modeled as an Ornstein-Uhlenbeck process using the Langevin equation (Van Kampen, 2007):

$$\frac{\mathrm{d}w(x)}{\mathrm{d}x} = -\frac{w(x)}{I_{\ln u}} + \sqrt{\frac{2}{I_{\ln u}}}\xi(x), \tag{3.20}$$

where $\xi(s)$ denotes a zero mean Gaussian white noise. Equation 3.20 is discretized as

$$w(x+\Delta x) = w(x) - \frac{w(x)\Delta x}{I_{\ln u}} + \sqrt{\frac{2\Delta x}{I_{\ln u}}}\zeta(x), \tag{3.21}$$

where $\zeta(x)$ is a standard normal random variable. The updated normal scores are backtransformed into velocities by:

$$u(x+\Delta x) = P_s^{-1}\{\Phi[w(x+\Delta x)]\}. \tag{3.22}$$

Finally, the particle position and travel time are updated according to equations 3.7 and 3.8.

3.3.2 Advective-Diffusive Transport

For purely advective particle motion, velocities change as particles move along streamlines as described by the SMM presented in the previous section. Advective velocity changes occur on the characteristic length scale $I_{\ln u}$. In the presence of diffusion, particle velocities can change also due to diffusive jumps across streamlines, which occur on a characteristic diffusion time scale τ_D. These two processes are in

competition, and during a transition, velocity changes are triggered by the process that acts fastest.

Transition Times

We consider particle transitions over the distance Δx between two observation planes according to equation 3.7. The advective time increment for a velocity transition to occur is:

$$\tau_a = \frac{\Delta x}{u(x)}. \tag{3.23}$$

The diffusive time increment τ_D for a velocity transition to occur is set equal to the escape time of a particle from a disk with radius R that is of the order of the transverse integral scale of the medium. Such an event resets the particle velocity. The solution of the escape problem is detailed in Appendix A. There, we show that the escape time distribution $\psi(t)$ can be represented by the exponential distribution:

$$\psi(t) = \frac{\exp(-t/\tau_m)}{\tau_m}, \qquad \tau_m = \frac{R^2}{8D}, \tag{3.24}$$

where τ_m is the mean escape time. The sampling of the steady flow field by diffusion is equivalent to volumetric sampling.

Velocity Transitions

The SMM for advective-diffusive transport can now be written as

$$x_{i+1} = x_i + \Delta x \tag{3.25}$$

$$t(x + \Delta x) = t(x) + \min[\tau_a(x), \tau_D]. \tag{3.26}$$

For an advective transition, that is, for $\tau_a(x) < \tau_D$, the next particle velocity is sampled from $p(u, \Delta x|u')$. For a diffusive transition, that is, for $\tau_D < \tau_a(x)$ it is sampled from the Eulerian velocity distribution $p_e(u)$. The reason for sampling from $p_e(u)$ is that by diffusion particles tend to uniformly cover space, which is equivalent to the volumetric sampling of flow velocities. This implies that after each diffusive transition, the Markov process, which models advective transitions, is reset and correlations to the previous velocities are lost. This means that the distribution $p_D(u, \Delta x|u', \tau')$ of particles velocities $u(x + \Delta x)$ conditional to the particle velocity $u(x) = u'$ and diffusion time $\tau_D = \tau'$ at the previous step is given by:

$$p_D(u, \Delta x|u', \tau') = \begin{cases} p(u, \Delta x|u') & \text{if } u' > \frac{\Delta x}{\tau'} \\ p_e(u) & \text{if } u' < \frac{\Delta x}{\tau'} \end{cases} \tag{3.27}$$

The presented algorithm is a simplification of the actual transport processes. In reality, particles gradually deviate from their advective trajectory by transverse diffusion, and the velocity experienced by the particles is decreasingly correlated with the velocity on the purely advective trajectory with increasing lateral distance. In fact, the covariance function of longitudinal velocities normal to the mean direction of flow is known to be of hole-type (Rubin, 1990). Considering this behavior would require keeping track of the lateral particle position and motion and using different transition probabilities of the longitudinal velocity for different lateral positions. Instead we consider a binary process. If transverse diffusion leads to a lateral distance

smaller than a given escape radius R, we consider exactly the same advective velocity that the particle would experience if it had stayed on the advective trajectory. This is what we denote the advective velocity transition. It corresponds to assuming perfect lateral velocity correlation for distances smaller than R. By contrast, if the transverse diffusion leads to a lateral distance larger than the given radius, the velocity in the next step does not correlate to the previous one at all. In the current application, where we target ensemble dispersion, these approximations are of insignificant effect. However, for an explicit focus on effective dispersion of plumes originating from point sources, these local processes need to be considered. Effective dispersion has been associated with effective diffusive mixing in heterogeneous media (Cirpka, 2002; Perez et al., 2020). Hence, we cannot make statements about mixing with the current approach.

3.3.3 Setup and Parameterization of the Spatial Markov Model

For the stochastic models, 10^6 trajectories are created for each combination of Pe and σ_Y^2. The particles are injected into the flux and follow a spatial step size of $\Delta x = 10^{-2} I_{\ln u}$.

The characteristic tube radius $R\left(\sigma_Y^2\right)$ as used for the calculation of the mean first-passage time in equation 3.24 depends on σ_Y^2 by the following empirical relationship:

$$R\left(\sigma_Y^2\right) = (2.164 - 0.048\sigma_Y^2) I_Y. \tag{3.28}$$

R decreases with increasing heterogeneity of the porous medium, which is in line with transport being increasingly concentrated along fewer preferential flow paths with increasing σ_Y^2 (Zehe et al., 2021). Increasing σ_Y^2 and thus decreasing the tube radius increases the probability for diffusive exchange, which reflects the well-known fact that mixing is enhanced by heterogeneity (Urroz et al., 1995; Weeks and Sposito, 1998).

We present two variants of the SMM: One based on the theoretical log-normal velocity distributions given in Section 3.3.1 and one based on empirical statistical velocity distributions, attained from averaging over the numerical Monte-Carlo simulations as described in Sections 2.2 & 3.2.2. The variants will be distinguished as theoretical SMM and empirical SMM.

The tortuosity used in equation 3.11 is computed as (Koponen et al., 1996):

$$\chi = \frac{\overline{\|\mathbf{v}(\mathbf{x})\|}}{\overline{v_1(\mathbf{x})}} \tag{3.29}$$

and has the same values as given by Cirpka et al. (2022) who found the following empirical relationship:

$$\chi = 1 + 0.059 \times \sigma_{lnK}^2. \tag{3.30}$$

3.4 Results & Discussion

3.4.1 Velocity Distributions

Figure 3.1 shows statistical distributions of tortuosity-corrected Eulerian velocity in the mean transport direction. Solid lines denote the average over the numerical velocity fields. Dashed lines are calculated from the theoretical marginal log-normal velocity distribution analogous to equations 3.13 & 3.18. With increasing variance

of hydraulic conductivity, the empirical distributions progressively deviate from the prescribed log-normal distributions towards higher velocities. Previous studies (Bellin et al., 1992; Le Borgne et al., 2007; Gotovac et al., 2009) share this observation, which is important for the evaluation of the proposed transport model.

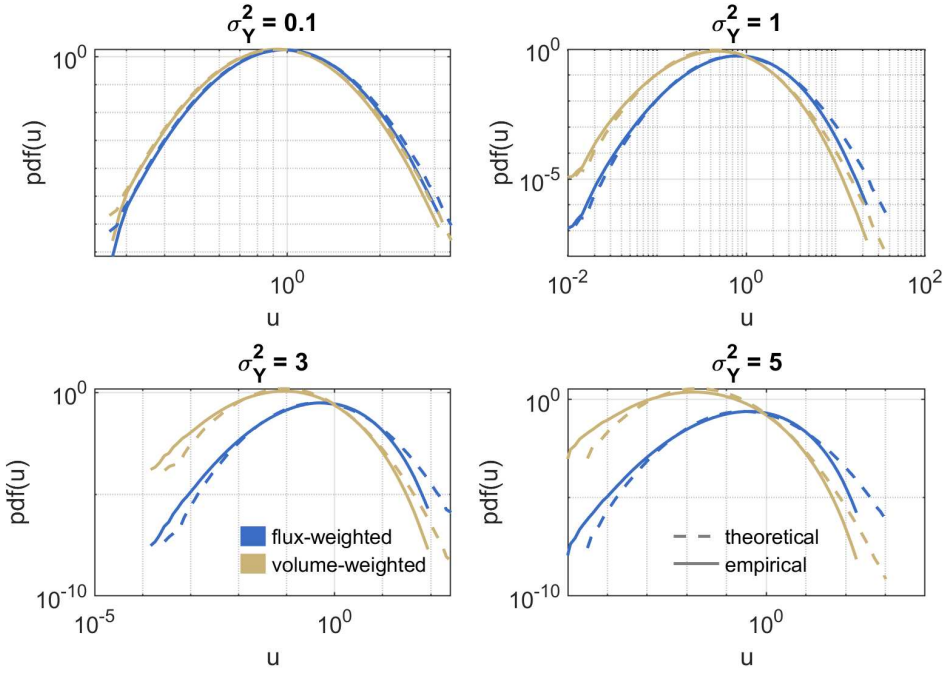

FIGURE 3.1: Double logarithmic plot of tortuosity-corrected Eulerian velocity distributions. Golden: volume-weighted distributions, blue: flux-weighted distributions, solid line: empirical distributions, dashed lines: theoretical, log-normal distributions.

3.4.2 Mean Arrival Times

Figure 3.2 shows the mean arrival times μ_τ at observation planes for the PTRW simulations and the stochastic model. There is a perfect agreement between the empirical and stochastic data for all hydraulic conductivity variances and Péclet numbers. As predicted for injection into the flux, the mean arrival time equals the travel distance divided by the mean Eulerian velocity (Demmy et al., 1999). Since the mean velocity is not affected by diffusion strength, all considered Péclet variants collapse onto one line.

3.4.3 Variances of Arrival Times

Figure 3.3 shows the variance of arrival times σ_τ^2 at different observation planes for the numerical and stochastic model. Increasing the heterogeneity of log-conductivity increases the variance of arrival times, as to be expected from theory predicting direct proportionality between the two metrics (e.g., Shapiro and Cvetkovic, 1988). The variance of arrival times decreases with increasing diffusion strength because in heterogeneous media transverse diffusion leads to a more efficient sampling of the velocity variability and thus limits the time during which a particle remains in an extreme part of the velocity spectrum (Andričević, 1998).

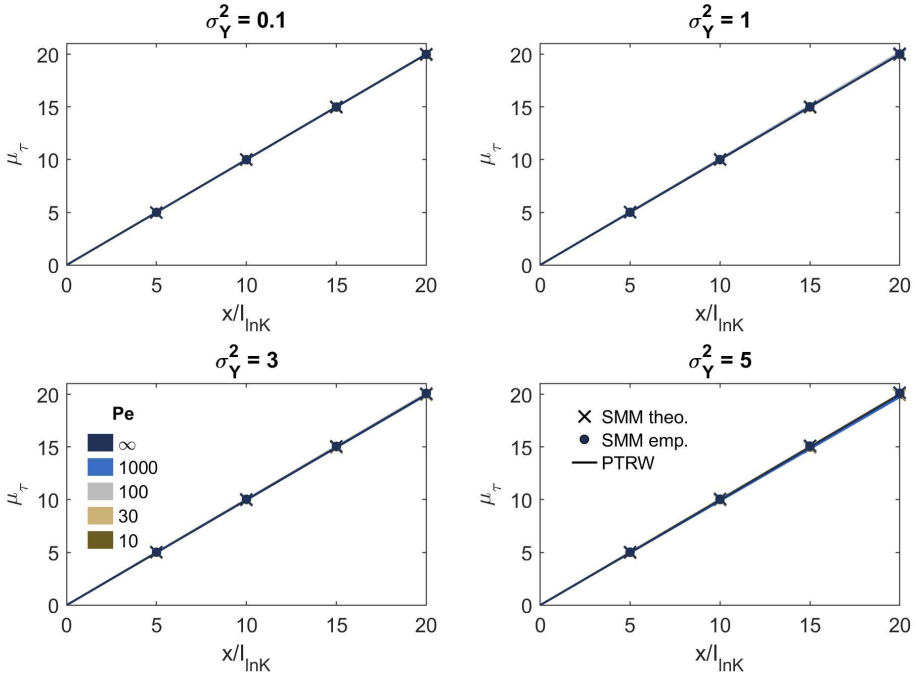

FIGURE 3.2: Mean arrival times for different hydraulic conductivity variances and Péclet numbers resulting from the PTRW simulations and the two variants of the stochastic model.

The agreement between the direct numerical simulations and the SMM is generally good, although it decreases slightly with increasing σ_Y^2. The theoretical SMM shows a systematic deviation towards slightly increased variances. The deviation increases with decreasing diffusion strength. Thus, fine-tuning the escape radius R to the theoretical SMM does not decrease the misfit because the SMM is most sensitive to R when diffusion is strongest, that is, in the low-Péclet cases where the fit is good as it is.

3.4.4 Breakthrough Curves

Figure 3.4 shows the BTC for purely advective transport at travel distances of 10 and 20 correlation lengths, comparing the PTRW and SMM models. Stronger heterogeneity leads to enhanced tailing and faster first arrival. This is visible in the peak arriving increasingly earlier than the expected mean arrival time, denoted by the colored vertical lines in the insets in figure 3.4. There is a good agreement between the PTRW results and the empirical SMM for all values of σ_Y^2. The theoretical SMM shows significant deviations from the PTRW results at early times, especially for large variances of log-conductivity. The breakthrough is too early in comparison to the PTRW results, which we attribute to the theoretical velocity distributions being shifted towards higher velocities in comparison to the empirical distributions (cf. figure 3.1).

Figures 3.5 & 3.6 show the BTC for infinite- and finite Péclet numbers of 10 and 100 computed by PTRW and the theoretical and empirical SMM, respectively. Like in the purely advective case, the theoretical model deviates from the PTRW results at early times. For the sake of clarity, we do not show the BTC for $Pe = 30$ and $Pe = 1000$. They follow the same behavior as discussed below. Figures 3.5 & 3.6

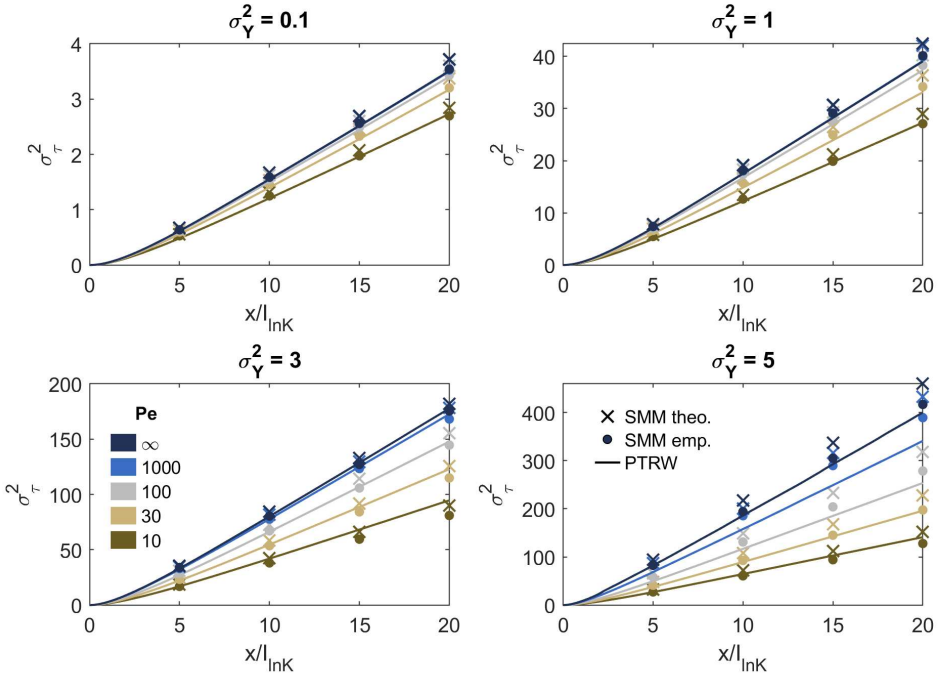

FIGURE 3.3: Variance of arrival times for different hydraulic conductivity variances and Péclet numbers for the PTRW simulations as well as the variants of the stochastic model.

allow us to discuss the effect of diffusion strength on particle breakthrough. As explained above, diffusion limits the effect of extreme velocities on the particle distribution. Therefore, stronger diffusion delays peak arrival (because particles are less influenced by the fastest velocity zones) and weakens tailing (because particles are less influenced by the slowest velocity zones), consistent with the observations of Fiori et al. (2011). Moreover, as measured by the decreasing variance of arrival times, the BTC becomes narrower with increasing diffusion strength. It is important to note that this behavior is specific to heterogeneous media and opposite to the behavior in homogeneous media, where plumes become wider with increasing diffusion strength. The behavior of the concentration peak depends on the combined effects of heterogeneity and Péclet number. In fields with weak heterogeneity, the peak arrival is not discernible from the mean arrival time, which is denoted by the black vertical lines in the insets of figures 3.5 & 3.6, and diffusion heightens the concentration peak. In fields with strong heterogeneity, preferential flow is more pronounced (Fiori and Jankovic, 2012), leading to the peak of the BTC arriving earlier than the mean arrival time. In this case, diffusion decreases the concentration peaks, because, as already stated, it cuts very fast arrival. The compacting of the BTC with increasing diffusion is still observable from the higher probability weight at the mean arrival time of the BTC for $Pe = 10$ compared to $Pe = 100$. All of these behaviors are captured by the theoretical and empirical SMM in accordance with the BTC data from the direct numerical simulations.

To quantitatively assess the performance of the two types of SMM, we compute the Cramér-von Mises criterion ω^2, which indicates the goodness of fit between two cumulative distribution functions Anderson, 1962:

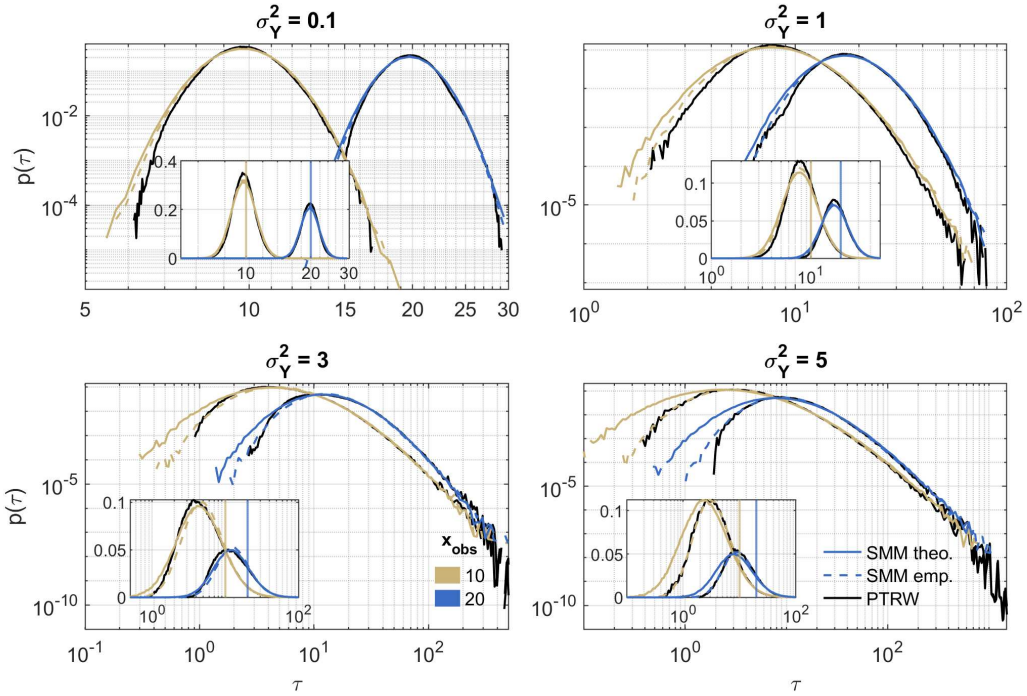

FIGURE 3.4: BTC at $x/I_Y = 10, 20$ for different hydraulic conductivity variances and purely advective transport. Double logarithmic display in main plots, semilogarithmic in insets. The inset axes have the same labels as the main plots. Solid black lines: PTRW results, colored lines: results from the SMM using the theoretical (solid) and empirical (dashed) velocity distributions. The colors indicate the position of the observation planes. The vertical colorful lines in the insets show the position where the dimensionless mean travel time equals the dimensionless coordinate of the observation planes.

$$\omega^2 = \int_{-\infty}^{\infty} \left[P_{SMM}(\tau) - P_{PTRW}(\tau)\right]^2 dP(\tau), \tag{3.31}$$

in which $P_{PTRW}(\tau)$ and $P_{SMM}(\tau)$ are the cdf of arrival times of the explicit and stochastic models.

Figure 3.7 shows a direct comparison between ω^2 for the theoretical and the empirical SMM. The smaller ω^2 the better the agreement between the SMM and the PTRW results. Generally, the empirical model performs better than the theoretical model, and the mismatch is smaller for milder heterogeneity. However, for $\sigma_Y^2 = 3$, the theoretical model performs better than the empirical model with the exception of the first observation plane. We attribute this irregularity to the difference between the represented averages: While the SMM represents a true ensemble average Sherman et al., 2021, the PTRW simulations are an average over a finite number of realizations which converge towards the ensemble average. We can rule out the fitting of R as the underlying reason because the theoretical model also outperforms the empirical model for the case of $Pe = \infty$.

The decision whether to use the theoretical or the empirical SMM depends on the given application. For cases of mild heterogeneity, the theoretical model is sufficiently accurate. For stronger heterogeneity and when the early breakthrough behavior is of great relevance, the empirical model is recommended.

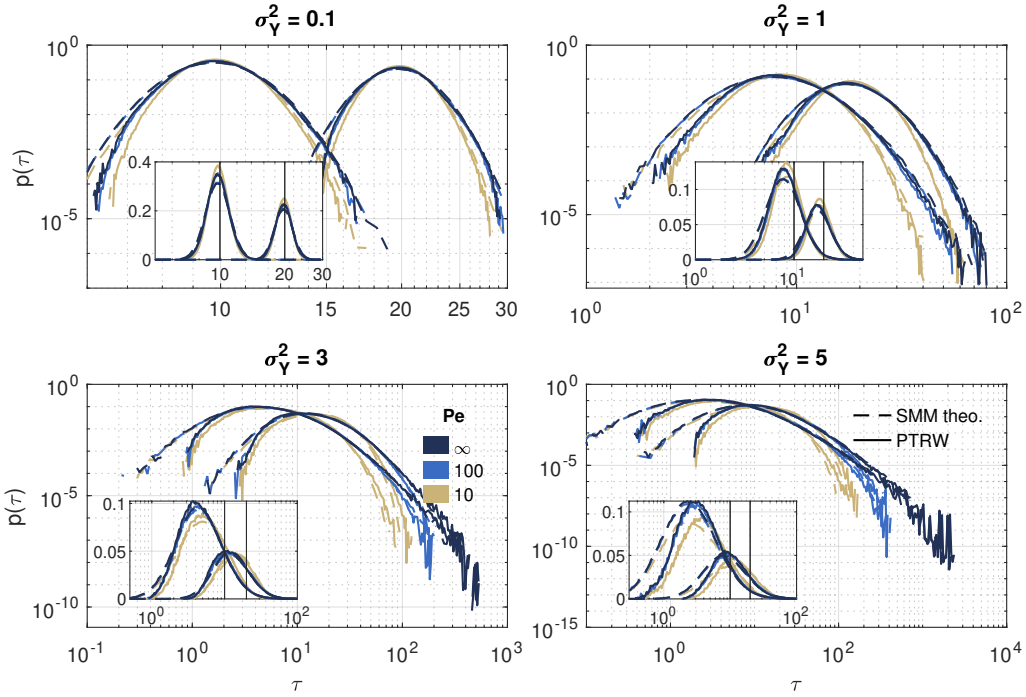

FIGURE 3.5: BTC at $x/I_{\ln K} = 10, 20$ for different hydraulic conductivity variances and Péclet numbers. Double logarithmic display in main plots, semilogarithmic in insets. The inset axes have the same labels as the main plots. Solid lines: PTRW results, dashed lines: results from the theoretical SMM. The vertical bold lines in the insets show the position where the dimensionless mean travel time equals the dimensionless coordinate of the observation planes.

3.5 Conclusions

In this work, we have presented a Spatial Markov Model for advective-diffusive transport based on the purely advective models of Cirpka et al. (2022) and Comolli et al. (2019). Our defined objective was to develop a process-based concept of diffusion while limiting the use of empirical data in an advective-diffusive SMM.

We successfully model diffusion as jumps between different advective trajectories which is translated into resetting the Markovian sequence of advective particle transitions. Diffusive exchange takes place at a spatial step if the diffusive travel time in transverse direction is shorter than the advective time in longitudinal direction. The diffusion probability depends on the Péclet number and the radius of the advective tube, which is a fitting parameter depending on σ_Y^2. Although it still relies on a fitting parameter and thus is not fully physically parameterized, our mechanistic concept for diffusion is an improvement over previous advective-diffusive SMM Le Borgne et al. (e.g., 2011), Sund et al. (2017b), Sund et al. (2017a), and Wright et al. (2021). The latter required input from transport simulations, which is in contrast to the goal of substituting the spatially explicit transport simulation by something computationally less costly.

The theoretical SMM assumes a log-normal velocity distribution and is solely derived from properties of the hydraulic conductivity field. However, its applicability is limited to fields of moderate heterogeneity. The empirical SMM requires the probability density function of the Eulerian velocity field. It is applicable to any degree of heterogeneity because, in contrast to the theoretical variant, it is not impacted by

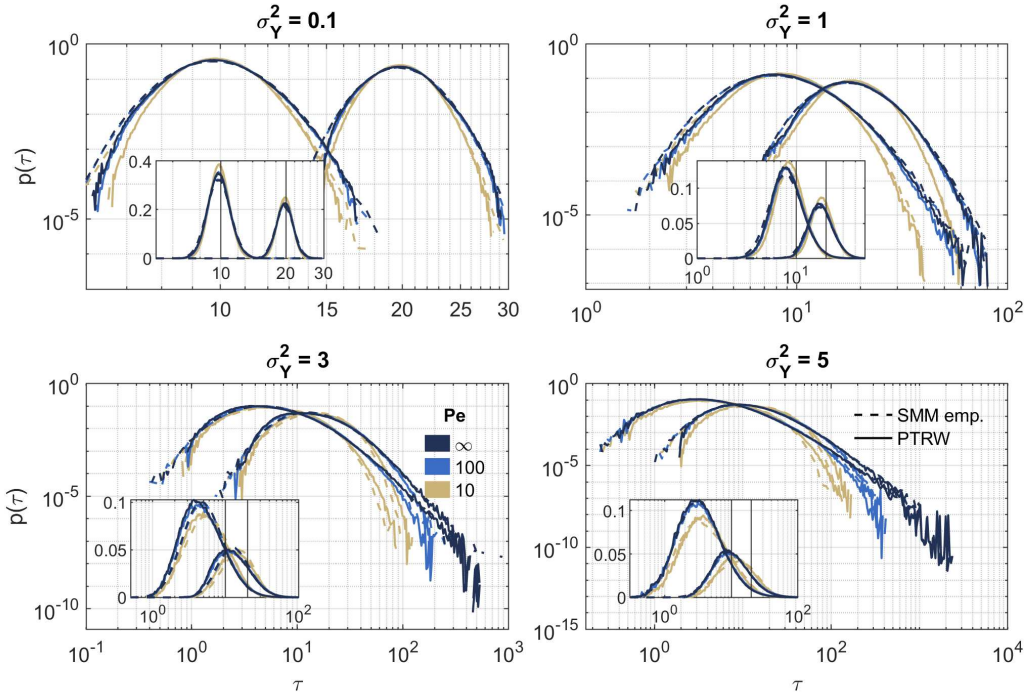

FIGURE 3.6: BTC at $x/I_Y = 10, 20$ for different hydraulic conductivity variances and Péclet numbers. Double logarithmic display in main plots, semilogarithmic in insets. The inset axes have the same labels as the main plots. Solid lines: PTRW results, dashed lines: results from the empirical SMM. The vertical bold lines in the insets show the position where the dimensionless mean travel time equals the dimensionless coordinate of the observation planes.

the increasing deviation between the log-normal prediction and the true empirical velocity distribution. For an approximate estimation of the temporal transport statistics, the theoretical SMM is quick and efficient. For cases where a high accuracy is needed and the heterogeneity is strong, it is important to use the exact velocity distribution which requires flow simulations. At least, in contrast to approaches relying on empirical transition matrices of Lagrangian velocities, it does not require solving a spatially explicit transport equation. In general, the proposed SMM is very flexible and can be used with any velocity distribution. Thus, it should be possible to advance it to be independent of empirical input altogether.

As mentioned in the introduction, the BTC and their moments analyzed here describe the average over a large ensemble of conductivity realizations. In real-world applications, this relates to the injection and observation of a solute over a wide cross section. The current framework cannot make statements about the expected spread of BTC at single observation points in single realizations, which has been used as a metric for mixing (Cirpka and Kitanidis, 2000). It would be of high interest to expand the analytical SMM framework to address local mixing phenomena that may control nonlinear mixing-controlled reactions. As stated in Section 3.3.2, the model in its current state is a simplification of the true correlation of longitudinal velocities in transverse direction. Incorporating a mechanism which allows for a gradual loss of correlation between particle pairs conditioned on their transverse distance might be a key to targeting mixing specifically. This is supported by Wright et al. (2019) who emphasize the importance of similitude between neighboring trajectories for

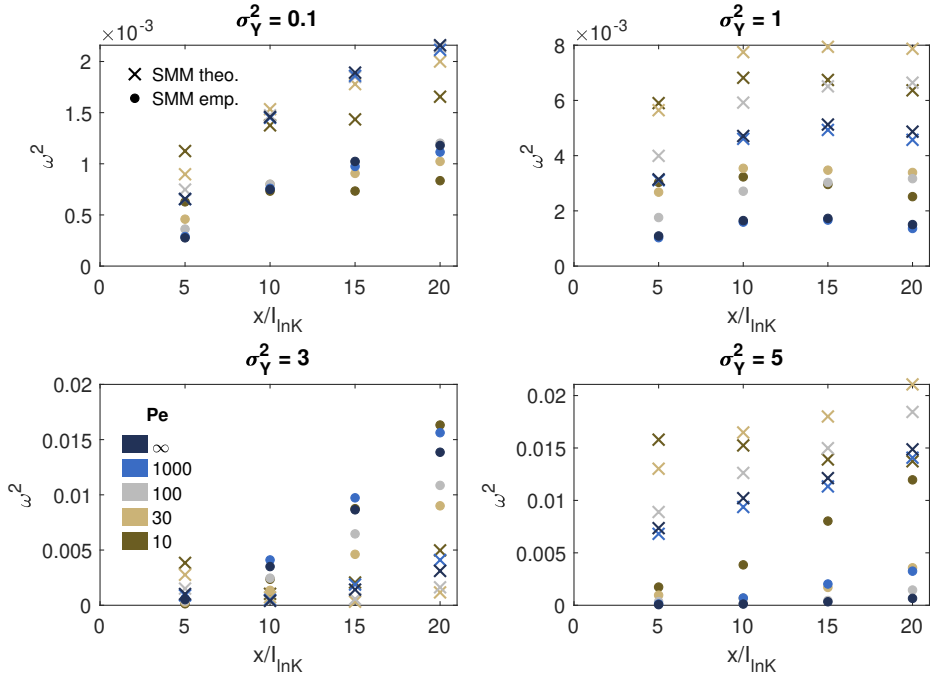

FIGURE 3.7: Cramér-von Mises criterion ω^2 for the agreement between the theoretical (cross symbols) or empirical (circles) SMM and the PTRW results for different hydraulic conductivity variances and Péclet numbers

mixing in their empirically parameterized SMM. To remain in the SMM framework, one would have to consider a coupled Markov model of longitudinal and transverse motion, or of absolute velocity and orientation, respectively (Meyer, 2018), in which the joint transition probabilities of two particles depend on their lateral distance. However, to develop a robust SMM framework that captures solute mixing further research is clearly needed.

Data Availability

All data and the Matlab codes for the SMM and to reproduce the figures are available at `https://doi.org/10.5281/zenodo.15389771` (Stettler et al., 2025) under the international Creative Commons license CC-BY-NC 4.0. Access to the Matlab codes for the three-dimensional numerical fields and particle-tracking simulations is described in Cirpka et al. (2022).

Chapter 4

Linear Stochastic Analysis of the Partial Reversibility of Ensemble and Effective Dispersion in Heterogeneous Porous Media

4.1 Introduction

Only mixing facilitates chemical reactions of reactants that are initially separated. Therefore it is of vital interest to separate the contributions of spreading and mixing to overall dispersion. Mixing is an irreversible process, whereas the deformation of a solute plume due to spatially variable advection is perfectly reversible. In thermodynamics, irreversibility implies an increase of entropy. Along these lines, Kitanidis (1994) introduced the dilution index as metric of solute mixing. With the exception of very simple cases, such as a truly Gaussian plume in a homogeneous flow field, the dilution index cannot be computed analytically. In heterogeneous aquifers with deformed plumes, evaluating the dilution index requires knowledge about the full 3-D concentration distribution, which has been calculated in numerical studies (e.g., Rolle et al., 2013; Dentz et al., 2018a), but is not measurable in the field. That is, while the dilution index is an accurate metric of mixing, it is not accessible under realistic field conditions. Therefore, other approaches are needed.

Applying the stream-tube approach, Cirpka (2002) considered advective-dispersive-reactive transport along independent stream tubes using the effective dispersion coefficient and a distribution of velocities among the stream tubes that reflected the variance of mean point-observed arrival times. The predictive capabilities of this parameterization for bimolecular reactions was excellent. Benson et al. (2019) compared the approach to 2-D simulations and a reactive-particle-tracking approach for bimolecular reactions in Poiseuille flow, confirming excellent agreement. Perez et al. (2019) and Perez et al. (2020) and Puyguiraud et al. (2019) used effective dispersion coefficients related to point injections to quantify mixing on the pore scale in a framework of lamellar mixing models. While these simulation results suggest that the longitudinal effective second central moment is a good predictor of longitudinal mixing in mixing-controlled reactive transport, it has not been tested whether it has all properties of a true mixing metric. In particular, the effective second central moment should not decrease upon flow reversal if it truly quantified mixing.

Reversibility of transport in creeping Couette flow has experimentally been demonstrated by Heller (1960), and the impact of diffusion on the reversibility of transport in such systems has been analyzed by Sundararajan et al. (2012), among

others. In the present study, we analyze to which extent second central spatial moments of solute plumes in heterogeneous porous media decrease upon reversal of the flow field. Because in natural porous media spatially variable advection and diffusive mixing interact, we expect that second central spatial moments decrease upon flow reversal but not to the same extent as they increased in the forward motion. Hence, solute dispersion should be addressed as a *partially reversible* process. This partial reversibility of second central moments is the main target of the present study.

The key idea is to analyze the behavior of solute clouds upon flow reversal in uniform-in-the-mean random velocity fields. Figure 4.1 exemplifies the reasoning by the simulated evolution of five point injections evenly spaced along a line in a 3-D heterogeneous domain. The top row of Figure 4.1 shows the depth-averaged concentration during forward motion. Due to the underlying heterogeneity, the individual particle clouds move with different advective velocities and are spread out in longitudinal direction while being transported downstream. Local-scale dispersion smears the initial point geometries. In the example, the flow direction is reversed after passing 10 integral scales in the mean. As shown in the bottom row of Figure 4.1, the positions of the receding plumes resemble those of the forward motion, meaning that the variability of the solute plumes' centers of gravity shrinks again upon flow reversal. However, the spread of the individual plumes is much less susceptible to flow reversal. The plumes seemingly continue expanding also in the reversed velocity field. The different behavior between the ensemble of all injected particles and the individual plumes illustrates the conceptual difference between ensemble and effective dispersion.

In field applications, the concept of reversing the flow field is known as push-pull test (Istok, 2013, and references therein). Here, solutes (or heat) are introduced in the water injected into a well (push phase) and are extracted from the same well upon water extraction (pull phase). Push-pull tests have been used to deduce various aquifer and transport properties (e.g. Leap and Kaplan, 1988; Vandenbohede et al., 2009; Rasmusson et al., 2014; Kang et al., 2015; Paradis et al., 2018), aside characterization of reactive transport (e.g. Istok et al., 1997; Ma et al., 2019; Kruisdijk and Breukelen, 2021). Because of flow reversibility, the spread of a conservative-tracer breakthrough curve is often considered to be unaffected by hydraulic heterogeneity, but the interpretation is hampered by ambient flow, mass-exchange into zones of immobile porosity, and the interplay between advective spreading and diffusive mixing (Hansen et al., 2016). Roth et al. (2021) performed laboratory-scale push-pull tracer experiments using refractive index matching in quasi two-dimensional homogeneous porous media and Neupauer et al. (2021) conducted corresponding numerical particle-tracking simulations for radial flow. In their numerical analysis of the laboratory experiments, diffusion was considered negligible, and consequently the authors observed complete reversibility of advective spreading.

For theoretical analyses, the radial flow geometry corresponding to push-pull tests is not advantageous as it introduces spatial non-stationarity (Neuweiler et al., 2001; Indelman, 2004; Di Dato et al., 2019). Previous works considering macroscopically uniform flow subject to flow reversal were performed by Berentsen et al. (2005) for the case of stratified formations. They developed an analytical solution for the ensemble moments demonstrating the partial reversibility of Taylor dispersion. Jha et al. (2009) and John et al. (2010) conducted purely numerical studies in multi-Gaussian random log-conductivity fields. The latter two investigated the influence

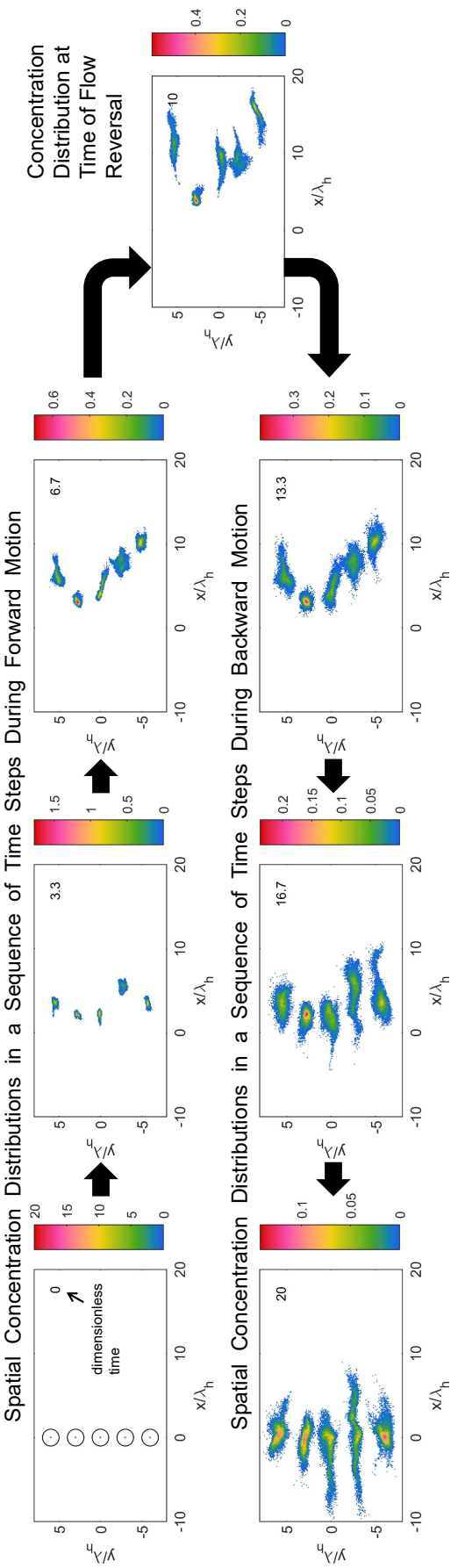

FIGURE 4.1: Numerical simulation of aligned point sources in a 3-D domain with flow reversal when the solute clouds have traveled 10 integral scales in the mean. $\sigma_Y^2 = 1.0$, $Pe = \bar{v}_0 \lambda_h / D_{loc} = 500$, length scales are normalized by the horizontal integral scale λ_h, times in the legends by $\lambda_h / \bar{v}_0$. Top row: depth-averaged concentration related to a line of point sources during forward movement (the circles in the top left panel highlight the injection points in their centers); bottom row: depth-averaged concentration during backward movement.

of flow reversal on the ensemble dispersion coefficient and how dispersivities in forward and reversed movement are influenced by geostatistical and transport characteristics, but they did not derive closed-form expressions. None of these studies analyzed effective moments, which are vital to address mixing dynamics.

Mixing in fields undergoing flow reversal is of practical interest in naturally oscillating systems, for example, contaminant transport and freshwater-seawater mixing in tidally influenced aquifers (La Licata et al., 2011; Pool et al., 2014), as well as in underground storage systems involving injection/extraction regimes, one example being hydrogen storage where an accurate prediction of mixing is required to assess the storage efficiency (Feldmann et al., 2016). As stated before, isolating the contribution of mixing to dispersion is of interest in order to accurately predict mixing-limited reactions, which are relevant for the remediation of contaminated sites (Kahler and Kabala, 2016). With our study we want to investigate how flow reversal can contribute to distinguishing between spreading and mixing.

In the present study we will analyze advective-diffusive transport in second-order stationary velocity fields affected by perfect flow reversal at time $t = T$ by linear stochastic theory and compare the theoretical results to particle-tracking random-walk simulations. Specifically, we analyze the ensemble and effective second central moments of plumes originating from point sources to quantify their partial reversibility.

By this analysis we address the following research questions:

1. Do effective second central moments for point sources decrease upon flow reversal? If this is the case, effective dispersion is an inaccurate metric of mixing.

2. Can ensemble second central moments after equally long forward and backward motion be used to estimate solute mixing? The answer to this question has implications for the design of practical tests. While spatial moments are difficult to measure in the field, the related temporal moments of breakthrough curves are accessible. If the question can be answered with "yes", the ensemble and effective second central moments must become identical again after equally long forward and backward motion.

3. How do geostatistical parameters of the log-conductivity field and transport parameters influence the partial reversibility of dispersion? We expect that the reversibility decreases with increasing variance of the log-hydraulic conductivity because stronger heterogeneity causes stronger spreading fostering enhanced mixing (Urroz et al., 1995). We also expect that larger local dispersion coefficients decrease the reversibility as diffusion destroys memory. We expect that a larger contrast between horizontal and vertical integral scales decreases the reversibility because the decisive diffusive mixing takes place in the transverse direction (e.g., Cirpka et al., 1999). Finally, we expect the reversibility to decrease with longer flow periods in both directions (corresponding to larger values of T) because the diffusive transport contribution becomes more relevant with time.

4. How long do the effects of flow reversal on second central moments prevail? Over which time do second central moments decrease, and how long does it take until the dispersion coefficients reach their asymptotic value after a flow reversal event?

5. What are the limits of linear stochastic theory when applied to the partial reversibility of ensemble and effective second central moments? The limits of linear theory have been intensively studied for asymptotic ensemble dispersion in forward motion, where the effects of local dispersion are typically minor. This is quite different for the moments after equally long forward and backward movement, posing a different, potentially harder test for linear stochastic theory.

The remainder of this paper is structured as follows: In Section 4.2 we present the mathematical description of flow and transport with flow reversal at $t = T$ and expand the analytical solution for ensemble and effective dispersion following linear stochastic theory (Dentz et al., 2000) to the case with flow reversal. In Section 4.3 we describe how we computationally evaluate the analytical solution in periodic media and how we numerically calculate spatial second central moments by particle-tracking random-walk simulations to test the analytical solution. In Section 4.4 we present how the reversibility of dispersion is influenced by different parameters and analyze characteristic times for transport in the reversed flow field. In Section 4.5 we conclude the paper by trying to answer the questions posed above.

4.2 Theory

4.2.1 Governing Equations for Flow and Transport with Flow Reversal

Starting point for the description of flow and transport through a 3-D heterogeneous domain is the steady-state groundwater flow equation 2.2:

$$\nabla \cdot (K \nabla h) = 0. \tag{4.1}$$

In order to account for flow reversal, it is subjected to transient forcings causing an immediate response of the groundwater flow system, rendering equation 4.1 to be at quasi-steady-state, in fact. As auxiliary condition of flow in an infinite domain, we assume that the mean hydraulic gradient $\mathbf{J}(t) = -\nabla \bar{h}$ [-] is spatially uniform but time dependent, in which the overbar denotes a large-scale spatial mean.

In line with linear stochastic theory (e.g., Dagan, 1989; Gelhar, 1993; Rubin, 2003), we consider the hydraulic conductivity $K(\mathbf{x})$ to be a log-normal random space function with uniform geometric mean K_g [LT^{-1}] and second-order stationary random fluctuations $Y'(\mathbf{x})$ [-] of log-conductivity with zero mean and covariance function $C(\mathbf{d})$ [-] with variance σ_Y^2 [-] and horizontal and vertical integral scales λ_h and λ_v [L]:

$$K(\mathbf{x}) = K_g \exp\left(Y'(\mathbf{x})\right), \tag{4.2}$$

$$\left\langle Y'(\mathbf{x}) \right\rangle = 0 \qquad \forall \mathbf{x}, \tag{4.3}$$

$$\left\langle Y'(\mathbf{x}) Y'(\mathbf{x}+\mathbf{d}) \right\rangle = C\left(\mathbf{d}, \sigma_Y^2, \lambda_h, \lambda_v\right) \forall \mathbf{x}, \tag{4.4}$$

where $\langle \cdot \rangle$ denotes the ensemble average, and $\mathbf{d}$ [L] is a distance vector. Note that the terms "integral scales" and "correlation lengths" are interchangeable if an exponential covariance function is used. Substituting equation 4.2 into equation 4.1 yields:

$$K_g \cdot \nabla \left[\exp\left(Y'\right) \cdot \nabla h\right] = 0, \tag{4.5}$$

subject to a time-dependent, uniform-in-the-mean hydraulic gradient. The related linear-groundwater-velocity field $\mathbf{v}(\mathbf{x}, t)$ [LT^{-1}] is described by:

$$\mathbf{v}(\mathbf{x}, t) = -\frac{K_g}{\theta} \exp\left[Y'(\mathbf{x})\right] \cdot \nabla h(\mathbf{x}, t), \tag{4.6}$$

where θ [-] is the effective porosity.

The advection-dispersion equation describes solute transport in this velocity field:

$$\frac{\partial c}{\partial t} + \mathbf{v} \cdot \nabla c - \nabla \cdot (\mathbf{D} \nabla c) = 0, \tag{4.7}$$

in which $c(\mathbf{x}, t)$ [ML^{-3}] is the solute concentration, $\mathbf{D}$ [$\mathrm{L}^2\mathrm{T}^{-1}$] is the dispersion tensor assumed spatially uniform for simplification. We assume a point-like initial distribution of the concentration and vanishing derivatives at the far-distance limit $x_i \to \pm\infty$, $i \in [1, 2, 3]$:

$$c(\mathbf{x}, 0) = m_0 \delta(\mathbf{x}), \tag{4.8}$$

$$\lim_{x_i \to \pm\infty} \frac{\partial^k c}{\partial x_i^k} = 0 \; \forall k \in \mathbb{N}_0, i \in [1, 2, 3], \tag{4.9}$$

in which m_0 [M] is the solute mass and $\delta(\cdot)$ is the Dirac delta function.

Since the velocity field $\mathbf{v}(\mathbf{x}, t)$ depends on the second-order stationary random log-K field it can be decomposed into a spatially uniform, time-dependent mean $\langle \mathbf{v}(t) \rangle$ [LT^{-1}] and second-order stationary spatial fluctuations $\mathbf{v}'(\mathbf{x}, t)$ [LT^{-1}] about the mean that have an expected value of zero:

$$\mathbf{v}(\mathbf{x}, t) = \langle \mathbf{v}(t) \rangle + \mathbf{v}'(\mathbf{x}, t). \tag{4.10}$$

Thus, the transport equation 4.7 can be written as:

$$\frac{\partial c}{\partial t} + \left(\langle \mathbf{v} \rangle + \mathbf{v}'\right) \cdot \nabla c - \nabla \cdot (\mathbf{D} \nabla c) = 0. \tag{4.11}$$

If we assume a uniform porosity and a quasi-steady-state flow field without internal sources and sinks, the velocity field is non-divergent:

$$\nabla \cdot \mathbf{v} = 0 \, \forall t. \tag{4.12}$$

With a uniform mean velocity $\langle \mathbf{v} \rangle$, the velocity fluctuations must have zero divergence, too:

$$\nabla \cdot \mathbf{v}' = 0 \, \forall t. \tag{4.13}$$

We consider the following special case with uniform-in-the-mean forward movement into direction x_1 until a time T of flow reversal, from which on the spatial distribution of velocity is exactly opposite of the original distribution:

$$\langle v_1(t)\rangle = \begin{cases} \bar{v}_0 & \text{if } t \leq T \\ -\bar{v}_0 & \text{if } t > T \end{cases}, \qquad \langle v_2(t)\rangle = \langle v_3(t)\rangle = 0 \; \forall t, \tag{4.14}$$

$$\mathbf{v}'(t) = \begin{cases} \mathbf{v}'_0(\mathbf{x}) & \text{if } t \leq T \\ -\mathbf{v}'_0(\mathbf{x}) & \text{if } t > T \end{cases}, \tag{4.15}$$

where $\bar{v}_0$ [LT^{-1}] is the mean velocity of the forward motion, being strictly oriented into direction x_1, and $\mathbf{v}'_0(\mathbf{x})$ [LT^{-1}] is the auto-correlated velocity fluctuation about the mean velocity in the forward motion.

Our model includes three time scales of transport: The advective time scale τ_a, which we use to make times non-dimensional, and the diffusive time scales in horizontal and vertical direction $\tau_{D,h}$ and $\tau_{D,v}$ [T]. They are given as (Attinger et al., 1999, e.g.):

$$\tau_a = \lambda_h / \bar{v}_0 \tag{4.16}$$

$$\tau_{D,h} = \lambda_h^2 / D \tag{4.17}$$

$$\tau_{D,v} = \lambda_v^2 / D \tag{4.18}$$

The ratio of τ_a and $\tau_{D,h}$ yields the Péclet number as defined in equation 2.7

4.2.2 Spatial Moments

The concentration fields are characterized by their zeroth, first, second raw and second central moments, $m_0\left(c\left(\mathbf{x},t\right)\right)$ [M], $\mathbf{m}_{\mathbf{x}}\left(c\left(\mathbf{x},t\right)\right)$ [ML], $\mathbf{M}_{\mathbf{x}\otimes\mathbf{x}}\left(c\left(\mathbf{x},t\right)\right)$ [ML^2], and $\mathbf{M}^c_{\mathbf{x}\otimes\mathbf{x}}\left(c\left(\mathbf{x},t\right)\right)$ [ML^2], which are functionals of the concentration field $c\left(\mathbf{x},t\right)$ defined by:

$$m_0\left(c\left(\mathbf{x},t\right)\right) = \int_{V_\infty} c\left(\mathbf{x},t\right) d\mathbf{x}, \tag{4.19}$$

$$\mathbf{m}_{\mathbf{x}}\left(c\left(\mathbf{x},t\right)\right) = \int_{V_\infty} \mathbf{x} c\left(\mathbf{x},t\right) d\mathbf{x}, \tag{4.20}$$

$$\mathbf{M}_{\mathbf{x}\otimes\mathbf{x}}\left(c\left(\mathbf{x},t\right)\right) = \int_{V_\infty} \mathbf{x}\otimes\mathbf{x} c\left(\mathbf{x},t\right) d\mathbf{x}, \tag{4.21}$$

$$\mathbf{M}^c_{\mathbf{x}\otimes\mathbf{x}}\left(c\left(\mathbf{x},t\right)\right) = \mathbf{M}_{\mathbf{x}\otimes\mathbf{x}}\left(c\left(\mathbf{x},t\right)\right) - \frac{\mathbf{m}_{\mathbf{x}}\left(c\left(\mathbf{x},t\right)\right)\otimes\mathbf{m}_{\mathbf{x}}\left(c\left(\mathbf{x},t\right)\right)}{m_0\left(c\left(\mathbf{x},t\right)\right)}, \tag{4.22}$$

in which $\otimes$ denotes the matrix product of two vectors.

The zeroth spatial moment $m_0\left(c\left(\mathbf{x},t\right)\right)$ is the solute mass in the total domain, $\mathbf{m}_{\mathbf{x}}\left(c\left(\mathbf{x},t\right)\right)/m_0\left(c\left(\mathbf{x},t\right)\right)$ [L] describes the position vector of the plume's center of gravity, and $\mathbf{M}^c_{\mathbf{x}\otimes\mathbf{x}}\left(c\left(\mathbf{x},t\right)\right)/m_0\left(c\left(\mathbf{x},t\right)\right)$ [L^2] the spatial spread of the solute cloud about its center of gravity. Half the rate of change of the normalized second central spatial moments operationally defines the dispersion tensor of the entire plume.

Following Kitanidis (1988) and Dentz et al. (2000), we distinguish between the matrix of second central moments of the expected concentration $\langle c\left(\mathbf{x},t\right)\rangle$, further on denoted ensemble moments, and the expected value of the second central moments, further on denoted effective moments, defined as:

$$\mathbf{M}^{c}_{\mathbf{x}\otimes\mathbf{x}}\left(\langle c\left(\mathbf{x},t\right)\rangle\right)=\mathbf{M}_{\mathbf{x}\otimes\mathbf{x}}\left(\langle c\left(\mathbf{x},t\right)\rangle\right)-\frac{\mathbf{m}_{\mathbf{x}}\left(\langle c\left(\mathbf{x},t\right)\rangle\right)\otimes\mathbf{m}_{\mathbf{x}}\left(\langle c\left(\mathbf{x},t\right)\rangle\right)}{m_0\left(c\left(\mathbf{x},t\right)\right)}, \tag{4.23}$$

$$\langle\mathbf{M}^{c}_{\mathbf{x}\otimes\mathbf{x}}\left(c\left(\mathbf{x},t\right)\right)\rangle=\mathbf{M}^{c}_{\mathbf{x}\otimes\mathbf{x}}\left(\langle c\left(\mathbf{x},t\right)\rangle\right)-\frac{\langle\mathbf{m}_{\mathbf{x}}\left(c\left(\mathbf{x},t\right)\right)\otimes\mathbf{m}_{\mathbf{x}}\left(c\left(\mathbf{x},t\right)\right)\rangle}{m_0\left(c\left(\mathbf{x},t\right)\right)}, \tag{4.24}$$

in which we have already made use of the zeroth moment $m_0\left(c\left(\mathbf{x},t\right)\right)$ of a conservative compound being constant when considering non-divergent flow in an infinite domain.
$\langle\mathbf{m}_{\mathbf{x}}\left(c\left(\mathbf{x},t\right)\right)\otimes\mathbf{m}_{\mathbf{x}}\left(c\left(\mathbf{x},t\right)\right)\rangle$ [$\mathrm{M^2L^2}$] is the covariance matrix of the first moments, expressing the uncertainty of tagging the spatial center of the solute plume.

We perform the spatial Fourier transformation of the concentration using ordinary frequencies:

$$\tilde{c}\left(\mathbf{s},t\right)=\int_{V_\infty}c\left(\mathbf{x},t\right)\exp\left(-2\pi i\mathbf{x}\cdot\mathbf{s}\right)d\mathbf{x}, \tag{4.25}$$

where $\tilde{c}\left(\mathbf{s},t\right)$ [M] is the Fourier transform of $c\left(\mathbf{x},t\right)$, $\mathbf{s}$ [$\mathrm{L^{-1}}$] is the vector of spatial frequencies, and i with the property $i^2=-1$ is the imaginary unit. The zeroth, first, and second spatial moments of $c\left(\mathbf{x},t\right)$ relate to the Fourier transform $\tilde{c}\left(\mathbf{s},t\right)$ of the concentration by:

$$m_0\left(c\left(\mathbf{x},t\right)\right)=\tilde{c}\left(\mathbf{0},t\right), \tag{4.26}$$

$$\mathbf{m}_{\mathbf{x}}\left(c\left(\mathbf{x},t\right)\right)=\frac{i}{2\pi}\,\nabla_{\mathbf{s}}\tilde{c}\left(\mathbf{s},t\right)|_{\mathbf{s}=\mathbf{0}}, \tag{4.27}$$

$$\mathbf{M}_{\mathbf{x}\otimes\mathbf{x}}\left(c\left(\mathbf{x},t\right)\right)=-\frac{1}{4\pi^2}\,\nabla_{\mathbf{s}}\otimes\nabla_{\mathbf{s}}\tilde{c}\left(\mathbf{s},t\right)|_{\mathbf{s}=\mathbf{0}}. \tag{4.28}$$

4.2.3 Dimensionless Expressions

Scaling the spatial coordinates with λ_h and time with $\tau_a=\lambda_h/\bar{v}_0$ leads to the dimensionless transport equation:

$$\frac{\partial c_*}{\partial t_*}+\left(\mathbf{e}_1+\mathbf{v}'_{0*}(t_*)\right)\cdot\nabla_* c_*-\nabla_*\cdot\left(\boldsymbol{\mathcal{E}}\nabla_* c_*\right)=0\qquad\text{if } t_*\le T_*, \tag{4.29}$$

$$\frac{\partial c_*}{\partial t_*}-\left(\mathbf{e}_1+\mathbf{v}'_{0*}(t_*)\right)\cdot\nabla_* c_*-\nabla_*\cdot\left(\boldsymbol{\mathcal{E}}\nabla_* c_*\right)=0\qquad\text{if } t_*>T_*, \tag{4.30}$$

$$c_*(\mathbf{x}_*,0)=\delta(\mathbf{x}_*), \tag{4.31}$$

in which $c_*=c\lambda_h^3/m_0$, $\mathbf{v}'_{0*}=\mathbf{v}'_0/\bar{v}_0$, $\mathbf{x}_*=\mathbf{x}/\lambda_h$, and $t_*=t/\tau_a$ are the dimensionless concentration, velocity fluctuations, spatial coordinates, and time, respectively, $\mathbf{e}_1=\left[1,0,0\right]^T$ is the unit vector in direction x_1, and $\boldsymbol{\mathcal{E}}=\mathbf{D}/\left(\lambda_h\bar{v}_0\right)$ is a dimensionless dispersion tensor, that is, a matrix of inverse Péclet numbers. For the case of isotropic local dispersion, $\mathcal{E}=D/\left(\lambda_h\bar{v}_0\right)=1/Pe$ is a scalar. For the case of a full local dispersion tensor, using the matrix $\boldsymbol{\mathcal{E}}$ of inverse Péclet numbers avoids the issue of inverting the local-dispersion tensor.

Like the states and properties in the spatial domain, the Fourier transformed concentration $\tilde{c}\left(\mathbf{s},t\right)$, the frequency vector $\mathbf{s}$, and the spatial moments are made

dimensionless by $\tilde{c}_* = \tilde{c}/m_0$,$\mathbf{s}_* = \mathbf{s}\lambda_h$, $m_{0*} = 1$, $\mathbf{m}_{\mathbf{x}*} = \mathbf{m}_\mathbf{x}/(m_0\lambda_h)$, $\mathbf{M}_{\mathbf{x}\otimes\mathbf{x}*} = \mathbf{M}_{\mathbf{x}\otimes\mathbf{x}}/(m_0\lambda_h^2)$, and $\mathbf{M}^c_{\mathbf{x}\otimes\mathbf{x}*} = \mathbf{M}^c_{\mathbf{x}\otimes\mathbf{x}}/(m_0\lambda_h^2)$. From here on, we drop the asterisks for brevity.

4.2.4 Evolution of Spatial Moments according to Linear Stochastic Theory

The following analysis adapts the derivation of Dentz et al. (2000) for effective and ensemble dispersion in second-order stationary velocity fields to the case of flow reversal at time T.

Concentration Fields

In the spectral domain, the dimensionless advection-dispersion equations for a point-like injection during forward and backward motion and the initial condition, equations 4.29-4.31, are:

$$\frac{\partial\tilde{c}\left(\mathbf{s},t\right)}{\partial t} + \left(4\pi^2\mathbf{s}\cdot\left(\boldsymbol{\mathcal{E}}\mathbf{s}\right) + 2\pi i\mathbf{e}_1\cdot\mathbf{s}\right)\tilde{c}\left(\mathbf{s},t\right) + 2\pi i\int\limits_{V_\infty}\mathbf{s}\cdot\tilde{\mathbf{v}}_0'\left(\mathbf{s}'\right)\tilde{c}\left(\mathbf{s}-\mathbf{s}',t\right)d\mathbf{s}' = 0 \text{ if } t\leq T, \tag{4.32}$$

$$\frac{\partial\tilde{c}\left(\mathbf{s},t\right)}{\partial t} + \left(4\pi^2\mathbf{s}\cdot\left(\boldsymbol{\mathcal{E}}\mathbf{s}\right) - 2\pi i\mathbf{e}_1\cdot\mathbf{s}\right)\tilde{c}\left(\mathbf{s},t\right) - 2\pi i\int\limits_{V_\infty}\mathbf{s}\cdot\tilde{\mathbf{v}}_0'\left(\mathbf{s}'\right)\tilde{c}\left(\mathbf{s}-\mathbf{s}',t\right)d\mathbf{s}' = 0 \text{ if } t> T, \tag{4.33}$$

$$\tilde{c}(\mathbf{s},0) = 1, \tag{4.34}$$

in which all variables with a tilde are Fourier transforms of the respective variables in the spatial domain.

Equations 4.32 & 4.33 are inhomogeneous first-order differential equations (ODE) that can be solved by the following recursive integrals:

$$\tilde{c}\left(\mathbf{s},t\right) = \tilde{c}_0\left(\mathbf{s},t\right) - 2\pi i\int\limits_0^t\frac{\tilde{c}_0\left(\mathbf{s},t\right)}{\tilde{c}_0\left(\mathbf{s},t'\right)}\int\limits_{V_\infty}\mathbf{s}\cdot\tilde{\mathbf{v}}_0'\left(\mathbf{s}'\right)\tilde{c}\left(\mathbf{s}-\mathbf{s}',t'\right)d\mathbf{s}'dt' \text{ if } t\leq T, \tag{4.35}$$

$$\begin{aligned}\tilde{c}\left(\mathbf{s},t\right) = \tilde{c}_0\left(\mathbf{s},t\right) &- 2\pi i\int\limits_0^T\frac{\tilde{c}_0\left(\mathbf{s},t\right)}{\tilde{c}_0\left(\mathbf{s},t'\right)}\int\limits_{V_\infty}\mathbf{s}\cdot\tilde{\mathbf{v}}_0'\left(\mathbf{s}'\right)\tilde{c}\left(\mathbf{s}-\mathbf{s}',t'\right)d\mathbf{s}'dt'\\ &+ 2\pi i\int\limits_T^t\frac{\tilde{c}_0\left(\mathbf{s},t\right)}{\tilde{c}_0\left(\mathbf{s},\tau\right)}\int\limits_{V_\infty}\mathbf{s}\cdot\tilde{\mathbf{v}}_0'\left(\mathbf{s}'\right)\tilde{c}\left(\mathbf{s}-\mathbf{s}',\tau\right)d\mathbf{s}'d\tau \qquad \text{if } t> T,\end{aligned} \tag{4.36}$$

in which the homogeneous solution $\tilde{c}_0\left(\mathbf{s},t\right)$ reads as:

$$\tilde{c}_0\left(\mathbf{s},t\right) = \exp\left(-\left(A+B\right)t\right) \qquad \text{if } t\leq T, \tag{4.37}$$

$$\tilde{c}_0\left(\mathbf{s},t\right) = \exp\left(-At - B\left(2T-t\right)\right) \text{if } t> T, \tag{4.38}$$

with the coefficients A and B related to local dispersion and mean advection:

$$A = 4\pi^2 \mathbf{s} \cdot (\boldsymbol{\mathcal{E}} \mathbf{s}), \tag{4.39}$$

$$B = 2\pi i \mathbf{e}_1 \cdot \mathbf{s}. \tag{4.40}$$

Substituting equation 4.35 into itself creates a series expansion of the concentration field which is the centerpiece in the approach of Dentz et al. (2000):

$$\tilde{c}(\mathbf{s}, t \leq T) = \tilde{c}_0(\mathbf{s}, t \leq T) + \tilde{c}_1(\mathbf{s}, t \leq T) + \tilde{c}_2(\mathbf{s}, t \leq T) + H.O.T., \tag{4.41}$$

in which $\tilde{c}_1$ and $\tilde{c}_2$ are the first- and second-order terms and $H.O.T.$ denotes higher-order terms. The expressions for $\tilde{c}_1$ and $\tilde{c}_2$ are given in Appendix B.1 as well as the derivation of the series expansion of the concentration field for $t > T$ and the expressions for the second-order expected concentrations which are the basis for the moment calculations.

Spatial Moments for $t \leq T$

Dentz et al. (2000) derived analytical expressions for the ensemble and effective dispersion tensors $\mathbf{D}_{ens}(t \leq T)$ and $\mathbf{D}_{eff}(t \leq T)$ in the spectral domain. The ensemble dispersion tensor is related to second central ensemble moment by

$$\mathbf{D}_{ens} = \frac{1}{2m_0} \frac{d\mathbf{M}^c_{\mathbf{x}\otimes\mathbf{x}}(\langle c(\mathbf{x}, t)\rangle)}{dt}, \tag{4.42}$$

and the effective dispersion tensor accordingly.

The second central ensemble moments for $t \leq T$ are given in perturbation theory by:

$$\mathbf{M}^c_{\mathbf{x}\otimes\mathbf{x}}(\langle c(\mathbf{x}, t \leq T)\rangle) = 2\boldsymbol{\mathcal{E}} t + 2 \int_{V_\infty} \mathbf{S}_{\mathbf{v}'_0\otimes\mathbf{v}'_0}(\mathbf{s}) \frac{(A-B)t + \exp((-A+B)t) - 1}{(A-B)^2} d\mathbf{s}. \tag{4.43}$$

The second central effective moments $\langle \mathbf{M}^c_{\mathbf{x}\otimes\mathbf{x}}(c(\mathbf{x}, t \leq T))\rangle$ are given by subtracting the covariance matrix of first moments (equation 4.44) from equation 4.43:

$$\left\langle \mathbf{m}'_{\mathbf{x}}(c(\mathbf{x}, t \leq T)) \otimes \mathbf{m}'_{\mathbf{x}}(c(\mathbf{x}, t \leq T)) \right\rangle = \int_{V_\infty} \mathbf{S}_{\mathbf{v}'_0\otimes\mathbf{v}'_0}(\mathbf{s}) \frac{\exp(-2At) - \exp(-At + Bt) - \exp(-At - Bt) + 1}{A^2 - B^2} d\mathbf{s}. \tag{4.44}$$

For a derivation of the expressions, the reader is referred to Dentz et al. (2000) or to Appendix B.2 where the spatial moments for $t > T$ are derived following the same steps.

Spatial Moments for $t > T$

The matrix of second central ensemble moments for $t > T$ reads as (c.f. Appendix B.2):

$$\mathbf{M}^{c}_{\mathbf{x}\otimes\mathbf{x}}\left(\langle c(\mathbf{x},t>T)\rangle\right)=2\boldsymbol{\mathcal{E}}t+2\int\limits_{V_\infty}\mathbf{S}_{\mathbf{v}_0'\otimes\mathbf{v}_0'}\left(\mathbf{s}\right)\left(\frac{\left(A-B\right)T+\exp\left(-AT+BT\right)-1}{\left(A-B\right)^2}\right.$$
$$-\frac{\exp\left(-At+B\left(2T-t\right)\right)-\exp\left(-\left(A+B\right)\left(t-T\right)\right)-\exp\left(-AT+BT\right)+1}{A^2-B^2}$$
$$\left.+\frac{\left(t-T\right)\left(A+B\right)+\exp\left(-\left(A+B\right)\left(t-T\right)\right)-1}{\left(A+B\right)^2}\right)d\mathbf{s}. \quad (4.45)$$

The covariance matrix of the first moments is given by (for the derivation see Appendix B.2):

$$\left\langle\mathbf{m}_{\mathbf{x}}'\left(c\left(\mathbf{x},t>T\right)\right)\otimes\mathbf{m}_{\mathbf{x}}'\left(c\left(\mathbf{x},t>T\right)\right)\right\rangle$$
$$=\int\limits_{V_\infty}\mathbf{S}_{\mathbf{v}_0'\otimes\mathbf{v}_0'}\left(\mathbf{s}\right)\left(\frac{\exp\left(\text{-}2AT\right)\text{-}\exp\left(\text{-}AT\text{+}BT\right)\text{-}\exp\left(\text{-}AT\text{-}BT\right)\text{+}1}{A^2\text{-}B^2}\right.$$
$$\text{-}\frac{\exp\left(\text{-}A\left(T\text{+}t\right)\text{-}B\left(T\text{-}t\right)\right)\text{-}\exp\left(\text{-}2AT\right)\text{-}\exp\left(\text{-}At\text{-}B\left(2T\text{-}t\right)\right)+\exp\left(\text{-}AT\text{-}BT\right)}{\left(A\text{-}B\right)^2}$$
$$\text{-}\frac{\exp\left(\text{-}A\left(T\text{+}t\right)\text{+}B\left(T\text{-}t\right)\right)\text{-}\exp\left(\text{-}2AT\right)\text{-}\exp\left(\text{-}At\text{+}B\left(2T\text{-}t\right)\right)+\exp\left(\text{-}AT\text{+}BT\right)}{\left(A\text{+}B\right)^2}$$
$$\left.+\frac{\exp\left(\text{-}2At\right)\text{-}\exp\left(\text{-}A\left(T\text{+}t\right)\text{-}B\left(T\text{-}t\right)\right)\text{-}\exp\left(\text{-}A\left(T\text{+}t\right)\text{+}B\left(T\text{-}t\right)\right)+\exp\left(\text{-}2AT\right)}{A^2\text{-}B^2}\right)d\mathbf{s}. \quad (4.46)$$

The matrix of second central effective moments $\langle\mathbf{M}^{c}_{\mathbf{x}\otimes\mathbf{x}}\left(c\left(\mathbf{x},t>T\right)\right)\rangle$ for $t>T$ is then given by subtracting equation 4.46 from equation 4.45, according to equation 4.24.

4.3 Application to Periodic Media

Our theoretical results involve integrals for which we do not have closed-form solutions. Thus, for the evaluation of the first-order analytical results, we discretize the periodic covariance function $C\left(\mathbf{d}\right)$ (equation 2.11) with a dimensionless grid spacing of $\Delta d_1\times\Delta d_2\times\Delta d_3$ and obtain the power spectrum $S_{Y'Y'}\left(\mathbf{s}\right)$ of log-conductivity fluctuations by discrete Fourier transformation using the FFTW-library implemented in Matlab (http://www.fftw.org). Because the heterogeneity-related contributions to the second central moments scale with σ_Y^2, it is sufficient fo perform the calculations with a single value of unity. The dimensionless velocity spectrum $\mathbf{S}_{\mathbf{v}_0'\otimes\mathbf{v}_0'}\left(\mathbf{s}\right)$ is then computed as (Dagan, 1989):

$$\mathbf{S}_{\mathbf{v}_0'\otimes\mathbf{v}_0'}\left(\mathbf{s}\right)=\left(\mathbf{e}_1-\frac{s_1}{\mathbf{s}\cdot\mathbf{s}}\mathbf{s}\right)\otimes\left(\mathbf{e}_1-\frac{s_1}{\mathbf{s}\cdot\mathbf{s}}\mathbf{s}\right)S_{Y'Y'}\left(\mathbf{s}\right), \quad (4.47)$$

which is substituted into Equations 4.43 and 4.45. The integrations in these equations are performed by summation over the discrete values of $\mathbf{s}$. The limits of the moment expressions for $\mathbf{s}\rightarrow\mathbf{0}$, which are needed for the computation of the various integrals, are given in Appendix B.3.

For the numerical simulations of flow and transport, two million particle pairs are injected via 50 evenly spaced injection planes perpendicular to the mean direction of flow. Within those planes, the starting locations are evenly distributed over the cross-section of the unit cell. The particles are tracked forward until $t = T$ and subsequently tracked backward until $t = 2T$, which is implemented by simply changing the sign of the velocity field. Injecting the particles distributed throughout the model domain rather than at the same location makes them sampling the flow variability of a single realization of the log-K field in a much more representative way. To remain in the framework of a point injection, the spatial moments are calculated from the particle displacements rather than spatial coordinates. Consequently, ergodicity can be achieved with fewer realizations. We average our numerical results over 10 realizations of the log-K field.

The mean longitudinal displacement and the ensemble second central moments of longitudinal displacements are computed by:

$$m_{x_1}\left(\langle c\left(\mathbf{x},t\right)\rangle\right) \approx \frac{1}{n_p}\sum_{i=1}^{n_p}\frac{1}{2}\left(x_{1,i,1}(t)+x_{1,i,2}(t)\right)-x_{1,i,1}(0), \tag{4.48}$$

$$M^c_{x_1x_1}\left(\langle c\left(\mathbf{x},t\right)\rangle\right) \approx \frac{1}{n_p-1}\sum_{i=1}^{n_p}\left(\frac{1}{2}\left(x_{1,i,1}(t)+x_{1,i,2}(t)\right)-x_{1,i,1}(0)-m_{x_1}(t)\right)^2, \tag{4.49}$$

in which $x_{1,i,j}(t)$ is the x_1-coordinate of the j-th particle starting at the i-th starting location. The effective second central moment of longitudinal displacements is evaluated as the two-particle semi-variogram of longitudinal displacements, which is why the particles are injected in pairs:

$$\left\langle M^c_{x_1x_1}\left(c\left(\mathbf{x},t\right)\right)\right\rangle \approx \frac{1}{n_p}\sum_{i=1}^{n_p}\frac{1}{2}\left(x_{1,i,1}(t)-x_{1,i,2}(t)\right)^2. \tag{4.50}$$

The standard configuration of the periodic unit cell, as described in Section 2.2, is adjusted to study the influence of different parameters onto the reversibility of dispersion. For the standard case, the log-K field is characterized by a variance of log-K fluctuations $\sigma_Y^2 = 0.3$ and is isotropic, that is, the vertical-to-horizontal anisotropy ratio $e = \lambda_v/\lambda_h$ equals unity.

In all calculations, we assume local dispersion to be isotropic. In the standard case, a Péclet number of $Pe = 1000$ is used, flow reversal takes place at $T = 10\tau_a$, and the spatial moments are calculated in a dimensionless temporal resolution of $dt = 0.1$. the anisotropic fields are generated by flattening the unit cell and thus the grid cells while keeping the number of cells constant.

The calculation of characteristic times requires very large domains and is exclusively performed by means of the analytical solution, for $\sigma_Y^2 = 1$ and $e = 1$. In order to keep the computational effort at a reasonable level, the model discretization normal to the mean direction of flow is altered to 100×100 cells of a spatial resolution of $\Delta d_2 = \Delta d_3 = 0.4\lambda_h$. In the direction of mean flow, we keep the spatial resolution of $\Delta d_1 = 0.1\lambda h$ and calculate the required length of the periodic unit cell as $L_1 = 2T/\tau_a$.

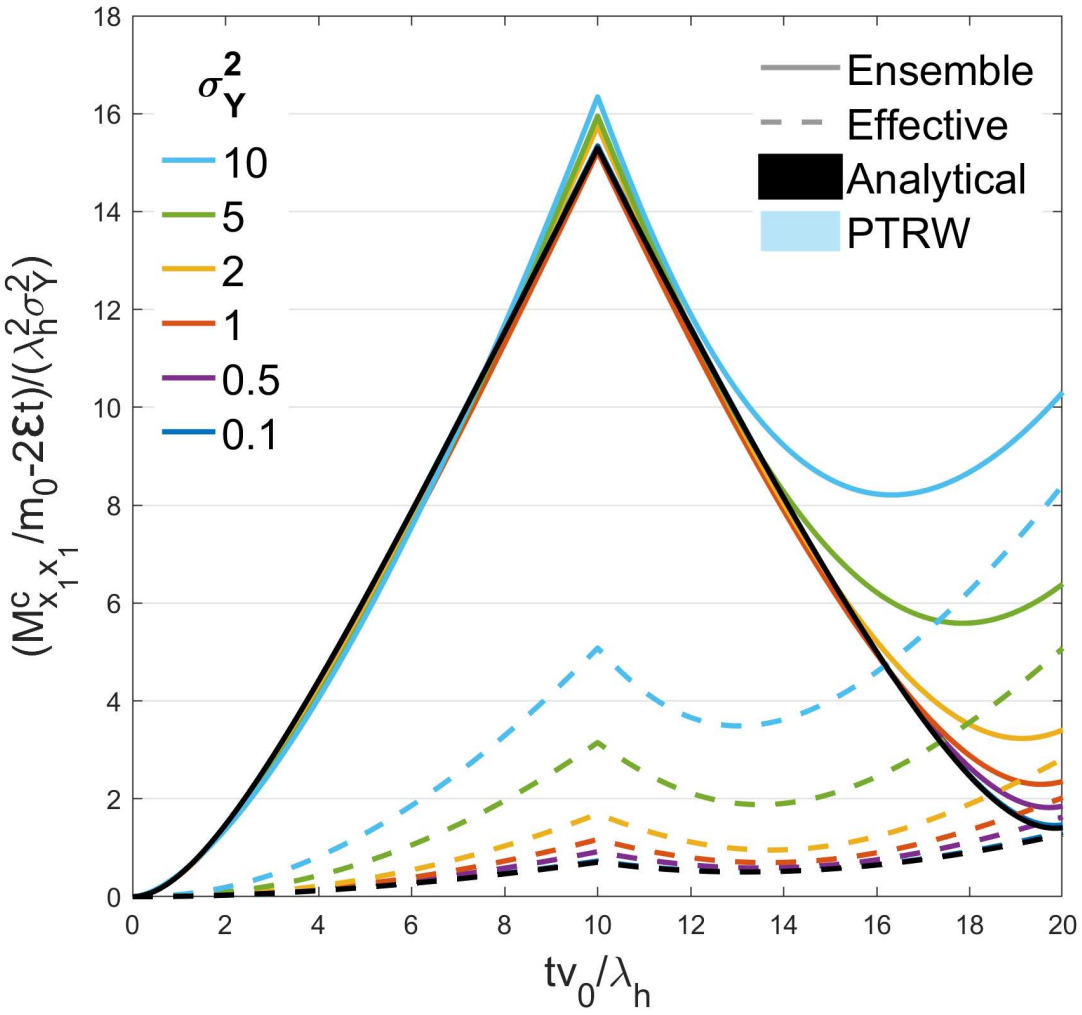

FIGURE 4.2: Analytical solution (black) and numerical results (colored) of the second central ensemble and effective spatial moments for different log-K variances σ_Y^2 after subtracting the purely diffusive contribution $2\mathcal{E}t$ scaled by σ_Y^2 for $Pe = 1000$ and $e = 1$.

4.4 Results and Discussion

4.4.1 Principle of Partial Reversibility

Figure 4.2 shows the ensemble and effective second central moments calculated analytically and numerically as function of time for different values of the log-conductivity variance σ_Y^2. Until flow reversal, both ensemble and effective second central moments follow the well-known behavior for a uniform-in-the-mean velocity field with a transition from a quadratic to a linear increase with time. Upon flow reversal, the ensemble and effective moments decrease until they reach a minimum after which they increase again. For effective moments, this happens much quicker than for ensemble moments. At $t = 2T$, ensemble and effective second central moments are much more similar than at $t = T$, but they still differ: The effective moments reach approximately 90% of the ensemble moments for low values of σ_Y^2 and approximately 80% for high values of σ_Y^2.

Dispersion becomes increasingly irreversible with increasing σ_Y^2 because stronger heterogeneity pronounces the effect of spreading by increasing the surface area of the plume over which transverse diffusion acts. However, with increasing σ_Y^2, there

is a decreasing agreement between the analytical and numerical results. While the first-order analytical solution scales strictly linearly with σ_Y^2, the numerical second central ensemble moments upon flow reversal and the effective moments increase more than linearly with σ_Y^2.

As both ensemble and effective moments undergo a phase of shrinking upon flow reversal, it is evident that they both measure a mixture of advective spreading and diffusive mixing. A true metric of mixing would not decrease upon flow reversal as mixing is an irreversible process. Nonetheless, the two types of second central moments are qualitatively different. The ensemble moments are dominated by spreading (at the given $\mathcal{E}$), while the effective moments are dominated by mixing. In the point-injection framework, effective second central moments begin to incorporate spreading once the volume of the plume has increased sufficiently by diffusion for it to experience different advective velocities. This explains why the effective second central moments are influenced by flow reversal. However, the plumes in individual realizations are much smaller than the ensemble-averaged plume. Upon flow reversal, consequently, a shorter time is needed to decorrelate the velocity fluctuations experienced within the individual plumes, implying that diffusion takes over earlier as the dominant mechanism of plume expansion in reversed flow.

Since the ensemble and effective moments do not reach the same value at $t = 2T$, the moments at this time cannot be considered representative for the mixing contribution in unidirectional transport for a duration of $2T$. Spreading and mixing are interdependent and apparently cannot be completely separated by mechanical flow reversal.

The minimum in the moments during backward flow marks the time point at which advective memory (leading to a decrease in spreading during backward flow) and the exploration of new travel paths by diffusion are in balance. We denote the time period between $t = T$ and the time at which the moments reach their minimum in the reversed flow field the shrinking time t_s. For $T < t < t_s$, the advective memory is still so strong that the plume shrinks in size, whereas for times $t > t_s$, diffusion has destroyed advective memory to an extent that the plume expands again. The definition of the shrinking time applies to both ensemble and effective moments. We will discuss the computed values in Section 4.4.4 in detail.

The decreasing agreement between the analytical and numerical results with increasing σ_Y^2 is attributed to the limitations of linear stochastic theory, which is strictly valid only at the limit $\sigma_Y^2 \to 0$. However, in applications to unidirectional flow linear stochastic theory has been found valid for $\sigma_Y^2 \leq 1$ (Gutjahr et al., 1978; Dagan et al., 2003). In the present case with flow reversal, the analytical solution substantially underestimates solute spreading during backward flow already for cases of very small heterogeneity while the spreading in the phase of forward flow is satisfactorily reproduced for all considered degrees of heterogeneity.

4.4.2 Influence of Diffusion Strength on Reversibility

We examine the influence of changing the diffusion strength onto the reversibility of dispersion by considering cases with different Péclet numbers Pe and cases with different vertical-to-horizontal anisotropy ratios e. Decreasing the latter corresponds to increasing the diffusion strength because in features of high oblateness, particles reach zones of a significantly different hydraulic conductivity already at a short transverse diffusion distance. For the case of forward motion, already Dentz et al. (2000) have shown that effective dispersion catches up faster with ensemble dispersion when the vertical-to-horizontal anisotropy ratio e is smaller.

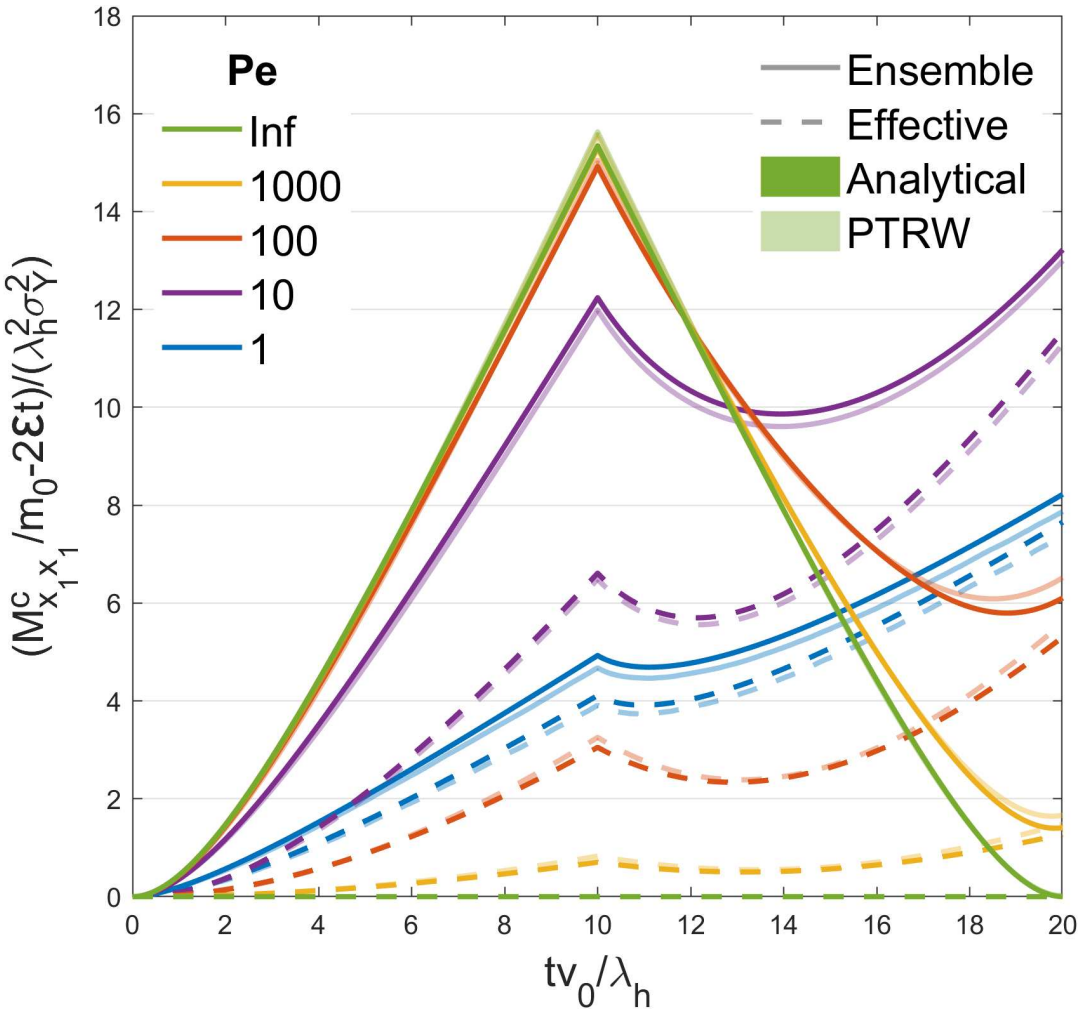

FIGURE 4.3: Analytical solution (bold colors) and numerical results (faded colors) for the second central ensemble and effective spatial moments for different local Péclet numbers Pe scaled by σ_Y^2 without the purely diffusive contribution $2\mathcal{E}t$ for $\sigma_Y^2 = 0.3$ and $e = 1$.

Figure 4.3 shows the influence of Pe on the time-dependent second central moments after subtracting the purely diffusive contribution $2\mathcal{E}t$ in equations 4.43 & 4.45. In the purely advective case ($Pe \to \infty$, or $\mathcal{E} = 0$), ensemble spreading is completely reversible, while the effective moments remain at zero, because in the absence of diffusion the considered point plume will never expand, and will thus be subject to a single velocity at any given time. In the other extreme case of $Pe = 1$ shown in Figure 4.3 (equal influence of diffusion and advection over travel distances of one integral scale of log-K), flow reversal has a very limited impact on the second central moments, as they increase again soon after the reversal and the ensemble and effective moments are almost identical. As a general trend, the smaller Pe, the closer to each other are ensemble and effective moments, the smaller are the ensemble moments (after subtracting the purely diffusive contribution) at $t = T$, the bigger are the effective moments at $t = T$, and the bigger are both moments at $t = 2T$.

Figure 4.4 shows the influence of the vertical-to-horizontal anisotropy ratio e on the ensemble and effective moments for the analytical solution and numerical results. Decreasing e has the same effect as decreasing Pe. The lower e, the higher are the effective second central moments at all times and the ensemble second central

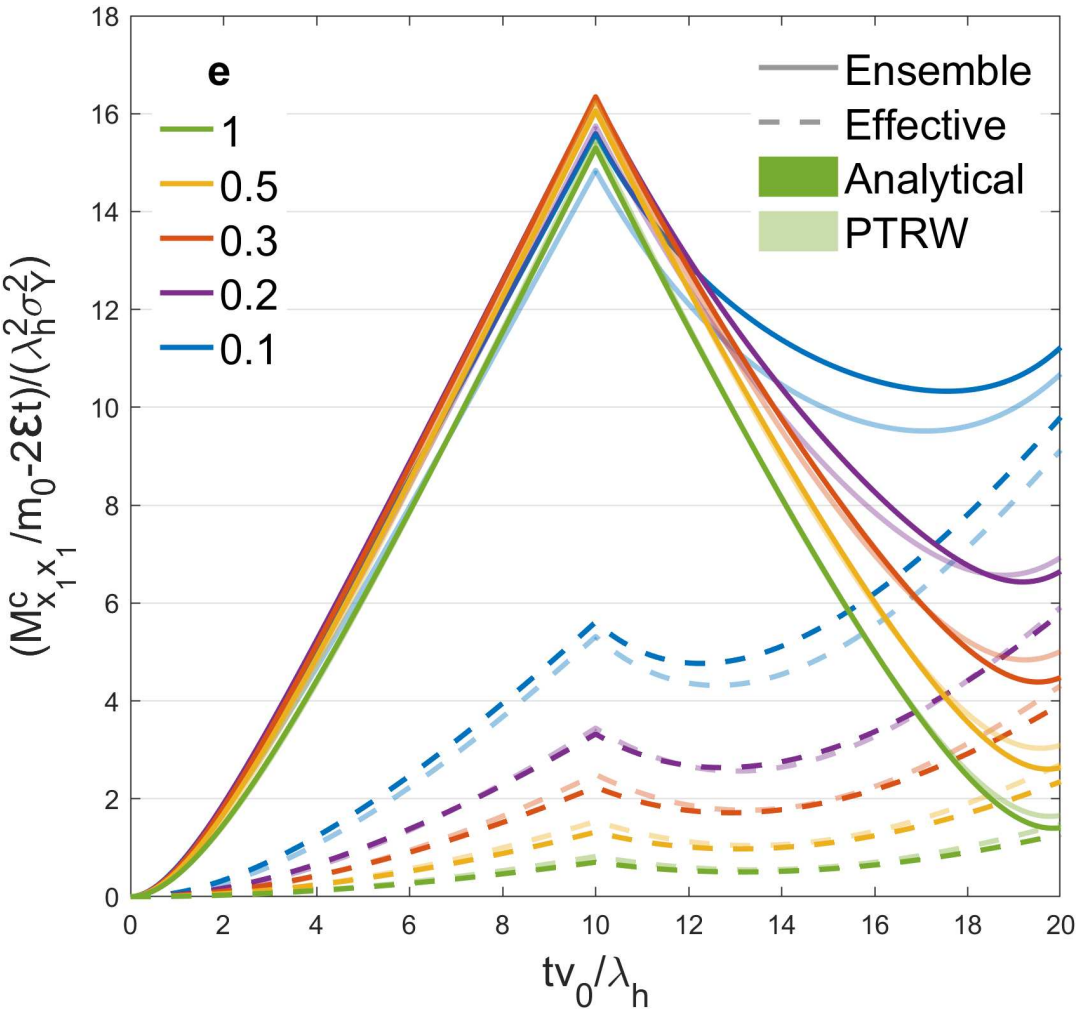

FIGURE 4.4: Analytical solution (bold colors) and numerical results (faded colors) of the second central ensemble and effective spatial moments after subtracting the purely diffusive contribution $2\mathcal{E}t$ and scaled by σ_Y^2 for different vertical-to-horizontal anisotropy ratios e for $\sigma_Y^2 = 0.3$ and $Pe = 1000$.

moments at $t = 2T$. This may be explained by diffusion destroying the advective memory so that dispersion becomes less reversible when diffusion get stronger in comparison to advection. The dimensionless diffusive time scales are $\tau_{D,h} = Pe$ in the horizontal and $\tau_{D,v} = e^2 Pe$ in the vertical direction. For diffusive mixing in heterogeneous media the transverse directions are more important than the vertical one. Hence, small values of e imply shorter mixing times, and have the same effect as smaller values of Pe (Dentz et al., 2000, sec. 3.2.3). In unidirectional movement, stronger diffusion leads to a decrease in the second central ensemble moments because transverse diffusion restricts advective spreading Andričević (1998).

At extremely small Péclet numbers the second central ensemble moments are larger than at small Péclet numbers also in forward movement, because the longitudinal diffusion is so strong that the heterogeneity becomes irrelevant. Note that our smallest Péclet numbers are not representative for natural groundwater flow in heterogeneous formations. To obtain very small Péclet numbers one needs either very low velocities or very small integral scales, which is more typical for pore-scale rather than field-scale dispersion (Huysmans and Dassargues, 2005; Yew et al., 2013).

When considering ranges of Pe typical for transport in natural aquifers and for all values of e, the impact of diffusion on second central moments is much larger in backwards than in forward flow, which can be seen in the second central ensemble moments spanning over a much wider range in backward than in forward movement. An increasing impact of diffusion reduces the distance over which advective memory prevails. This memory is irrelevant in forward flow, whereas in reversed flow it causes the reversion of advective spreading. This reversion is hampered by diffusion-caused amnesia.

4.4.3 Influence of the Reversal Time T on Reversibility

Figure 4.5 shows the influence of the reversal time T on the second central ensemble moments at $t = 2T$, that is, at the time point when the plume's center of gravity has returned to its origin, for different Péclet numbers. The higher T, the higher are the second central moments at $t = 2T$ and therefore the less reversible is dispersion. This is so because longer travel times allow diffusion to destruct advective memory more efficiently.

For short reversal times, smaller Péclet numbers imply higher second central moments at $t = 2T$. However, for very long reversal times the relationship loses its monotonicity and the lines corresponding to different Péclet numbers are arranged according to their order in unidirectional movement (cf. difference in order from lowest to highest ensemble moment in Figure 4.3 between $t = T$ and $t = 2T$). The inset in Figure 4.5 exemplifies that the lines of different Pe do not simply converge but intersect, leading to a non-monotonous relationship between Pe and the second central ensemble moments at $t = 2T$. The change in order is complete once the reversal times exceed the time during which advective memory has any influence on the dispersion process for all Péclet numbers considered. Note that our simulation maximum of $T = 3000$ is not sufficient to reach this point. For these very large reversal times the asymptotic macrodispersive behavior is reached in backward motion before the plumes have returned to their origin. The relevant time is the setting time $t_{s,rev}$ introduced in the next section 4.4.4.

The considerations of the second central moments at $t = 2T$ for different Péclet numbers are of practical interest. Under the assumption that the second central spatial moments at $t = 2T$ can be related to the second central temporal moments at the starting plane upon flow reversal, a series of push-pull tracer experiments with different reversal times could be used to determine Pe.

4.4.4 Characteristic Times

Figure 4.6A shows the development of the second central ensemble moments with time for different reversal times for $Pe = 10$ and Figure 4.6B shows the corresponding ensemble dispersion coefficients, defined as half the rate of change of the second central ensemble moments. In both plots, we consider the time since flow reversal. In Figure 4.6A, the ensemble moments at the time of reversal are subtracted from the ensemble moments at all times because we want to concentrate on what is happening after flow reversal. The subsets of Figures 4.6A & 4.6B are enlargements focusing on the time shortly after the time of flow reversal. These subsets also illustrate the definition of the shrinking time t_{sh}, which is the duration between the time of flow reversal and the point at which the second central moments begin to increase again. Figure 4.6A shows this point as a minimum, and Figure 4.6B correspondingly where the ensemble dispersion coefficient is zero.

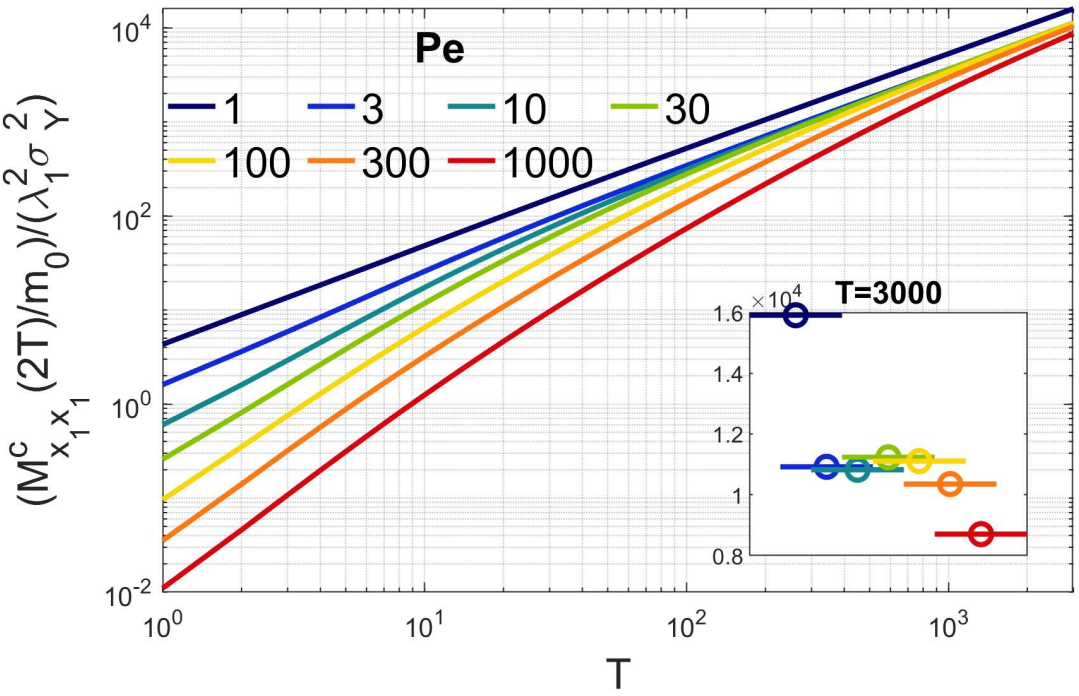

FIGURE 4.5: Second central ensemble moments at $t = 2T$ for different reversal times T and Péclet numbers, $\sigma_Y^2 = 1$, $e = 1$. The inset shows the second central ensemble moments at $t = 2T$ for the case of $T = 3000$, with symbols scattered horizontally to improve readability.

The shrinking time t_{sh} measures how long the reduction in spreading under reversed flow due to advective memory prevails over the diffusive destruction of memory making the plume explore parts of the velocity field that have not been explored in the forward motion.

Figure 4.6C shows the dependence of the shrinking time on the reversal time for ensemble and effective moments. Both shrinking times converge to the same asymptotic limit for large values of T. For small to intermediate values of the reversal time T, the shrinking time of the effective moments is smaller than that of the ensemble moments. The reversal time needed for the shrinking time to reach the asymptotic limit is considerably larger for the effective than for the ensemble moments. This behavior reflects that individual plumes originating from a point source need very long forward motion until they sample the full heterogeneity of the flow field in a representative manner. Only when this point is reached, the shrinking time upon flow reversal is independent of the time of forward motion. In comparison, the ensemble-averaged point-related plumes sample the full heterogeneity much quicker so that also the asymptotic shrinking time is reached in a setup with a smaller reversal time T.

As second characteristic time, we consider the setting time, which was introduced by Fiori (1996) for unidirectional flow as the time needed for the dispersion coefficient to reach 99% of its asymptotic value, which the latter authors used to define the beginning of the macrodispersive plume behavior. We distinguish between the setting time $t_{s,uni}$ for unidirectional flow and the setting time $t_{s,rev}$ after flow reversal in the reversed flow field:

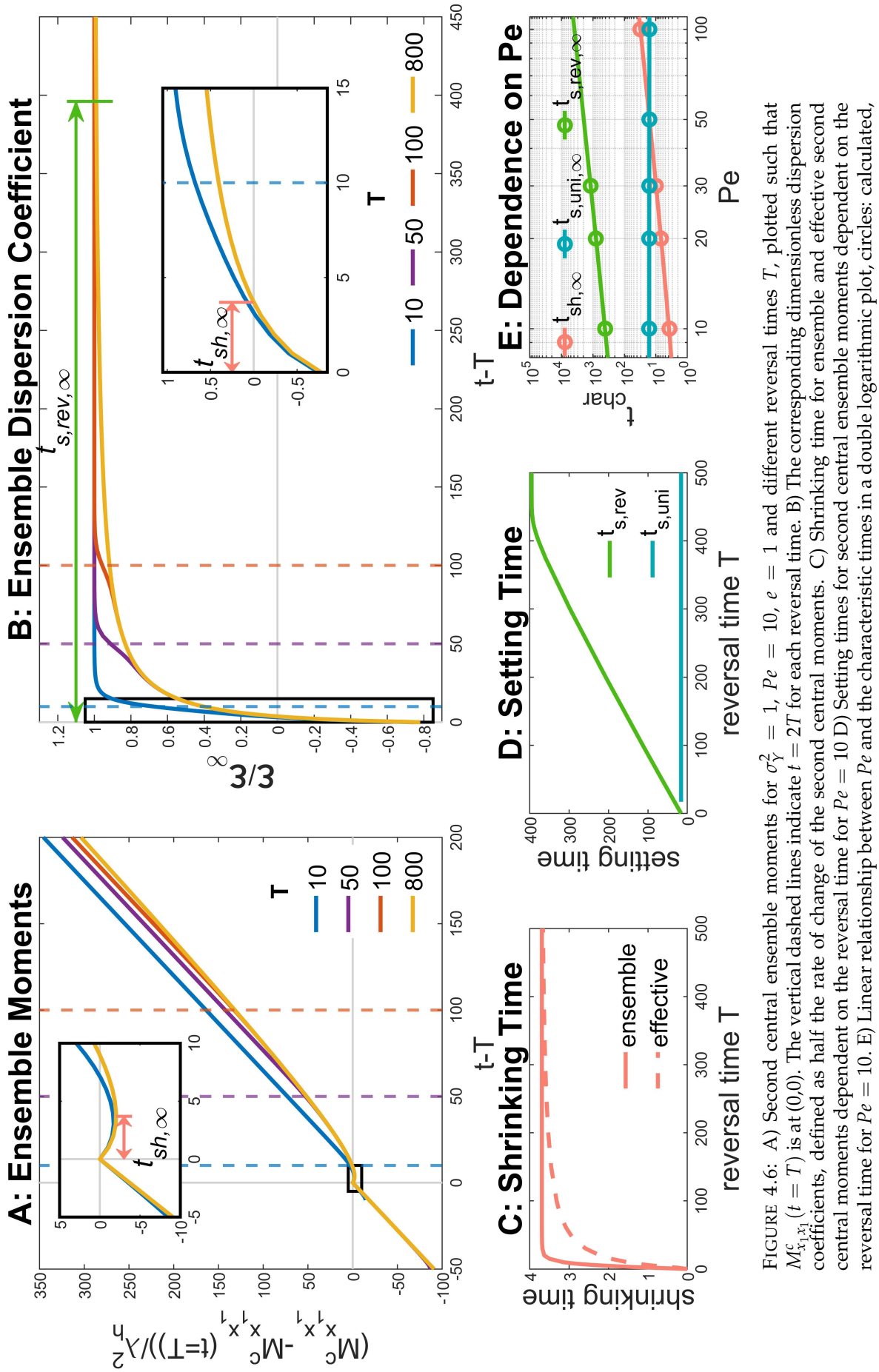

FIGURE 4.6: A) Second central ensemble moments for $\sigma_Y^2 = 1$, $Pe = 10$, $e = 1$ and different reversal times T, plotted such that $M^c_{x_1x_1}(t = T)$ is at (0,0). The vertical dashed lines indicate $t = 2T$ for each reversal time. B) The corresponding dimensionless dispersion coefficients, defined as half the rate of change of the second central moments. C) Shrinking time for ensemble and effective second central moments dependent on the reversal time for $Pe = 10$ D) Setting times for second central ensemble moments dependent on the reversal time for $Pe = 10$. E) Linear relationship between Pe and the characteristic times in a double logarithmic plot, circles: calculated, lines: linear fit.

$$\mathcal{E}\left(t_{s,uni}\right) = 0.99\mathcal{E}_\infty \quad \text{if } t \leq T, \tag{4.51}$$

$$\mathcal{E}\left(T + t_{s,rev}\right) = 0.99\mathcal{E}_\infty \quad \text{if } t > T. \tag{4.52}$$

$t_{s,rev}$ is a measure for the dimensionless time after flow reversal over which advective memory affects dispersion, i.e. the duration over which the onset of macrodispersive plume behavior is delayed. For times $t > t_{s,rev} + T$, flow reversal has lost all influence on the plume spreading and the moments begin to increase at the same rate as if the movement had been unidirectional from the beginning on.

Figure 4.6D shows the setting times $t_{s,uni}$ and $t_{s,rev}$ as function of the reversal time T for ensemble dispersion. For very short T, $t_{s,uni}$ is not defined. These are the cases where the duration of forward flow is too short for the plume behavior to become macrodispersive. Once this point is reached, $t_{s,uni}$ remains at a constant value independent of T. Conversely, $t_{s,rev}$ is defined for all T. The minimum value is identical to the constant value of $t_{s,uni}$, followed by a linear increase of $t_{s,rev}$ with T until the constant asymptotic value $t_{s,rev,\infty}$ is attained for very large values of T. $t_{s,rev,\infty}$ is significantly higher than $t_{s,uni,\infty}$, pointing at the strong persistence of advective memory in reversed flow.

The dashed vertical lines in Figures 4.6A & 4.6B mark the time point at which the center of gravity of the plume has returned to the origin ($t = 2T$). For times $t \gtrsim 2T$ there is no more influence of advective memory on the moments because the plume (in the mean) begins to move through parts of the domain it has not been exposed to before. (This does not happen at exactly $t = 2T$ because the rear parts of the plume are still in the known part of the domain and thus are influenced by advective memory.) Thus at $t \approx 2T$, the moments begin to increase linearly with time (Figure 4.6A), and respectively their temporal derivatives move quickly to their asymptotic limit (Figure 4.6B). For $T < t_{s,rev,\infty}$ the linear relationship between T and $t_{s,rev}$ is observed, because here, the setting time is not determined by the balance between advective memory and diffusive mixing but by the length of the explored domain. The asymptotic setting time is attained for $T \geq t_{s,rev,\infty}$, indicating that macrodispersive plume behavior in backward motion has been reached before the plume has passed the original starting location.

Figure 4.6E shows the dependence of the discussed asymptotic characteristic times on the Péclet number in a log-log plot. While $t_{sh,\infty}$ and $t_{s,rev,\infty}$ increase linearly with Pe, $t_{s,uni,\infty}$ remains at a constant value. This difference in behavior between the two setting times illustrates the increased importance of diffusion strength in reversed flow, in which the advective and diffusive contributions to dispersion have opposing effects. Generally, increasing Pe increases the characteristic times because higher Péclet numbers imply that diffusive mixing needs longer to overrule the plume-shrinking effect of advective memory (in the case of t_{sh}) or to completely erase advective memory (in the case of $t_{s,rev}$), respectively. The slope of the linear relationship between Pe and $t_{s,rev,\infty}$ is especially steep, thus we are numerically limited to evaluate the characteristic times for low Péclet numbers, where diffusion is very strong. When extrapolating to Pe-ranges typical for natural aquifers, the characteristic times reach such high values that the necessary travel distances to reach their asymptotic values exceed reasonable lengths over which aquifer statistics can be assumed to be stationary. As a consequence, the influence of flow reversal on plume behavior in realistic settings seems to persist until the plume has returned to its origin.

Note that all analyses on characteristic times were conducted using the analytical solution only.

4.5 Conclusions

We investigated the reversibility of dispersion in heterogeneous porous media by analyzing ensemble and effective second central spatial moments for uniform-in-the-mean transport with flow reversal. Based on our analytical and numerical results, we formulate the following answers to the research questions raised in the introduction:

1. For finite Péclet numbers, both ensemble and effective second central moments undergo a phase of shrinking upon flow reversal and do not return to their initial value. This shows that effective dispersion is not a measure for pure mixing, although it has successfully been applied as such (e.g., Cirpka, 2002; Benson et al., 2019).

2. Generally, it is well known that ensemble dispersion in forward motion is not a metric of mixing. We were hoping that the ensemble moments after equally long forward and backward motion could provide insights on mixing. However, comparing the second central moments at $t = 2T$ to their initial state (thus comparing the plume shape between the two time points at which the plume's center of gravity is at the origin) we were not able to derive an exact quantitative measure of solute mixing. Spreading, stretching-enhanced diffusive mixing, and the destruction of advective memory by diffusion are strongly interrelated and the ensemble moments after equally long forward and backward motion contain contributions of both mixing and spreading. Although effective dispersion contains reversible elements as well, it is still a better suited metric, and we encourage its use over ensemble dispersion in parameterizing mixing.

3. Our expectations regarding the influence of geostatistical and transport parameters have been confirmed. Parameter changes favoring diffusion over advection decrease the reversibility of dispersion. Thus the reversibility of dispersion decreases with increasing variance σ_Y^2 of log-conductivity, decreasing vertical-to-horizontal anisotropy ratio e and local Péclet number Pe and increasing reversal time T. The influence of parameter changes on the second central moments is much more pronounced after equally long forward and reversed flow than in unidirectional flow, which we attribute to diffusion and advection acting opposingly. Thus, flow reversal allows for a better qualitative assessment of advective and diffusive influences on dispersion than it is possible in unidirectional transport.

4. We defined two characteristic times: the shrinking time, which measures over which time period the second central moments shrink upon flow removal, and the setting time, which quantifies how long the influence of advective memory on the plume behavior persists. Stronger reversibility of dispersion is marked by higher characteristic times. For sufficiently long durations of forward motion, the characteristic times reach asymptotic values that depend linearly on the Péclet number. However, the asymptotic setting times in reversed flow are so high that it is very doubtful whether they are ever reached in real aquifers. This in turn means that under realistic conditions the advective memory is so

strong that the change of second central moments will be influenced by the preceding forward motion and flow reversal until the plume has returned to its origin. Only for unrealistically long times of forward motion, diffusion has the chance to completely destroy the advective memory in the backward motion before reaching the origin, so that asymptotic ensemble dispersion coefficients are achieved.

5. Linear stochastic theory is valid only for conductivity fields with mild heterogeneity. The comparison of the analytical second central moments to the numerical results obtained by particle-tracking random-walk simulations shows that the range of log-conductivity variances in which linear stochastic theory is applicable is more restricted for transport with flow reversal than for unidirectional flow. This is a direct result of the higher impact of local dispersion on second central moments when the flow field is reversed. In the limit of $\sigma_Y^2 \to 0$, linear stochastic theory solution predicts solute spreading accurately for any given value of Pe and e.

With our results from both linear stochastic theory and numerical simulations, we are able to quantify the partial reversibility of dispersion. Other than initially hoped for, the approach of flow reversal does not facilitate a complete distinction between advective and diffusive processes. While we can qualitatively assess different influences, we have no handle to quantify the spreading and mixing contributions to dispersion separately. This also puts the interpretation of dispersion coefficients obtained by fitting breakthrough curves in standard push-pull tests into question. These coefficients are not material properties of the formation; they cannot distinctively be related to the formations heterogeneity; neither do they apply to transport under natural-gradient flow conditions, nor do they quantify mixing (unless within the borehole during the push-pull test itself). Possibly, a series of push-pull experiments with different injection times and mean flow velocities could help in disentangling the various contributions to the observed dispersion. Deriving such approaches, however, is beyond the scope of the current study.

Data Availability

The in-house Matlab codes used to generate the data are available at `https://doi.org/10.5281/zenodo.7023202` (Stettler and Cirpka, 2022) under the international Creative Commons license CC-BY-NC 4.0. The HSL-MI20 algebraic multigrid (AMG) preconditioner used to solve the system of equations resulting from discretizing the flow equation is taken from the HSL library, a collection of Fortran codes for large-scale scientific computation (`http://www.hsl.rl.ac.uk/catalogue/hsl_mi20.html`).

Chapter 5

Conclusions & Outlook

5.1 Synthesis of Major Findings

In this thesis, I have approached the issue of understanding and quantitatively describing solute transport and dispersion in groundwater flow through heterogeneous aquifers from different angles. The general scope of investigation lies in recognizing and quantifying the interactions between spreading and mixing and their individual contributions to dispersion. In the following, I will first highlight the methodical achievements and then focus on answering the content-related research questions posed in the introduction.

Methodically, two theoretical approaches have been extended. Study A introduces a Spatial Markov Model which incorporates both advective and diffusive velocity transitions and can successfully model temporal moments and breakthrough curves under different Péclet regimes. A SMM using velocity transitions derived analytically from field properties that mechanistically includes diffusion has not existed for realistic heterogeneous porous media before. I have successfully developed and implemented such a method for the case of mild heterogeneity of the field. Here, the velocity statistics are derived from properties of the $\ln K$ distribution, which is assumed log-normal. However, for values of $\sigma_Y^2 > 1$, the model relies on numerical flow simulations to attain the velocity distributions because the actual velocity distributions increasingly deviate from log-normal shapes with increasing heterogeneity. Yet, contrasting previous studies (e.g. Le Borgne et al., 2011; Sund et al., 2017b), no simulations of transport are necessary because the diffusion implementation is based on mechanistic considerations rather than on a diffusive transition matrix. Specifically, particles can leave their current advective trajectory (resulting in a momentary loss of velocity correlation) if they diffuse further away from the center of the stream tube than a given escape radius over which the longitudinal velocity is assumed constant.

Study B expands the small perturbation solution by Dentz et al. (2000) for the evolution of spatial moments and related ensemble and effective dispersion to flow reversal. The analytical approximation is based on a series expansion in the spectral domain of the concentration field emerging from a point injection. As is the case for linear stochastic theory in general (e.g. Dagan, 2002), the solution is restricted to moderate heterogeneity, especially during the transport phase following flow reversal and for effective dispersion. This shows that the deviation between the analytical solution and the numerical results is higher in cases where the role of diffusion is enhanced. However, when taking its limitations into account, it is very convenient to resort to an analytical solution rather than performing numerical simulations, particularly when fully explicit 3-D schemes are computationally too expensive, as is the case in the present study for the examination of the evolution and asymptotic behavior of characteristic transport times (Figures 4.5 & 4.6).

Concentrating on the content contributions, the overarching research questions as stated in the introduction (Section 1.4), can be answered as follows:

- How does diffusion strength influence breakthrough curves, ensemble and effective moments and the degree of reversibility of dispersion?

For transport through heterogeneous media, ensemble dispersion (slightly) decreases with increasing diffusion strength (Fiori et al., 2002). Both studies confirm this result. The BTCs in Study A become narrower and more symmetrical the stronger diffusion acts. Increasing the field heterogeneity has the opposite effect. The study exemplifies the competition between the plume spreading due to heterogeneity and the smoothing effect of random diffusion by limiting the influence of extreme velocities. Study B confirms that the effect of diffusion does not only depend on the Péclet number (e.g. Tonina and Bellin, 2008). With longer travel and reversal times, diffusion becomes more and more dominant over advection. Additionally, the diffusion strength grows by its interaction with the heterogeneity and the anisotropy of the field. To correctly assess the influence of diffusion strength on solute transport, the perspective is important, especially for point injections: Over the ensemble average - when the uncertainty of the center of mass is included - mixing decreases the plume variance by breaking velocity correlations. When looking at individual plumes originating from point injections (effective dispersion), mixing increases the plume variance by allowing a plume to sample different velocities. Those effects are reflected in the respective decrease and increase in ensemble and effective dispersion with increasing diffusion strength. The degree of reversibility of dispersion decreases with increasing diffusion strength both for ensemble and effective dispersion because diffusion destroys the advective memory which is required for reversibility.

- Are effective moments under flow reversal an adequate measure for mixing?

Study B shows that both ensemble and effective dispersion are partially reversible upon flow reversal. Thus, effective moments are not a direct measure for mixing. A true mixing metric can never decrease since under mass conservation diffusion leads to a monotonous increase of the system's entropy and is completely irreversible (Chiogna and Rolle, 2017). However, since effective moments are generally more descriptive for individual plumes (Barros and Dentz, 2016) and we can see from Study B that they are much less influenced by flow reversal, they are certainly more suited to infer mixing information than ensemble moments.

- How can flow reversal contribute to understanding the interplay between mixing and spreading?

From the degree of reversibility of dispersion upon flow reversal, we can deduce information about the relative strengths of advection and diffusion and associated spreading and mixing. The less reversible dispersion, the more dominant is diffusion over advection. However, this assessment remains qualitative. Solely based on moment analysis, no quantitative statements are possible because ensemble and effective dispersion are influenced by both transport processes. Obviously, the interactions between spreading and mixing are too complex and persistent to be fully disentangled by flow reversal. Thus, considering additional metrics for pure mixing would be very instructive. Nevertheless, applying flow reversal provides a perspective on the interplay between spreading and mixing as opposed to unidirectional flow, in which the processes remain indiscernible. The observed partial reversibility

of dispersion raises the question what information is provided by dispersion coefficients gained through single-well push-pull tests. The signal after a complete push-pull cycle is strongly influenced by its path, over which spreading is reduced in parts, yet mixing is not isolated from it. In fact, we observe the combined effect of spreading and mixing on path memory which does not appear as such in unidirectional transport. Thus, since a dispersion coefficient determined from such an experiment carries a very specific signature it is debatable whether it can reasonably be applied to more general cases which usually would be its purpose.

To condense the above to a minimum: The core contribution of study A lies in the method development of an analytically based advective-diffusive SMM with a mechanistic diffusion implementation. The core contribution of Study B lies in a better understanding of the information content of effective dispersion and of the potential that flow reversal carries to differentiate between transport processes.

5.2 Research Perspectives

Several research avenues arise from the present studies.

First, it is of high interest to enhance the advective-diffusive SMM so that it can be applied even more widely and flexibly. I identify three main progression points for the SMM: (i) Advance the model to be independent of numerical or empirical input. This involves finding a distribution other than the log-normal one which correctly represents the K and corresponding velocity fields also at high variances (cf. Loáiciga et al., 2006; Meerschaert et al., 2013). Additionally, this requires a physically based derivation of the stream-tube radius rather than relying on the empirical relationship between σ_Y^2 and R (equation 3.28). (ii) Include flow reversal. This demands an implementation of path memory. For a purely advective scenario, this memory is easily created by storing the full history of all experienced velocities for every particle. However, when including diffusion which naturally destroys memory, this becomes a more challenging task. (iii) Forge the model to allow for measurements of effective dispersion as well as ensemble dispersion. This can be attained by injecting particles in pairs, meaning two particles originate with the same initial velocity, and then deriving the effective dispersion from observing how their covariance evolves. Here, the challenge lies in finding a mechanism which allows for a gradual loss of correlation with travel distance between particles making up a pair rather than a binary system where the particles are either perfectly correlated or not correlated at all.

All three progression points have one aspect in common: Information about the correlation of longitudinal velocities in transverse direction is useful or even necessary to attain them. However, the presented SMM cannot account for the correlation of longitudinal velocities between neighboring stream tubes. Once a particle leaves its current trajectory, the first velocity on the new trajectory is drawn fully independently from the last velocity. This complete loss of correlation does not represent the true covariance function of longitudinal velocities normal to the mean direction of flow. Only when incorporating some knowledge about transverse velocity correlation, we can develop a physical law for tube radii, account for path memory correctly and represent mixing from a single-plume perspective. A first step towards this goal could be to examine what correlation can be found between a particle's current velocity and the velocity gradient in transverse direction (cf. Aquino and Le Borgne, 2021). However, a strong advantage of SMM lies in their simplicity of breaking down

the three-dimensional reality to a one-dimensional stochastic process. So the challenge is to add the required amount of information and complexity while remaining in the reduced stochastic framework.

Second, the theoretical findings would be strongly supported by an experimental verification. A possible experimental set-up to measure both temporal and spatial moments of an evolving plume under flow reversal could be the following: Inject a (dye) tracer into a quasi-2-D transparent experiment box, filled with a combination of an artificial sediment (homogeneously or heterogeneously packed) and a fluid whose refractive indices are matched. Like this, the tracer plume will be visible integrated over the full thickness of the box, in the ideal case without any optical distortion from the matrix (Wiederseiner et al., 2011). Once the wanted reversal time is met, invert the direction of the pump while keeping the net pumping rate constant. The full concentration field required for calculation of spatial moments is acquired from relating the light intensity from pictures taken of the plume during the experiment run time to the tracer concentration (e.g. Zinn et al., 2004; Roth et al., 2021; Rousseau et al., 2023). Temporal moments can be determined by measuring the tracer concentration at the outlet of the box. Applying the stream-tube approach, by taking samples at several locations along the box rather than integrated over the full width, local breakthrough corresponding to effective moments can be determined (e.g. Jose et al., 2004; Ye et al., 2016).

Moreover, additional measures like the dilution index (Kitanidis, 1994) and the mixing area or volume (Basilio Hazas et al., 2023) which are directly measuring mixing and thus expected to be unaffected by flow reversal can be calculated based on the fully resolved concentration fields. Comparing these measures to the ensemble and effective moments which Study B has shown to be affected by flow reversal should shed light on the remaining open question about the respective strength of the individual contributions of spreading and mixing to overall dispersion and to describe the interplay between the processes not just qualitatively but quantitatively as well. Furthermore, performing these push-pull experiments under variable controlled conditions could clarify what information we actually gain from single-well push-pull tests and their associated dispersion coefficients.

Finally, experimentally generated physical data could be the core of an integrative study, combining all theoretical and numerical methods presented in this thesis.

Appendix A

Appendix to Study A

A.1 Exponential Approximation of first-passage-time distribution

In order to determine the first-passage or escape time from a tube of radius R, we consider radial diffusion:

$$\frac{\partial c(r,t)}{\partial t} - D\frac{1}{r}\frac{\partial}{\partial r}\left(r\frac{\partial}{\partial r}c(r,t)\right) = 0 \tag{A.1}$$

with a uniform initial condition $c(r, t = 0) = 1$ and the boundary condition $c(r = R, t) = 0$. This implies, that we assume that particles are initially uniformly distributed across the tube. The first-passage-time distribution is then given by:

$$\psi(t) = -2D\pi R\frac{\partial c(r = R, t)}{\partial r}. \tag{A.2}$$

The solution can be found in Laplace space (Harvey and Gorelick, 1995):

$$\psi^*(s) = \frac{2}{\sqrt{s\tau_0}}\frac{I_1(\sqrt{s\tau_0})}{I_0(\sqrt{s\tau_0})}, \tag{A.3}$$

where I_i is the modified Bessel function of the first type of order i, s is the Laplace variable, and $\tau_0 = R^2/D$. For times $t < \tau_0$ it decays as $t^{-1/2}$, and for $t > \tau_0$ it decays exponentially fast. The leading exponential mode is given by (Haggerty and Gorelick, 1995):

$$\psi_0(t) = \frac{4\exp(-\alpha_0^2 t/\tau_D)}{\tau_D}, \tag{A.4}$$

where $\alpha_0 = 2.4048$ is the first zero of the Bessel function $J_0(z)$.

The mean first-passage time can be determined from $\psi^*(s)$ by differentiation:

$$\tau_m = -\left.\frac{\mathrm{d}\psi(s)}{\mathrm{d}s}\right|_{\lambda=0} = \frac{\tau_0}{8}. \tag{A.5}$$

The first-passage-time distribution $\psi(t)$ can be approximated by the exponential distribution:

$$\psi(t) = \frac{\exp(-t/\tau_m)}{\tau_m}. \tag{A.6}$$

Figure A.1 shows examples for the first-passage-time distributions and their exponential approximation:

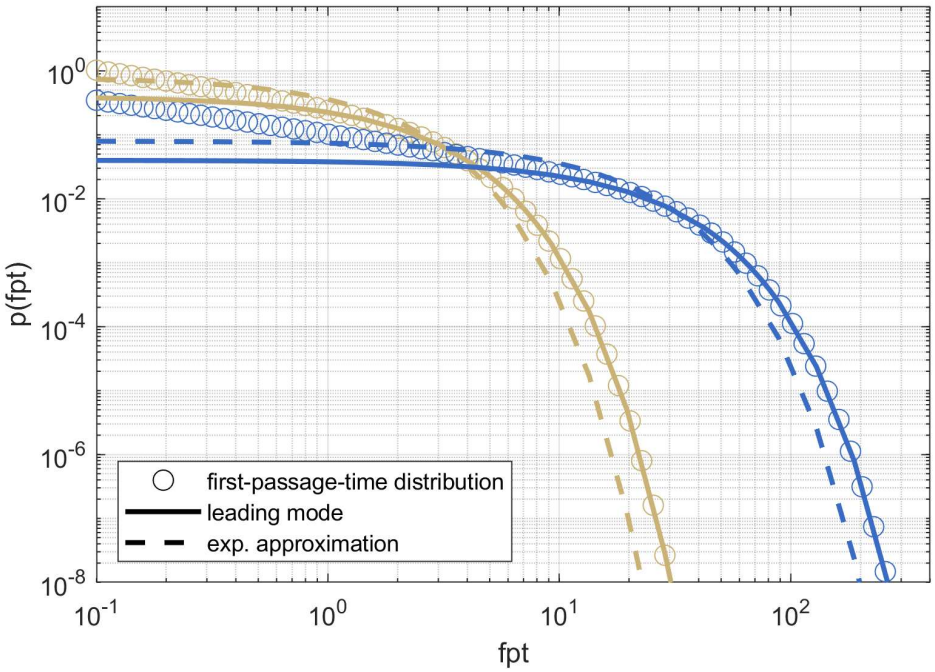

FIGURE A.1: First-passage-time distribution. Open circles: obtained by inverse Laplace transform of equation A.3 for $\tau_0 = 10$ (gold) and 100 (blue); solid lines: dominant mode given by equation A.4; dashed lines: exponential approximation given by equation A.6.

Appendix B

Appendix to Study B

B.1 Derivation of Concentration Fields according to Linear Stochastic Theory

The first- and second-order terms $\tilde{c_1}$ and $\tilde{c_2}$ in equation 4.41 read as:

$$\tilde{c}_1(\mathbf{s}, t \leq T) = -2\pi i \int_{V_\infty} \int_0^t \frac{\tilde{c}_0(\mathbf{s}, t)}{\tilde{c}_0(\mathbf{s}, t')} \mathbf{s} \cdot \tilde{\mathbf{v}}_0'(\mathbf{s}') \tilde{c}_0(\mathbf{s} - \mathbf{s}', t') dt' d\mathbf{s}' \tag{B.1}$$

$$\tilde{c}_2(\mathbf{s}, t \leq T) = -4\pi^2 \int_{V_\infty} \int_{V_\infty} \int_0^t \int_0^{t'} \frac{\tilde{c}_0(\mathbf{s}, t)}{\tilde{c}_0(\mathbf{s}, t')} \mathbf{s} \cdot \tilde{\mathbf{v}}_0'(\mathbf{s}') \frac{\tilde{c}_0(\mathbf{s} - \mathbf{s}', t')}{\tilde{c}_0(\mathbf{s} - \mathbf{s}', t'')} (\mathbf{s} - \mathbf{s}') \cdot \tilde{\mathbf{v}}_0'(\mathbf{s}'') \tilde{c}_0(\mathbf{s} - \mathbf{s}' - \mathbf{s}'', t'') dt'' dt' d\mathbf{s}'' d\mathbf{s}'. \tag{B.2}$$

Truncating equation 4.41 after the second-order term and taking expected values leads to the following expression for the Fourier transform of the expected concentration $\langle \tilde{c}(\mathbf{s}, t) \rangle$ in macroscopically unidirectional flow:

$$\langle \tilde{c}(\mathbf{s}, t \leq T) \rangle = \tilde{c}_0(\mathbf{s}, t \leq T) - 4\pi^2 \int_{V_\infty} \int_0^t \int_0^{t'} \frac{\tilde{c}_0(\mathbf{s}, t)}{\tilde{c}_0(\mathbf{s}, t')} \frac{\tilde{c}_0(\mathbf{s} - \mathbf{s}', t')}{\tilde{c}_0(\mathbf{s} - \mathbf{s}', t'')} \tilde{c}_0(\mathbf{s}, t'') \mathbf{s} \cdot \left(\mathbf{S}_{\mathbf{v}_0' \otimes \mathbf{v}_0'}(\mathbf{s}') \mathbf{s} \right) dt'' dt' d\mathbf{s}', \tag{B.3}$$

in which the incompressibility condition (equation 4.13) in the spectral domain, $\mathbf{s}' \cdot \tilde{\mathbf{v}}'(\mathbf{s}') = 0$, has been used and $\mathbf{S}_{\mathbf{v}_0' \otimes \mathbf{v}_0'}$ is the cross-power spectrum of velocity fluctuations, calculated using the identity $\langle \tilde{\mathbf{v}}_0'(\mathbf{s}') \otimes \tilde{\mathbf{v}}_0'(\mathbf{s}'') \rangle = \mathbf{S}_{\mathbf{v}_0' \otimes \mathbf{v}_0'}(\mathbf{s}') \delta(\mathbf{s}' + \mathbf{s}'')$. Equation B.3 is used to calculate the moments of the expected concentration before flow reversal.

With flow reversal at $t = T$, the series expansion is constructed by substituting equation 4.35 into the first recursive integral of equation 4.36 and the latter into the second recursive integral of itself:

$$\tilde{c}(\mathbf{s}, t > T) = \tilde{c}_0(\mathbf{s}, t > T) - 2\pi i \int_{V_\infty} \int_0^T \frac{\tilde{c}_0(\mathbf{s}, t)}{\tilde{c}_0(\mathbf{s}, t')} \mathbf{s} \cdot \tilde{\mathbf{v}}_0'(\mathbf{s}')\, \tilde{c}_0(\mathbf{s} - \mathbf{s}', t') dt' d\mathbf{s}'$$
$$- 4\pi^2 \int_{V_\infty} \int_{V_\infty} \int_0^T \int_0^{t'} \frac{\tilde{c}_0(\mathbf{s}, t)}{\tilde{c}_0(\mathbf{s}, t')} \mathbf{s} \cdot \tilde{\mathbf{v}}_0'(\mathbf{s}')\, \frac{\tilde{c}_0(\mathbf{s} - \mathbf{s}', t')}{\tilde{c}_0(\mathbf{s} - \mathbf{s}', t'')} (\mathbf{s} - \mathbf{s}')$$
$$\cdot \tilde{\mathbf{v}}_0'(\mathbf{s}'')\, \tilde{c}_0(\mathbf{s} - \mathbf{s}' - \mathbf{s}'', t'') dt'' dt' d\mathbf{s}'' d\mathbf{s}'$$
$$+ 2\pi i \int_{V_\infty} \int_T^t \frac{\tilde{c}_0(\mathbf{s}, t)}{\tilde{c}_0(\mathbf{s}, \tau)} \mathbf{s} \cdot \tilde{\mathbf{v}}_0'(\mathbf{s}')\, \tilde{c}_0(\mathbf{s} - \mathbf{s}', \tau) d\tau d\mathbf{s}'$$
$$+ 4\pi^2 \int_{V_\infty} \int_{V_\infty} \int_T^t \int_0^T \frac{\tilde{c}_0(\mathbf{s}, t)}{\tilde{c}_0(\mathbf{s}, \tau)} \mathbf{s} \cdot \tilde{\mathbf{v}}_0'(\mathbf{s}')\, \frac{\tilde{c}_0(\mathbf{s} - \mathbf{s}', \tau)}{\tilde{c}_0(\mathbf{s} - \mathbf{s}', t')} (\mathbf{s} - \mathbf{s}')$$
$$\cdot \tilde{\mathbf{v}}_0'(\mathbf{s}'')\, \tilde{c}_0(\mathbf{s} - \mathbf{s}' - \mathbf{s}'', t') dt' d\tau d\mathbf{s}'' d\mathbf{s}'$$
$$- 4\pi^2 \int_{V_\infty} \int_{V_\infty} \int_T^t \int_T^\tau \frac{\tilde{c}_0(\mathbf{s}, t)}{\tilde{c}_0(\mathbf{s}, \tau)} \mathbf{s} \cdot \tilde{\mathbf{v}}_0'(\mathbf{s}')\, \frac{\tilde{c}_0(\mathbf{s} - \mathbf{s}', \tau)}{\tilde{c}_0(\mathbf{s} - \mathbf{s}', \tau')} (\mathbf{s} - \mathbf{s}')$$
$$\cdot \tilde{\mathbf{v}}_0'(\mathbf{s}'')\, \tilde{c}_0(\mathbf{s} - \mathbf{s}' - \mathbf{s}'', \tau') d\tau' d\tau d\mathbf{s}'' d\mathbf{s}' + H.O.T.. \quad \text{(B.4)}$$

Now, the second-order expected concentration in the spectral domain reads as:

$$\langle \tilde{c}\,(\mathbf{s}, t > T) \rangle = \tilde{c}_0\,(\mathbf{s}, t > T)$$
$$- 4\pi^2 \int_{V_\infty} \int_0^T \int_0^{t'} \frac{\tilde{c}_0\,(\mathbf{s}, t)}{\tilde{c}_0\,(\mathbf{s}, t')} \frac{\tilde{c}_0\,(\mathbf{s} - \mathbf{s}', t')}{\tilde{c}_0\,(\mathbf{s} - \mathbf{s}', t'')} \tilde{c}_0\,(\mathbf{s}, t'')\, \mathbf{s} \cdot \left(\mathbf{S}_{\mathbf{v}_0' \otimes \mathbf{v}_0'}\,(\mathbf{s}')\, \mathbf{s} \right) dt'' dt' d\mathbf{s}'$$
$$+ 4\pi^2 \int_{V_\infty} \int_T^t \int_0^T \frac{\tilde{c}_0\,(\mathbf{s}, t)}{\tilde{c}_0\,(\mathbf{s}, \tau)} \frac{\tilde{c}_0\,(\mathbf{s} - \mathbf{s}', \tau)}{\tilde{c}_0\,(\mathbf{s} - \mathbf{s}', t')} \tilde{c}_0\,(\mathbf{s}, t')\, \mathbf{s} \cdot \left(\mathbf{S}_{\mathbf{v}_0' \otimes \mathbf{v}_0'}\,(\mathbf{s}')\, \mathbf{s} \right) dt' d\tau d\mathbf{s}'$$
$$- 4\pi^2 \int_{V_\infty} \int_T^t \int_T^\tau \frac{\tilde{c}_0\,(\mathbf{s}, t)}{\tilde{c}_0\,(\mathbf{s}, \tau)} \frac{\tilde{c}_0\,(\mathbf{s} - \mathbf{s}', \tau)}{\tilde{c}_0\,(\mathbf{s} - \mathbf{s}', \tau')} \tilde{c}_0\,(\mathbf{s}, \tau')\, \mathbf{s} \cdot \left(\mathbf{S}_{\mathbf{v}_0' \otimes \mathbf{v}_0'}\,(\mathbf{s}')\, \mathbf{s} \right) d\tau' d\tau d\mathbf{s}', \quad \text{(B.5)}$$

which is the basis for the moment expressions for $t > T$.

B.2 Derivation of Spatial Moments for $t > T$ according to Linear Stochastic Theory

B.2.1 Zeroth Moment

Evaluating the series expansion of equation B.4 at $\mathbf{s} = \mathbf{0}$, yields the zeroth moment of the concentration field for $t > T$:

$$m_0\,(c\,(\mathbf{x}, t > T)) = \tilde{c}_0\,(\mathbf{0}, t > T) = 1, \quad \text{(B.6)}$$

which is consistent with the total mass of the solute in the domain being conserved at all times.

B.2.2 First Moment

The first moments of the expected value of the concentration $\mathbf{m}_{\mathbf{x}}\left(\langle c\left(\mathbf{x}, t>T\right)\rangle\right)$ for $t>T$ are derived by applying equation 4.27 to equation B.5:

$$\mathbf{m}_{\mathbf{x}}\left(\langle c\left(\mathbf{x}, t>T\right)\rangle\right)=\frac{i}{2\pi}\nabla_{\mathbf{s}}\left(\tilde{c}_0\left(\mathbf{s}, t>T\right)\right)_{\mathbf{s}=\mathbf{0}}=\mathbf{e}_1\left(2T-t\right). \tag{B.7}$$

The first moments of the actual concentrations $\mathbf{m}_{\mathbf{x}}\left(c\left(\mathbf{x}, t>T\right)\right)$ for $t>T$ are derived by applying equation 4.27 to equation B.4. In a first-order approximation, all second- and higher order terms in the latter are neglected:

$$\begin{aligned}\mathbf{m}_{\mathbf{x}}\left(c\left(\mathbf{x}, t>T\right)\right) \approx\ & \mathbf{e}_1\left(2T-t\right)\\ &+\int_{V_\infty}\int_0^T \tilde{\mathbf{v}}_0'(\mathbf{s}')\tilde{c}_0(-\mathbf{s}', t')dt'd\mathbf{s}'-\int_{V_\infty}\int_T^t \tilde{\mathbf{v}}_0'(\mathbf{s}')\tilde{c}_0(-\mathbf{s}', \tau)d\tau d\mathbf{s}'.\end{aligned} \tag{B.8}$$

The expected value of first moments $\langle\mathbf{m}_{\mathbf{x}}\left(c\left(\mathbf{x}, t>T\right)\right)\rangle$ equals the first moments of the expected concentration $\mathbf{m}_{\mathbf{x}}\left(\langle c\left(\mathbf{x}, t>T\right)\rangle\right)$ even to the second order because the expected value of the velocity fluctuations in equation B.8 is zero and the second-order terms in equation B.4 are accounted for in equation B.5.

Using $\mathbf{m}_{\mathbf{x}}=\langle\mathbf{m}_{\mathbf{x}}\rangle+\mathbf{m}_{\mathbf{x}}'$, the first-order deviation $\mathbf{m}_{\mathbf{x}}'\left(c\left(\mathbf{x}, t>T\right)\right)$ is:

$$\mathbf{m}_{\mathbf{x}}'\left(c\left(\mathbf{x}, t>T\right)\right)=\int_{V_\infty}\int_0^T \tilde{\mathbf{v}}_0'(\mathbf{s}')\tilde{c}_0(-\mathbf{s}', t')dt'd\mathbf{s}'-\int_{V_\infty}\int_T^t \tilde{\mathbf{v}}_0'(\mathbf{s}')\tilde{c}_0(-\mathbf{s}', \tau)d\tau d\mathbf{s}'. \tag{B.9}$$

The covariance matrix of first moments $\langle\mathbf{m}_{\mathbf{x}}'\left(c\left(\mathbf{x}, t>T\right)\right)\otimes\mathbf{m}_{\mathbf{x}}'\left(c\left(\mathbf{x}, t>T\right)\right)\rangle$ for $t>T$ is calculated by computing the product of first-moment deviations and taking the expected value, leading to:

$$\begin{aligned}&\left\langle\mathbf{m}_{\mathbf{x}}'\left(c\left(\mathbf{x}, t>T\right)\right)\otimes\mathbf{m}_{\mathbf{x}}'\left(c\left(\mathbf{x}, t>T\right)\right)\right\rangle=\\ &\qquad\int_{V_\infty}\int_0^T\int_0^T \tilde{c}_0(-\mathbf{s}', t')\mathbf{S}_{\mathbf{v}_0'\otimes\mathbf{v}_0'}\left(\mathbf{s}'\right)\tilde{c}_0(\mathbf{s}', t'')dt''dt'd\mathbf{s}'\\ &\qquad-\int_{V_\infty}\int_0^T\int_T^t \tilde{c}_0(-\mathbf{s}', t')\mathbf{S}_{\mathbf{v}_0'\otimes\mathbf{v}_0'}\left(\mathbf{s}'\right)\tilde{c}_0(\mathbf{s}', \tau)d\tau dt'd\mathbf{s}'\\ &\qquad-\int_{V_\infty}\int_T^t\int_0^T \tilde{c}_0(-\mathbf{s}', \tau)\mathbf{S}_{\mathbf{v}_0'\otimes\mathbf{v}_0'}\left(\mathbf{s}'\right)\tilde{c}_0(\mathbf{s}', t')dt'd\tau d\mathbf{s}'\\ &\qquad+\int_{V_\infty}\int_T^t\int_T^t \tilde{c}_0(-\mathbf{s}', \tau)\mathbf{S}_{\mathbf{v}_0'\otimes\mathbf{v}_0'}\left(\mathbf{s}'\right)\tilde{c}_0(\mathbf{s}', \tau')d\tau'd\tau d\mathbf{s}',\end{aligned} \tag{B.10}$$

in which $\langle\tilde{\mathbf{v}}_0'(\mathbf{s}')\otimes\tilde{\mathbf{v}}_0'(\mathbf{s}'')\rangle=\mathbf{S}_{\mathbf{v}_0'\otimes\mathbf{v}_0'}\left(\mathbf{s}'\right)\delta\left(\mathbf{s}'+\mathbf{s}''\right)$ has been used.

The temporal integrals in equation B.10 can be evaluated explicitly, yielding equation 4.46.

B.2.3 Second Raw Moment

Applying equation 4.28 to equation B.5, yields the second raw moment of the ensemble concentration:

$$\begin{aligned}\mathbf{M}_{\mathbf{x}\otimes\mathbf{x}}\left(\langle c(\mathbf{x},t>T)\rangle\right) &= 2\boldsymbol{\mathcal{E}}t+\mathbf{e}_1\otimes\mathbf{e}_1\left(2T-t\right)^2\\ &+2\int\limits_{V_\infty}\int\limits_0^T\int\limits_0^{t'}\frac{\tilde{c}_0\left(-\mathbf{s}',t'\right)}{\tilde{c}_0\left(-\mathbf{s}',t''\right)}\mathbf{S}_{\mathbf{v}_0'\otimes\mathbf{v}_0'}\left(\mathbf{s}'\right)dt''dt'd\mathbf{s}'\\ &-2\int\limits_{V_\infty}\int\limits_T^t\int\limits_0^T\frac{\tilde{c}_0\left(-\mathbf{s}',\tau\right)}{\tilde{c}_0\left(-\mathbf{s}',t'\right)}\mathbf{S}_{\mathbf{v}_0'\otimes\mathbf{v}_0'}\left(\mathbf{s}'\right)dt'd\tau d\mathbf{s}'\\ &+2\int\limits_{V_\infty}\int\limits_T^t\int\limits_T^\tau\frac{\tilde{c}_0\left(-\mathbf{s}',\tau\right)}{\tilde{c}_0\left(-\mathbf{s}',\tau'\right)}\mathbf{S}_{\mathbf{v}_0'\otimes\mathbf{v}_0'}\left(\mathbf{s}'\right)d\tau'd\tau d\mathbf{s}', \quad \text{(B.11)}\end{aligned}$$

which is identical to the expected value of the second raw moments:

$$\left\langle\mathbf{M}_{\mathbf{x}\otimes\mathbf{x}}(c(\mathbf{x},t>T))\right\rangle=\mathbf{M}_{\mathbf{x}\otimes\mathbf{x}}\left(\langle c(\mathbf{x},t>T)\rangle\right). \quad \text{(B.12)}$$

The temporal integrals in equation B.11 are evaluated analytically, leading to the following expression for $\mathbf{M}_{\mathbf{x}\otimes\mathbf{x}}\left(\langle c(\mathbf{x},t>T)\rangle\right)$:

$$\begin{aligned}\mathbf{M}_{\mathbf{x}\otimes\mathbf{x}}\left(\langle c(\mathbf{x},t>T)\rangle\right) &= 2\boldsymbol{\mathcal{E}}t+\mathbf{e}_1\otimes\mathbf{e}_1\left(2T-t\right)^2\\ &+2\int\limits_{V_\infty}\mathbf{S}_{\mathbf{v}_0'\otimes\mathbf{v}_0'}\left(\mathbf{s}\right)\left(\frac{\left(A-B\right)T+\exp\left(-AT+BT\right)-1}{\left(A-B\right)^2}\right.\\ &-\frac{\exp\left(-At+B\left(2T-t\right)\right)-\exp\left(-\left(A+B\right)\left(t-T\right)\right)-\exp\left(-AT+BT\right)+1}{A^2-B^2}\\ &\left.+\frac{\left(t-T\right)\left(A+B\right)+\exp\left(-\left(A+B\right)\left(t-T\right)\right)-1}{\left(A+B\right)^2}\right)d\mathbf{s}. \quad \text{(B.13)}\end{aligned}$$

B.2.4 Second Central Moment

Finally, inserting equations B.13 & 4.46 into equation 4.23 yields the matrix of second central ensemble moments for $t > T$, equation 4.45.

B.3 Limits of Moment Expressions for $\mathbf{s} \to \mathbf{0}$

B.3.1 Limits for $t \leq T$

The fraction in equation 4.43 becomes at the limit of $\mathbf{s} \to \mathbf{0}$:

$$\lim_{\mathbf{s}\to\mathbf{0}}\frac{\left(A-B\right)t+\exp\left(\left(-A+B\right)t\right)-1}{\left(A-B\right)^2}=\frac{t^2}{2}. \quad \text{(B.14)}$$

The fraction in equation 4.44 becomes at the limit of $\mathbf{s} \to \mathbf{0}$:

$$\lim_{\mathbf{s}\to\mathbf{0}} \frac{\exp(-2At) - \exp(-At + Bt) - \exp(-At - Bt) + 1}{A^2 - B^2} = t^2. \tag{B.15}$$

B.3.2 Limits for $t > T$

Summing up the fractions inside the integral of equation 4.45 and taking the limit $\mathbf{s} \to \mathbf{0}$ yields:

$$\lim_{\mathbf{s}\to\mathbf{0}} \left(\frac{\cdot}{\cdot} - \frac{\cdot}{\cdot} + \frac{\cdot}{\cdot} \right) = \frac{1}{2} (2T - t)^2 . \tag{B.16}$$

Summing up the fractions inside the integral of equation 4.46 and taking the limit $\mathbf{s} \to \mathbf{0}$ yields:

$$\lim_{\mathbf{s}\to\mathbf{0}} \left(\frac{\cdot}{\cdot} - \frac{\cdot}{\cdot} - \frac{\cdot}{\cdot} + \frac{\cdot}{\cdot} \right) = (2T - t)^2 . \tag{B.17}$$

Bibliography

Aeschbach-Hertig, W. and T. Gleeson (2012). "Regional strategies for the accelerating global problem of groundwater depletion". In: *Nature Geoscience* 5 (12), pp. 853–861. DOI: 10.1038/ngeo1617.

Akomolafe, O. J., B. Ghanbarian, and J. D. Hyman (2024). "Fluid flow and solute transport simulations in tight geologic formations: Discrete fracture network and continuous time random walk analyses". In: *Journal of Hydrology* 635, p. 131109. DOI: 10.1016/j.jhydrol.2024.131109.

Anderson, T. W. (1962). "On the distribution of the two-sample Cramer-von Mises criterion". In: *The Annals of Mathematical Statistics*, pp. 1148–1159. DOI: 10.1214/aoms/1177704477.

Andrés, S., M. Dentz, and L. Cueto-Felgueroso (2025). "First-order multirate mass transfer for modeling coupled flow and deformation in heterogeneous fractured media". In: *Journal of Hydrology* 650, p. 132521. ISSN: 0022-1694. DOI: 10.1016/j.jhydrol.2024.132521.

Andričević, R. (1998). "Effects of local dispersion and sampling volume on the evolution of concentration fluctuations in aquifers". In: *Water Resources Research* 34 (5), pp. 1115–1129. DOI: 10.1029/98WR00260.

Aquino, T. and T. Le Borgne (2021). "The diffusing-velocity random walk: a spatial-Markov formulation of heterogeneous advection and diffusion". In: *Journal of Fluid Mechanics* 910, A12. DOI: 10.1017/jfm.2020.957.

Attinger, S., M. Dentz, H. Kinzelbach, and W. Kinzelbach (1999). "Temporal Behaviour of a Solute Cloud in a Chemically Heterogeneous Porous Medium". In: *Journal of Fluid Mechanics* 386, pp. 77–104. DOI: 10.1017/S0022112099004334.

Bandopadhyay, A., T. Le Borgne, Y. Méheust, and M. Dentz (2017). "Enhanced reaction kinetics and reactive mixing scale dynamics in mixing fronts under shear flow for arbitrary Damköhler numbers". In: *Advances in Water Resources* 100, pp. 78–95. DOI: 10.1016/j.advwatres.2016.12.008.

Bannick, C. et al. (2008). "Grundwasser in Deutschland". In: *Bundesministerium für Umwelt, Naturschutz und Reaktorsicherheit*.

Barros, F. P. J. de and M. Dentz (2016). "Pictures of blockscale transport: Effective versus ensemble dispersion and its uncertainty". In: *Advances in Water Resources* 91, pp. 11–22. DOI: 10.1016/j.advwatres.2016.03.004.

Basilio Hazas, M., F. Ziliotto, J. Lee, M. Rolle, and G. Chiogna (2023). "Evolution of plume geometry, dilution and reactive mixing in porous media under highly transient flow fields at the surface water-groundwater interface". In: *Journal of Contaminant Hydrology* 258, p. 104243. DOI: https://doi.org/10.1016/j.jconhyd.2023.104243.

Bear, J. (1972). *Dynamics of Fluids in Porous Media*. New York: American Elsevier.

Bellin, A., P. Salandin, and A. Rinaldo (1992). "Simulation of dispersion in heterogeneous porous formations: Statistics, first-order theories, convergence of computations". In: *Water Resources Research* 28 (9), pp. 2211–2227. DOI: 10.1029/92WR00578.

Benson, D. A., S. Pankavich, and D. Bolster (2019). "On the separate treatment of mixing and spreading by the reactive-particle-tracking algorithm: An example of accurate upscaling of reactive Poiseuille flow". In: *Advances in Water Resources* 123, pp. 40–53. DOI: 10.1016/j.advwatres.2018.11.001.

Berentsen, C. W. J., M. L. Verlaan, and C. P. J. W. van Kruijsdijk (2005). "Upscaling and reversibility of Taylor dispersion in heterogeneous porous media". In: *Physical Review E* 71 (4), p. 046308. DOI: 10.1103/PhysRevE.71.046308.

Berkowitz, B., A. Cortis, M. Dentz, and H. Scher (2006). "Modeling Non-Fickian Transport in Geological Formations as a Continuous Time Random Walk". In: *Reviews of Geophysics* 44 (2), RG2003. DOI: 10.1029/2005RG000178.

Bolster, D., Y. Méheust, T. Le Borgne, J. Bouquain, and P. Davy (2014). "Modeling preasymptotic transport in flows with significant inertial and trapping effects - The importance of velocity correlations and a spatial Markov model". In: *Advances in Water Resources* 70, pp. 89–103. DOI: 10.1016/j.advwatres.2014.04.014.

Bolster, D., K. R. Roche, and V. L. Morales (2019). "Recent advances in anomalous transport models for predicting contaminants in natural groundwater systems". In: *Current Opinion in Chemical Engineering* 26, pp. 72–80. ISSN:

2211-3398. DOI: 10.1016/j.coche.2019.09.006.

Cherry, J. (2023). "In My Experience: The Lessons from Dispersion–Don't Believe Everything You Read". In: *Ground Water Monitoring & Remediation* 43 (3). DOI: 10.1111/gwmr.12603.

Chiogna, G., D. L. Hochstetler, A. Bellin, P. K. Kitanidis, and M. Rolle (2012). "Mixing, entropy and reactive solute transport". In: *Geophysical Research Letters* 39 (20). DOI: 10.1029/2012GL053295.

Chiogna, G. and M. Rolle (2017). "Entropy-based critical reaction time for mixing-controlled reactive transport". In: *Water Resources Research* 53 (8), pp. 7488–7498. DOI: 10.1002/2017WR020522.

Cirpka, O. A. (2002). "Choice of Dispersion Coefficients in Reactive Transport Calculations on Smoothed Fields". In: *Journal of Contaminant Hydrology* 58 (3-4), pp. 261–282. DOI: 10.1016/S0169-7722(02)00039-6.

Cirpka, O. A., E. O. Frind, and R. Helmig (1999). "Numerical simulation of biodegradation controlled by transverse mixing". In: *Journal of Contaminant Hydrology* 40 (2), pp. 159–182. DOI: 10.1016/S0169-7722(99)00044-3.

Cirpka, O. A. and P. K. Kitanidis (2000). "Characterization of mixing and dilution in heterogeneous aquifers by means of local temporal moments". In: *Water Resources Research* 36 (5), pp. 1221–1236. DOI: 10.1029/1999WR900354.

Cirpka, O. A., M.-M. Stettler, and M. Dentz (2022). "Spatial Markov Model for the Prediction of Travel-Time-Based Solute Dispersion in Three-Dimensional Heterogeneous Media". In: *Water Resources Research* 58 (6), e2022WR032215. DOI: 10.1029/2022WR032215.

Close, M., J. Bright, F. Wang, L. Pang, and M. Manning (2008). "Key features of artificial aquifers for use in modeling contaminant transport". In: *Groundwater* 46 (6), pp. 814–828. DOI: 10.1111/j.1745-6584.2008.00474.x.

Comolli, A., V. Hakoun, and M. Dentz (2019). "Mechanisms, Upscaling, and Prediction of Anomalous Dispersion in Heterogeneous Porous Media". In: *Water Resources Research* 55 (10), pp. 8197–8222. DOI: 10.1029/2019WR024919.

Cvetkovic, V., A. Fiori, and G. Dagan (2014). "Solute transport in aquifers of arbitrary variability: A time-domain random walk formulation". In: *Water Resources Research* 50 (7), pp. 5759–5773. DOI: 10.1002/2014WR015449.

Dagan, G. (1984). "Solute transport in heterogeneous porous formations". In: *Journal of Fluid Mechanics* 145, pp. 151–177. DOI: 10.1017/S0022112084002858.

Dagan, G. (1988). "Time-dependent macrodispersion for solute transport in anisotropic heterogeneous aquifers". In: *Water Resources Research* 24 (9), pp. 1491–1500. DOI: 10.1029/WR024i009p01491.

Dagan, G. (1989). *Flow and transport in porous formations*. New York: Springer Verlag. DOI: 10.1007/978-3-642-75015-1.

Dagan, G., V. D. Cvetkovic, and A. Shapiro (1992). "A solute flux approach in transport in heterogeneous formations : 1. The general framework". In: *Water Resources Research* 28 (5), pp. 1369–1376. DOI: 10.1029/91WR03086.

Dagan, G. and A. Fiori (1997). "The influence of pore-scale dispersion on concentration statistical moments in transport through heterogeneous aquifers". In: *Water Resources Research* 33 (7), pp. 1595–1605. DOI: 10.1029/97WR00803.

Dagan, G., A. Fiori, and I. Janković (2003). "Flow and transport in highly heterogeneous formations: 1. Conceptual framework and validity of first-order approximations". In: *Water Resources Research* 39 (9). DOI: 10.1029/2002WR001717.

Dagan, G. (1987). "Theory of solute transport by groundwater". In: *Annual review of fluid mechanics* 19 (1), pp. 183–213. DOI: 10.1146/annurev.fl.19.010187.001151.

Dagan, G. (2002). "An overview of Stochastic Modeling of Groundwater Flow and Transport: From Theory to Applications". In: *Eos, Transactions American Geophysical Union* 83 (53), pp. 621–622. DOI: 10.1029/2002EO000421.

de Anna, P., J. Jimenez-Martinez, H. Tabuteau, R. Turuban, T. Le Borgne, M. Derrien, and Y. Méheust (2014). "Mixing and reaction kinetics in porous media: An experimental pore scale quantification". In: *Environmental Science & Technology* 48 (1), pp. 508–516. DOI: 10.1021/es403105b.

Demmy, G., S. Berglund, and W. Graham (1999). "Injection Mode Implications for Solute Transport in Porous Media: Analysis in a Stochastic Lagrangian Framework". In: *Water Resources Research* 35 (7), pp. 1965–1973. DOI: 10.1029/1999WR900027.

Dentz, M., F. P. J. de Barros, T. L. Borgne, and D. R. Lester (2018a). "Evolution of solute blobs in heterogeneous porous media". In: *Journal of Fluid Mechanics* 853, pp. 621–646. DOI: 10.1017/jfm.2018.588.

Dentz, M., T. L. Borgne, A. Englert, and B. Bijeljic (2011). "Mixing, spreading and reaction in heterogeneous media: A brief review". In: *Journal of Contaminant Hydrogeology* 120-121, pp. 1–17. DOI: 10.1016/j.jconhyd.2010.05.002.

Dentz, M., M. Icardi, and J. J. Hidalgo (2018b). "Mechanisms of dispersion in a porous medium". In: *Journal of Fluid Mechanics* 841, pp. 851–882. DOI: 10.1017/jfm.2018.120.

Dentz, M., P. K. Kang, A. Comolli, T. L. Borgne, and D. R. Lester (2016). "Continuous time random walks for the evolution

of Lagrangian velocities". In: *Physical Review Fluids* 1 (7), p. 074004. DOI: 10.1103/PhysRevFluids.1.074004.

Dentz, M., H. Kinzelbach, S. Attinger, and W. Kinzelbach (2000). "Temporal behavior of a solute cloud in a heterogeneous porous medium 1. Point-like injection". In: *Water Resources Research* 36 (12), pp. 3591–3604. DOI: 10.1029/2000WR900162.

Dentz, M., J. J. Hidalgo, and D. Lester (2023). "Mixing in porous media: concepts and approaches across scales". In: *Transport in Porous Media* 146 (1-2), pp. 5–53. DOI: 10.1007/s11242-022-01852-x.

Di Dato, M., A. Bellin, and A. Fiori (2019). "Convergent radial transport in three-dimensional heterogeneous aquifers: The impact of the hydraulic conductivity structure". In: *Advances in Water Resources* 131, p. 103381. DOI: 10.1016/j.advwatres.2019.103381.

Ding, X.-H., S.-J. Feng, and Q.-T. Zheng (2022). "Forward and back diffusion of reactive contaminants through multi-layer low permeability sediments". In: *Water Research* 222, p. 118925. DOI: 10.1016/j.watres.2022.118925.

Elhanati, D., I. Dror, and B. Berkowitz (2023). "Impact of Time-Dependent Velocity Fields on the Continuum-Scale Transport of Conservative Chemicals". In: *Water Resources Research* 59 (9), e2023WR035266. DOI: 10.1029/2023WR035266.

Engdahl, N. B. and T. Aquino (2022). "Upscaled models for time-varying solute transport: Transient spatial-Markov dynamics". In: *Advances in Water Resources* 166, p. 104271. DOI: 10.1016/j.advwatres.2022.104271.

Feehley, C. E., C. Zheng, and F. J. Molz (2000). "A dual-domain mass transfer approach for modeling solute transport in heterogeneous aquifers: Application to the Macrodispersion Experiment (MADE) site". In: *Water Resources Research* 36 (9), pp. 2501–2515. DOI: 10.1029/2000WR900148.

Feldmann, F., B. Hagemann, L. Ganzer, and M. Panfilov (2016). "Numerical simulation of hydrodynamic and gas mixing processes in underground hydrogen storages". In: *Environmental Earth Sciences* 75, pp. 1–15. DOI: 10.1007/s12665-016-5948-z.

Fernàndez-Garcia, D., H. Rajaram, and T. H. Illangasekare (2005). "Assessment of the predictive capabilities of stochastic theories in a three-dimensional laboratory test aquifer: Effective hydraulic conductivity and temporal moments of breakthrough curves". In: *Water Resources Research* 41 (4). DOI: 10.1029/2004WR003523.

Ferrara, A., M. Marseguerra, and E. Zio (1999). "A comparison between the advection-dispersion and the Kolmogorov-Dmitriev model for groundwater contaminant transport". In: *Annals of Nuclear Energy* 26 (12), pp. 1083–1096. ISSN: 0306-4549. DOI: 10.1016/S0306-4549(98)00112-1.

Fetter, C. W., T. Boving, and D. Kreamer, eds. (2017). *Contaminant Hydrogeology*. 3rd. Long Grove: Waveland Press.

Fiori, A. (1996). "Finite Peclet extensions of Dagan's solutions to transport in anisotropic heterogeneous formations". In: *Water Resources Research* 32, pp. 193–198. DOI: 10.1029/95wr02768.

Fiori, A. and G. Dagan (2000). "Concentration Fluctuations in Aquifer Transport: A Rigorous First-Order Solution and Applications". In: *Journal of Contaminant Hydrology* 45 (1-2), pp. 139–163. DOI: 10.1016/S0169-7722(00)00123-6.

Fiori, A., I. Jankovic, and G. Dagan (2011). "The impact of local diffusion upon mass arrival of a passive solute in transport through three-dimensional highly heterogeneous aquifers". In: *Advances in Water Resources* 34 (12), pp. 1563–1573. DOI: 10.1016/j.advwatres.2011.08.010.

Fiori, A., S. Berglund, V. Cvetkovic, and G. Dagan (2002). "A first-order analysis of solute flux statistics in aquifers: The combined effect of pore-scale dispersion, sampling, and linear sorption kinetics". In: *Water Resources Research* 38 (8), pp. 12–1. DOI: 10.1029/2001WR000678.

Fiori, A. and I. Jankovic (2012). "On Preferential Flow, Channeling and Connectivity in Heterogeneous Porous Formations". In: *Mathematical Geosciences* 44, pp. 133–145. DOI: 10.1007/s11004-011-9365-2.

Fiori, A., I. Janković, and G. Dagan (2006). "Modeling flow and transport in highly heterogeneous three-dimensional aquifers: Ergodicity, Gaussianity, and anomalous behavior - 2. Approximate semianalytical solution". In: *Water Resources Research* 42 (6). DOI: 10.1029/2005WR004752.

Fiori, A., A. Zarlenga, H. Gotovac, I Jankovic, E. Volpi, V. Cvetkovic, and G. Dagan (2015). "Advective transport in heterogeneous aquifers: Are proxy models predictive?" In: *Water Resources Research* 51 (12), pp. 9577–9594. DOI: 10.1002/2015WR017118.

Foster, S. and T. K. Bjerre (2023). "Diffuse agricultural pollution of groundwater: addressing impacts in Denmark and Eastern England". In: *Water Quality Research Journal* 58 (1), pp. 14–21. DOI: 10.2166/wqrj.2022.022.

Gelhar, L. W. (1993). *Stochastic Subsurface Hydrology*. Englewood Cliffs, NJ: Prentice-Hall.

Gelhar, L. W. and C. L. Axness (1983). "Three-dimensional stochastic analysis of macrodispersion in aquifers". In: *Water Resources Research* 19 (1), pp. 161–180. DOI: 10.1029/WR019i001p00161.

Goeppert, N., N. Goldscheider, and B. Berkowitz (2020). "Experimental and modeling evidence of kilometer-scale anomalous tracer transport

in an alpine karst aquifer". In: *Water Research* 178, p. 115755. DOI: 10.1016/j.watres.2020.115755.

Gotovac, H., V. Cvetković, and R. Andričević (2009). "Flow and travel time statistics in highly heterogeneous porous media". In: *Water Resources Research* 45 (W07402). DOI: 10.1029/2008WR007168.

Gouze, P., T. Le Borgne, R Leprovost, G Lods, T Poidras, and P Pezard (2008). "Non-Fickian dispersion in porous media: 1. Multiscale measurements using single-well injection withdrawal tracer tests". In: *Water Resources Research* 44 (6). DOI: 10.1029/2007WR006278.

Gouze, P., A. Puyguiraud, D. Roubinet, and M. Dentz (2023). "Pore-scale transport in rocks of different complexity modeled by random walk methods". In: *Transport in Porous Media* 146 (1), pp. 139–158. DOI: 10.1007/s11242-021-01675-2.

Gramling, C. M., C. F. Harvey, and L. C. Meigs (2002). "Reactive Transport in Porous Media: A Comparison of Model Prediction with Laboratory Visualization". In: *Environmental Science & Technology* 36 (11), pp. 2508–2514. DOI: 10.1021/es0157144.

Guo, Z., C. V. Henri, G. E. Fogg, Y. Zhang, and C. Zheng (2020). "Adaptive Multirate Mass Transfer (aMMT) model: A new approach to upscale regional-scale transport under transient flow conditions". In: *Water Resources Research* 56 (2), e2019WR026000. DOI: 10.1029/2019WR026000.

Gutjahr, A. L., L. W. Gelhar, A. A. Bakr, and J. R. MacMillan (1978). "Stochastic Analysis of Spatial Variability in Subsurface Flows 2. Evaluation and Application". In: *Water Resources Research* 14 (5), pp. 953–959. DOI: 10.1029/WR014i005p00953.

Haggerty, R. and S. M. Gorelick (1995). "Multiple-Rate Mass Transfer for Modeling Diffusion and Surface Reactions in Media with Pore-Scale Heterogeneity." In: *Water Resources Research* 31 (10), pp. 2382–2400. DOI: 10.1029/95WR10583.

Hansen, S. K., C. P. Haslauer, O. A. Cirpka, and V. V. Vesselinov (2018). "Direct Breakthrough Curve Prediction From Statistics of Heterogeneous Conductivity Fields". In: *Water Resources Research* 54 (1), pp. 271–285. DOI: 10.1002/2017WR020450.

Hansen, S. K., B. Berkowitz, V. V. Vesselinov, D. O'Malley, and S. Karra (2016). "Push-pull tracer tests: Their information content and use for characterizing non-Fickian, mobile-immobile behavior". In: *Water Resources Research* 52 (12), pp. 9565–9585. DOI: 10.1002/2016WR018769.

Harvey, C. F. and S. M. Gorelick (1995). "Temporal Moment-Generating Equations: Modeling Transport and Mass-Transfer in Heterogeneous Aquifers". In: *Water Resources Research* 31 (8), pp. 1895–1911. DOI: 10.1029/95WR01231.

Heller, J. P. (1960). "An Unmixing Demonstration". In: *American Journal of Physics* 28, p. 348. DOI: 10.1119/1.1935802.

Hilpert, M., B. A. Mora, J. Ni, A. M. Rule, and K. E. Nachman (2015). "Hydrocarbon release during fuel storage and transfer at gas stations: environmental and health effects". In: *Current Environmental Health Reports* 2, pp. 412–422. DOI: 10.1007/s40572-015-0074-8.

Huysmans, M. and A. Dassargues (2005). "Review of the use of Peclet numbers to determine the relative imporance of advection and diffusion in low permeability environments". In: *Hydrogeology Journal* 13 (5), pp. 895–904. DOI: 10.1007/s10040-004-0387-4.

Hyman, J. D. and M. Dentz (2021). "Transport Upscaling under Flow Heterogeneity and Matrix-Diffusion in Three-Dimensional Discrete Fracture Networks". In: *Advances in Water Resources* 155, p. 103994. DOI: 10.1016/j.advwatres.2021.103994.

Indelman, P. (2004). "On macrodispersion in uniform - radial divergent flow through weakly heterogeneous aquifers". In: *Stochastic Environmental Research and Risk Assessment* 18 (1), pp. 16–21. DOI: 10.1007/s00477-003-0165-1.

Istok, J. D. (2013). *Push-Pull tests for Site Characterization*. Heidelberg: Springer. DOI: 10.1007/978-3-642-13920-8.

Istok, J., M. Humphrey, M. Schroth, M. Hyman, and K. OReilly (1997). "Single-well, "push-pull" test for in situ determination of microbial activities". In: *Groundwater* 35 (4), pp. 619–631. DOI: 10.1111/j.1745-6584.1997.tb00127.x.

Jha, R. K., A. K. John, S. L. Bryant, and L. W. Lake (2009). "Flow Reversal and Mixing". In: *SPE Journal* 14 (01), pp. 41–49. DOI: 10.2118/103054-PA.

John, A. K., L. W. Lake, S. L. Bryant, and J. W. Jennings (2010). "Investigation of Mixing in Field-Scale Miscible Displacements Using Particle-Tracking Simulations of Tracer Floods With Flow Reversal". In: *SPE Journal* 15 (03), pp. 598–609. DOI: 10.2118/113429-PA.

Jose, S. C. and O. A. Cirpka (2004). "Measurement of Mixing-Controlled Reactive Transport in Homogeneous Porous Media and its Prediction from Conservative Tracer Test Data". In: *Environmental Science & Technology* 38 (7), pp. 2089–2096. DOI: 10.1021/es034586b.

Jose, S. C., M. A. Rahman, and O. A. Cirpka (2004). "Large-Scale Sandbox Experiment on Longitudinal Effective Dispersion in Heterogeneous Porous Media". In: *Water Resources*

Research 40 (12), W12415. DOI: 10.1029/2004WR003363.

Kahler, D. M. and Z. J. Kabala (2016). "Acceleration of groundwater remediation by deep sweeps and vortex ejections induced by rapidly pulsed pumping". In: *Water Resources Research* 52 (5), pp. 3930–3940. DOI: 10.1002/2015WR017157.

Kang, P. K., M. Dentz, T. Le Borgne, and R. Juanes (2011). "Spatial Markov Model of Anomalous Transport Through Random Lattice Networks". In: *Physical Review Letters.* 107, p. 180602. DOI: 10.1103/PhysRevLett.107.180602.

Kang, P. K., P. de Anna, J. P. Nunes, B. Bijeljic, M. J. Blunt, and R. Juanes (2014). "Pore-scale intermittent velocity structure underpinning anomalous transport through 3-D porous media". In: *Geophysical Research Letters* 41 (17), pp. 6184–6190. DOI: 10.1002/2014GL061475.

Kang, P. K., T. Le Borgne, M. Dentz, O. Bour, and R. Juanes (2015). "Impact of velocity correlation and distribution on transport in fractured media: Field evidence and theoretical model". In: *Water Resources Research* 51 (2), pp. 940–959. DOI: 10.1002/2014WR015799.

Kapoor, V. and P. K. Kitanidis (1996). "Concentration fluctuations and dilution in two-dimensionally periodic heterogeneous porous media". In: *Transport in Porous Media* 22, pp. 91–119. DOI: 10.1029/97WR03608.

Kitanidis, P. K. (1988). "Prediction by the method of moments of transport in heterogeneous formations". In: *Journal of Hydrology* 102 (1-4), pp. 453–473. DOI: 10.1016/0022-1694(88)90111-4.

Kitanidis, P. K. (1994). "The concept of the dilution index". In: *Water Resources Research* 30 (7), pp. 2011–2026. DOI: 10.1029/94WR00762.

Koponen, A., M. Kataja, and J. Timonen (1996). "Tortuous flow in porous media". In: *Physical Review E* 54 (1), pp. 406–410. DOI: 10.1103/PhysRevE.54.406.

Kruisdijk, E. and B. M. van Breukelen (2021). "Reactive transport modelling of push-pull tests: A versatile approach to quantify aquifer reactivity". In: *Applied Geochemistry* 131, p. 104998. DOI: 10.1016/j.apgeochem.2021.104998.

Kruse, E., S. Eslamian, K. Ostad-Ali-Askari, and S. Z. Hosseini-Teshnizi (2018). "Borehole Investigations". In: *Encyclopedia of Engineering Geology*. Ed. by P. Bobrowsky and B. Marker. Cham: Springer International Publishing, pp. 1–6. ISBN: 978-3-319-12127-7. DOI: 10.1007/978-3-319-12127-7_32-1.

Kuang, X. et al. (2024). "The changing nature of groundwater in the global water cycle". In: *Science* 383 (6686), eadf0630. DOI: 10.1126/science.adf0630.

La Licata, I., C. D. Langevin, A. M. Dausman, and L. Alberti (2011). "Effect of tidal fluctuations on transient dispersion of simulated contaminant concentrations in coastal aquifers". In: *Hydrogeology Journal* 19 (7), pp. 1313–1322. DOI: 10.1007/s10040-011-0763-9.

Larocque, M., P. G. Cook, K. Haaken, and C. T. Simmons (2009). "Estimating flow using tracers and hydraulics in synthetic heterogeneous aquifers". In: *Groundwater* 47 (6), pp. 786–796. DOI: 10.1111/j.1745-6584.2009.00595.x.

Le Borgne, T., M. Dentz, and E. Villermaux (2015). "The lamellar description of mixing in porous media". In: *Journal of Fluid Mechanics* 770, pp. 458–498. DOI: 10.1017/jfm.2015.117.

Le Borgne, T., D. Bolster, M. Dentz, P. de Anna, and A. Tartakovsky (2011). "Effective pore-scale dispersion upscaling with a correlated continuous time random walk approach". In: *Water Resources Research* 47 (12). DOI: 10.1029/2011WR010457.

Le Borgne, T., M. Dentz, and J. Carrera (2008a). "Lagrangian Statistical Model for Transport in Highly Heterogeneous Velocity Fields". In: *Physical Review Letters.* 101 (9), p. 090601. DOI: 10.1103/PhysRevLett.101.090601.

Le Borgne, T., M. Dentz, and J. Carrera (2008b). "Spatial Markov processes for modeling Lagrangian particle dynamics in heterogeneous porous media". In: *Physical Review E* 78 (2), p. 026308. DOI: 10.1103/PhysRevE.78.026308.

Le Borgne, T., M. Dentz, and E. Villermaux (2013). "Stretching, Coalescence, and Mixing in Porous Media". In: *Physical Review Letters* 110 (20), p. 204501. DOI: 10.1103/PhysRevLett.110.204501.

Le Borgne, T., J.-R. de Dreuzy, P. Davy, and O. Bour (2007). "Characterization of the velocity field organization in heterogeneous media by conditional correlation". In: *Water Resources Research* 43 (2). DOI: 10.1029/2006WR004875.

Leap, D. I. and P. G. Kaplan (1988). "A single-well tracing method for estimating regional advective velocity in a confined aquifer: theory and preliminary laboratory verification". In: *Water Resources Research* 24 (7), pp. 993–998. DOI: 10.1029/WR024i007p00993.

Lester, D. R., M. Dentz, and T. Le Borgne (2016). "Chaotic mixing in three-dimensional porous media". In: *Journal of Fluid Mechanics* 803, pp. 144–174. DOI: 10.1017/jfm.2016.486.

Li, J. B. (2007). "Stochastic Risk Assessment of Groundwater Contamination under Uncertainty: A Canadian Case Study". In: *Journal of Environmental Informatics* 9 (2). DOI: 10.3808/jei.200700089.

Li, N. and L. Ren (2009). "Application of continuous time random walk theory to nonequilibrium transport in soil". In: *Journal of Contaminant Hydrology* 108 (3), pp. 134–151. DOI: 10.1016/j.jconhyd.2009.07.002.

Loáiciga, H. A., W. W.-G. Yeh, and M. A. Ortega-Guerrero (2006). "Probability density functions in the analysis of hydraulic conductivity data". In: *Journal of Hydrologic Engineering* 11

(5), pp. 442–450. DOI: 10.1061/(ASCE)1084-0699(2006)11:5(442).

Lowe, J. and P. F. Zaccheo (1991). "Subsurface Explorations and Sampling". In: *Foundation Engineering Handbook*. Ed. by H.-Y. Fang. Boston, MA: Springer US, pp. 1–71. ISBN: 978-1-4615-3928-5. DOI: 10.1007/978-1-4615-3928-5_1.

Lu, Z. and D. Zhang (2003). "On importance sampling Monte Carlo approach to uncertainty analysis for flow and transport in porous media". In: *Advances in Water Resources* 26 (11), pp. 1177–1188. DOI: 10.1016/S0309-1708(03)00106-4.

Ma, M., P. Dillon, and Y. Zheng (2019). "Determination of Sulfamethoxazole Degradation Rate by an in Situ Experiment in a Reducing Alluvial Aquifer of the North China Plain". In: *Environmental Science & Technology* 53 (18), pp. 10620–10628. DOI: 10.1021/acs.est.9b00832.

Maliva, R. G. (2016). "Aquifer Characterization Techniques". In: Cham: Springer, pp. 1–617. ISBN: 978-3-319-32137-0. DOI: 10.1007/978-3-319-32137-0.

Meerschaert, M. M., M. Dogan, R. L. Van Dam, D. W. Hyndman, and D. A. Benson (2013). "Hydraulic conductivity fields: Gaussian or not?" In: *Water Resources Research* 49 (8), pp. 4730–4737. DOI: 10.1002/wrcr.20376.

Mettier, R., G. Kosakowski, and O. Kolditz (2006). "Influence of Small-Scale Heterogeneities on Contaminant Transport in Fractured Crystalline Rock". In: *Groundwater* 44 (5), pp. 687–696. DOI: 10.1111/j.1745-6584.2006.00236.x.

Meyer, D. W. (2018). "A simple velocity random-walk model for macrodispersion in mildly to highly heterogeneous subsurface formations". In: *Advances in Water Resources* 121, pp. 57–67. DOI: 10.1016/j.advwatres.2018.07.015.

Molz, F. and M. Widdowson (1988). "Internal inconsistencies in dispersion-dominated models that incorporate chemical and microbial kinetics". In: *Water Resources Research* 24 (4), pp. 615–619. DOI: 10.1029/WR024i004p00615.

Molz, F. (2015). "Advection, dispersion, and confusion". In: *Groundwater* 53 (3). DOI: 10.1111/gwat.12338.

Montero, M. and J. Masoliver (2007). "Nonindependent continuous-time random walks". In: *Physical Review E* 76 (6), p. 061115. DOI: 10.1103/PhysRevE.76.061115.

Morales, V., M. Dentz, M. Willmann, and M. Holzner (2017). "Stochastic dynamics of intermittent pore-scale particle motion in three-dimensional porous media: Experiments and theory". In: *Geophysical Research Letters* 44 (18), pp. 9361–9371. DOI: 10.1002/2017GL074326.

Moroni, M., N. Kleinfelter, and J. H. Cushman (2007). "Analysis of dispersion in porous media via matched-index particle tracking velocimetry experiments". In: *Advances in Water Resources* 30 (1), pp. 1–15. DOI: 10.1016/j.advwatres.2006.02.005.

Neuman, S. P., C. L. Winter, and C. M. Newman (1987). "Stochastic theory of field-scale Fickian dispersion in anisotropic porous media". In: *Water Resources Research* 23 (3), pp. 453–466. DOI: 10.1029/WR023i003p00453.

Neuman, S. P. and D. M. Tartakovsky (2009). "Perspective on theories of non-Fickian transport in heterogeneous media". In: *Advances in Water Resources* 32 (5), pp. 670–680. DOI: 10.1016/j.advwatres.2008.08.005.

Neupauer, R. M., E. J. Roth, J. P. Crimaldi, D. C. Mays, and L. J. Sather (2021). "Demonstration of Reversible Dispersion in a Darcy-Scale Push-Pull Laboratory Experiment". In: *Transport in Porous Media* 146 (1-2), pp. 351–367. DOI: 10.1007/s11242-021-01682-3.

Neuweiler, I., S. Attinger, and W. Kinzelbach (2001). "Macrodispersion in a radially diverging flow field with finite Peclet numbers 1. Perturbation theory approach". In: *Water Resources Research* 37 (3), pp. 481–493. DOI: 10.1029/2000WR900313.

Paradis, C. J., L. D. McKay, E. Perfect, J. D. Istok, and T. C. Hazen (2018). "Push-pull tests for estimating effective porosity: expanded analytical solution and in situ application". In: *Hydrogeology Journal* 26 (2), pp. 381–393. DOI: 10.1007/s10040-017-1672-3.

Pasetto, D., A. Guadagnini, and M. Putti (2014). "A reduced-order model for Monte Carlo simulations of stochastic groundwater flow". In: *Computational Geosciences* 18, pp. 157–169. DOI: 10.1007/s10596-013-9389-4.

Pavliotis, G. A. (2014). *Stochastic Processes and Applications*. New York: Springer. DOI: 10.1007/978-1-4939-1323-7.

Perez, L. J., J. J. Hidalgo, and M. Dentz (2019). "Upscaling of Mixing-Limited Bimolecular Chemical Reactions in Poiseuille Flow". In: *Water Resources Research* 55 (1), pp. 249–269. DOI: 10.1029/2018WR022730.

Perez, L. J., J. J. Hidalgo, A. Puyguiraud, J. Jimenez-Martinez, and M. Dentz (2020). "Assessment and Prediction of Pore-Scale Reactive Mixing From Experimental Conservative Transport Data". In: *Water Resources Research* 56 (6). DOI: 10.1029/2019WR026452.

Piscopo, A. N., R. M. Neupauer, and D. C. Mays (2013). "Engineered injection and extraction to enhance reaction for improved in situ remediation". In: *Water Resources Research* 49 (6), pp. 3618–3625. DOI: 10.1002/wrcr.20209.

Pollock, D. W. (1988). "Semianalytical computation of path lines for finite-difference models". In: *Groundwater* 26 (6), pp. 743–750. DOI: 10.1111/j.1745-6584.1988.tb00425.x.

Pool, M., V. E. Post, and C. T. Simmons (2014). "Effects of tidal fluctuations on mixing and spreading in coastal aquifers: Homogeneous case". In: *Water Resources Research* 50 (8), pp. 6910–6926. DOI: 10.1002/2014WR015534.

Puyguiraud, A., P. Gouze, and M. Dentz (2019). "Upscaling of Anomalous Pore-Scale Dispersion". In: *Transport in Porous Media* 128 (2), pp. 837–855. DOI: 10.1007/s11242-019-01273-3.

Rasmusson, K., M. Rasmusson, F. Fagerlund, J. Bensabat, Y. Tsang, and A. Niemi (2014). "Analysis of alternative pushpull-test-designs for determining in situ residual trapping of carbon dioxide". In: *International Journal of Greenhouse Gas Control* 27, pp. 155–168. ISSN: 1750-5836. DOI: 10.1016/j.ijggc.2014.05.008.

Raveh-Rubin, S., Y. Edery, I. Dror, and B. Berkowitz (2015). "Nickel migration and retention dynamics in natural soil columns". In: *Water Resources Research* 51 (9), pp. 7702–7722. DOI: 10.1002/2015WR016913.

Rhodes, M. E., B. Bijeljic, and M. J. Blunt (2008). "Pore-to-field simulation of single-phase transport using continuous time random walks". In: *Advances in Water Resources* 31 (12), pp. 1527–1539. DOI: 10.1016/j.advwatres.2008.04.006.

Risken, H. (1996). *The Fokker-Planck Equation*. 2nd. Berlin Heidelberg: Springer. DOI: 10.1007/978-3-642-61544-3_4.

Rolle, M., G. Chiogna, D. L. Hochstetler, and P. K. Kitanidis (2013). "On the importance of diffusion and compound-specific mixing for groundwater transport: An investigation from pore to field scale". In: *Journal of Contaminant Hydrology* 153, pp. 51–68. DOI: 10.1016/j.jconhyd.2013.07.006.

Rolle, M., C. Eberhardt, G. Chiogna, O. A. Cirpka, and P. Grathwohl (2009). "Enhancement of Dilution and Transverse Reactive Mixing in Porous Media: Experiments and Model-Based Interpretation". In: *Journal of Contaminant Hydrology* 110 (3-4), pp. 130–142. DOI: 10.1016/j.jconhyd.2009.10.003.

Roth, E. J., D. C. Mays, R. M. Neupauer, L. J. Sather, and J. P. Crimaldi (2021). "Methods for Laser-Induced Fluorescence Imaging of Solute Plumes at the Darcy Scale in Quasi-Two-Dimensional, Refractive Index-Matched Porous Media". In: *Transport in Porous Media* 136 (3), pp. 879–898. DOI: 10.1007/s11242-021-01545-x.

Rousseau, G., S. Izumoto, T. Le Borgne, and J. Heyman (2023). "Dispersion versus diffusion in mixing fronts". In: *Water Resources Research* 59 (11), e2023WR035848. DOI: 10.1029/2023WR035848.

Rubin, Y. (1990). "Stochastic modeling of macrodispersion in heterogeneous porous media". In: *Water Resources Research* 26 (1), pp. 133–141. DOI: 10.1029/WR026i001p00133.

Rubin, Y. (2003). *Applied Stochastic Hydrogeology*. Oxford: Oxford University Press. DOI: 10.1093/oso/9780195138047.001.0001.

Rubin, Y. and S. Ezzedine (1997). "The Travel Times of Solutes at the Cape Cod Tracer Experiment: Data Analysis, Modeling, and Structural Parameters Inference". In: *Water Resources Research* 33 (7), pp. 1537–1547. DOI: 10.1029/96WR00016.

Santucci, L., E. Carol, and C. Tanjal (2018). "Industrial waste as a source of surface and groundwater pollution for more than half a century in a sector of the Río de la Plata coastal plain (Argentina)". In: *Chemosphere* 206, pp. 727–735. DOI: 10.1016/j.chemosphere.2018.05.084.

Shapiro, A. M. and V. D. Cvetkovic (1988). "Stochastical analysis of solute arrival time in heterogeneous porous media". In: *Water Resources Research* 24 (10), pp. 1711–1718. DOI: 10.1029/WR024i010p01711.

Sherman, T., N. B. Engdahl, G. Porta, and D. Bolster (2021). "A review of spatial Markov models for predicting pre-asymptotic and anomalous transport in porous and fractured media". In: *Journal of Contaminant Hydrology* 236, p. 103734. DOI: 10.1016/j.jconhyd.2020.103734.

Sherman, T., A. Foster, D. Bolster, and K. Singha (2018). "Predicting Downstream Concentration Histories From Upstream Data in Column Experiments". In: *Water Resources Research* 54 (11), pp. 9684–9694. DOI: 10.1029/2018WR023420.

Siebert, S., J. Burke, J. M. Faures, K. Frenken, J. Hoogeveen, P. Döll, and F. T. Portmann (2010). "Groundwater use for irrigation – a global inventory". In: *Hydrology and Earth System Sciences* 14 (10), pp. 1863–1880. DOI: 10.5194/hess-14-1863-2010.

Smith, M., K. Cross, M. Paden, and P. Laban (2016). "Spring–Managing groundwater sustainably". In: *IUCN, Gland, Switzerland*. DOI: 10.2305/IUCN.CH.2016.WANI.8.en.

Sprenger, M. et al. (2019). "The Demographics of Water: A Review of Water Ages in the Critical Zone". In: *Reviews of Geophysics* 57 (3), pp. 800–834. DOI: 10.1029/2018RG000633.

Srzic, V., V. Cvetkovic, R. Andricevic, and H. Gotovac (2013). "Impact of aquifer heterogeneity structure and local-scale dispersion on solute concentration uncertainty". In: *Water Resources Research* 49 (6), pp. 3712–3728. DOI: 10.1002/wrcr.20314.

Stettler, M.-M. and O. A. Cirpka (2022). *Electronic Appendix to Linear Stochastic Analysis of the Partial Reversibility of Ensemble and Effective Dispersion in Heterogeneous Porous Media*. DOI: 10.5281/zenodo.7023203.

Stettler, M.-M., M. Dentz, and O. A. Cirpka (2023). "Linear Stochastic Analysis of the

Partial Reversibility of Ensemble and Effective Dispersion in Heterogeneous Porous Media". In: *Water Resources Research* 59 (1), e2022WR033570. DOI: 10.1029/2022WR033570.

Stettler, M.-M., M. Dentz, and O. A. Cirpka (2025). *Electronic Appendix to: Spatial Markov Model of Advective-Diffusive Transport in Heterogeneous Domains*. DOI: 10.5281/zenodo.15389771.

Stettler, M.-M., M. Dentz, and O. A. Cirpka (2026). "Spatial Markov Model of Advective-Diffusive Transport in Heterogeneous Domains". In: *Water Resources Research* 62 (1), e2025WR041175. DOI: 10.1029/2025WR041175.

Sund, N., G. Porta, D. Bolster, and R. Parashar (2017a). "A Lagrangian Transport Eulerian Reaction Spatial (LATERS) Markov Model for Prediction of Effective Bimolecular Reactive Transport". In: *Water Resources Research* 53 (11), pp. 9040–9058. DOI: 10.1002/2017WR020821.

Sund, N. L., G. M. Porta, and D. Bolster (2017b). "Upscaling of dilution and mixing using a trajectory based Spatial Markov random walk model in a periodic flow domain". In: *Advances in Water Resources* 103, pp. 76–85. DOI: 10.1016/j.advwatres.2017.02.018.

Sundararajan, P., J. D. Kirtland, D. L. Koch, and A. D. Stroock (2012). "Impact of chaos and Brownian diffusion on irreversibility in Stokes flows". In: *Physical Review E* 86 (4), p. 046203. DOI: 10.1103/PhysRevE.86.046203.

Tecklenburg, J., I. Neuweiler, J. Carrera, and M. Dentz (2016). "Multi-rate mass transfer modeling of two-phase flow in highly heterogeneous fractured and porous media". In: *Advances in Water Resources* 91, pp. 63–77. DOI: 10.1016/j.advwatres.2016.02.010.

Tonina, D. and A. Bellin (2008). "Effects of Pore-Scale Dispersion, Degree of Heterogeneity, Sampling Size, and Source Volume on the Concentration Moments of Conservative Solutes in Heterogeneous Formations". In: *Advances in Water Resources* 31 (2), pp. 339–354. DOI: 10.1016/j.advwatres.2007.08.009.

Urroz, G. E., Y. Ma, and M. W. Kemblowski (1995). "Advective and dispersive mixing in stratified formations". In: *Transport in Porous Media* 18 (3), pp. 231–243. DOI: 10.1007/bf00616933.

Van Kampen, N. G. (2007). *Stochastic Processes in Physics and Chemistry*. 3rd. Amsterdam Boston London: Elsevier. DOI: 10.1016/B978-0-444-52965-7.X5000-4.

Vandenbohede, A., A. Louwyck, and L. Lebbe (2009). "Conservative Solute Versus Heat Tranport in Porous Media During Push-Pull Tests". In: *Transport in Porous Media* 76 (8), pp. 265–287. DOI: 10.1007/s11242-008-9246-4.

Vanderborght, J. and H. Vereecken (2002). "Estimation of Local Scale Dispersion from Local Breakthrough Curves During a Tracer Test in a Heterogeneous Aquifer: The Lagrangian Approach". In: *Journal of Contaminant Hydrology* 54 (1-2), pp. 141–171. DOI: 10.1016/S0169-7722(01)00143-7.

Weeks, S. W. and G. Sposito (1998). "Mixing and stretching efficiency in steady and unsteady groundwater flows". In: *Water Resources Research* 34 (12), pp. 3315–3322. DOI: 10.1029/98WR02535.

Wiederseiner, S., N. Andreini, G. Epely-Chauvin, and C. Ancey (2011). "Refractive-index and density matching in concentrated particle suspensions: a review". In: *Experiments in fluids* 50 (5), pp. 1183–1206. DOI: 10.1007/s00348-010-0996-8.

Wright, E. E., N. L. Sund, D. H. Richter, G. M. Porta, and D. Bolster (2019). "Upscaling Mixing in Highly Heterogeneous Porous Media via a Spatial Markov Model". In: *Water* 11 (1), p. 53. DOI: 10.3390/w11010053.

Wright, E. E., N. L. Sund, D. H. Richter, G. M. Porta, and D. Bolster (2021). "Upscaling bimolecular reactive transport in highly heterogeneous porous media with the LAgrangian Transport Eulerian Reaction Spatial (LATERS) Markov model". In: *Stochastic Environmental Research and Risk Assessment* 35 (8), pp. 1529–1547. DOI: 10.1007/s00477-021-02006-z.

Ye, Y., G. Chiogna, O. A. Cirpka, P. Grathwohl, and M. Rolle (2016). "Experimental investigation of transverse mixing in porous media under helical flow conditions". In: *Physical Review E* 94 (1), 013113. DOI: 10.1103/PhysRevE.94.013113.

Yeh, T.-C. J. (1992). "Stochastic Modelling of Groundwater Flow and Solute Transport in Aquifers". In: *Hydrological Processes* 6 (4), pp. 369–395. DOI: 10.1002/hyp.3360060402.

Yew, A. G., D. Pinero, A. H. Hsieh, and J. Atencia (2013). "Low Peclet number mass and momentum transport in microcavities". In: *Applied Physics Letters* 102 (8), p. 084108. DOI: 10.1063/1.4794058.

Yoon, S., M. Dentz, and P. K. Kang (2021). "Optimal fluid stretching for mixing-limited reactions in rough channel flows". In: *Journal of Fluid Mechanics* 916, A45. DOI: 10.1017/jfm.2021.208.

Zehe, E., R. Loritz, Y. Edery, and B. Berkowitz (2021). "Preferential pathways for fluid and solutes in heterogeneous groundwater systems: self-organization, entropy, work". In: *Hydrology and Earth System Sciences* 25 (10), pp. 5337–5353. DOI: 10.5194/hess-25-5337-2021.

Zerovnik, G., A. Trkov, D. L. Smith, and R. Capote (2013). "Transformation of correlation coefficients between normal and lognormal distribution and implications for nuclear applications". In: *Nuclear Instruments and Methods in Physics Research* 727, pp. 33–39. DOI: 10.1016/j.nima.2013.06.025.

Zhang, D. (2002). *Stochastic Methods for Flow in Porous Media*. San Diego: Academic Press.

Zinn, B., L. C. Meigs, C. F. Harvey, R. Haggerty, W. J. Peplinski, and C. F. V. Schwerin (2004). "Experimental Visualization of Solute Transport and Mass Transfer Processes in Two-Dimensional Conductivity Fields with Connected Regions of High Conductivity". In: *Environmental Science & Technology* 38 (14), pp. 3916–3926. DOI: 10.1021/es034958g.

Zivar, D., S. Kumar, and J. Foroozesh (2021). "Underground hydrogen storage: A comprehensive review". In: *International Journal of Hydrogen Energy* 46 (45), pp. 23436–23462. DOI: 10.1016/j.ijhydene.2020.08.138.